BERICHTE
aus dem Fachbereich Geowissenschaften
der Universität Bremen

No. 176

Bruhns, P.

CRYSTAL CHEMICAL CHARACTERIZATION OF HEAVY METAL INCORPORATION IN BRICK BURNING PROCESSES

Berichte, Fachbereich Geowissenschaften, Universität Bremen, No. 176,
93 pages, Bremen 2001

ISSN 0931-0800

The "Berichte aus dem Fachbereich Geowissenschaften" are produced at irregular intervals by the Department of Geosciences, Bremen University.

They serve for the publication of experimental works, Ph.D.-theses and scientific contributions made by members of the department.

Reports can be ordered from:

Gisela Boelen

Sonderforschungsbereich 261

Universität Bremen

Postfach 330 440

D 28334 BREMEN

Phone: (49) 421 218-4124

Fax: (49) 421 218-3116

e-mail: boelen@uni-bremen.de

Citation:

Bruhns, P.

Crystal Chemical Characterization of Heavy Metal Incorporation in Brick Burning Processes.

Berichte, Fachbereich Geowissenschaften, Universität Bremen, No. 176, 93 pages, Bremen, 2001.

ISSN 0931-0800

Crystal chemical characterization of heavy metal incorporation in brick burning processes

Dissertation

zur Erlangung des

Doktorgrades der Naturwissenschaften

im Fachbereich 5 - Geowissenschaften

der Universität Bremen

vorgelegt von

Petra Bruhns

Bremen 2001

Tag des Kolloquiums: 18.06.2001

Gutachter:

1. Prof. Dr. R. X. Fischer

2. Dr. K. Hamer

Prüfer:

1. Prof. Dr. O. Brockamp

2. Prof. Dr. H. Villinger

Preface

The aim of this study is the detailed description of the processes occurring during brick burning upon addition of selected heavy metal compounds to the raw clay material. Brick manufacturers test the feasibility of heavy metal contaminated wastes (e.g. sewage sludges, incineration ashes, etc.) with regard to the properties of a technical product. The immobilization of heavy metals in general is tested by leaching experiments as described in DEV S4 (DIN 38414).

We were interested in the crystal-chemical processes concerning the heavy metal incorporation. The detailed knowledge of the reactions in which heavy metals are involved or which are triggered by heavy metals yields a basis for the judgement of the product's stability. The determination of mineral phases incorporating heavy metal ions concedes the judgement of the stability of fixation.

The next chapter, the *Introduction*, of this PhD thesis gives an overview of previous studies. The following part, the *Experimental and analyses*, describes syntheses, experiments, and analyses performed. In the third chapter, *Publications*, the manuscripts are presented. At the moment, two of them are published: "*Crystallization of cristobalite and tridymite in the presence of vanadium*" and "*Phase reactions in the brick firing process of V doped clay*", both in the European Journal of Mineralogy. "*Phase reactions in the brick firing process of clay in the presence of Cr, Cu, and Pb*" and "*Incorporation and leaching of heavy metals in clay annealed with Pb, Cu, and V*" are submitted. In part four of this study, *Conclusion*, a survey and interpretation of the results are given.

Table of contents

Part I Introduction

The utilization of heavy metal contaminated wastes based on thermal treatment is discussed by several authors (e.g. Rosenwinkel, 1998). The products are mainly used as construction materials like clay pipes, bricks, or granules. In this study, we focussed on bricks and especially on the crystal-chemical processes occurring during brick burning. In comparison with experiments performed with natural clay, the mineral reactions and formations yield informations on the influence of heavy metals on the brick burning process.

Natural clay consists of clay minerals, quartz, feldspars, and accessory minerals. The individual compositions of clays, especially the type of clay minerals and their concentrations, vary significantly. Obviously, the brick burning process and its products depend on the composition of the raw material.

Salmang and Scholze (1983) describe the mineralizations of natural clay upon thermal treatment. Generally, clay minerals are decomposed in rather low temperature regions. The clay investigated in this study contained kaolinite and illite. Kaolinite at room temperature is a layer clay mineral with the chemical composition $Al_2Si_2O_5(OH)_4$. Two sheets, a tetrahedral sheet consisting of SiO_4 groups and an octahedral ($AlO_2(OH)_4$) sheet are linked together. The symmetry is triclinic with space group *C 1* and unit cell parameters $a = 5.1554$ Å, $b = 8.9448$ Å, $c = 7.4048$ Å, $\alpha = 91.7°$, $\beta = 104.862°$, $\gamma = 89.822°$ (Bish & Von Dreele, 1989). No structure model is available so far for illite. Zöller (1994) investigated illite using electron diffraction and described a close relationship of the illite structure and the muscovite structure. In this study, illite is described in the symmetry of muscovite in the monoclinic space group *C 2/c* and cell parameters $a = 5.1988$ Å, $b = 9.0266$ Å, $c = 20.1058$ Å, $\beta = 95.782°$ as given by Richardson & Richardson (1982).

At temperatures up to 600° C water is separated from the clay minerals, especially kaolinite. Kaolinite transforms to mullite upon further heating. Mullite ($Al_{4+2x}Si_{2-2x}O_{10-x}$, $0.25 \leq x \leq 0.4$) is an important component of ceramics. The transformation occurs in several steps: firstly, dehydroxylation between 500° and 600° C yields metakaolinite. The nature of metakaolinite has been uncertain over a long time as it gives no distinct X-ray pattern. Brindley & Nakahira (1959) postulated that the Si-O network of kaolinite is retained essentially unchanged in metakaolinite. Gualtieri & Bellotto (1998) also describe a relatively uncollapsed framework with strong relations to the parent kaolinite. During the dehydroxylation process they observed a change in the coordination of Al cations from 6 (in kaolinite) to 4. One out of 8 OH is preserved in the metakaolinite structure. The remaining -OH groups are removed in the temperature range up to 950° C. After complete dehydroxylation, a new phase is observed: its symmetry is cubic and it is often described as a spinel-type (Brindley & Nakahira, 1959). It serves as precursor of mullitization: further heating forms mullite in the range between 1100° and 1400° C (Brindley & Nakahira, 1959). According to the reaction scheme:

$$3\ Al_2(Si_2O_5)(OH)_4 \rightarrow 3\ Al_2O_3 \cdot 2SiO_2 + 4\ SiO_2 + 6\ H_2O.$$

silica is released simultaneously. In this temperature range silica crystallizes as cristobalite. The presence of cristobalite in ceramics and bricks is not desirable. During the cooling process, cristobalite undergoes a phase transition between 180° and 270° C from the high-temperature modification (β) in space group $Fd\bar{3}m$ with unit cell parameter a = 7.12 Å (Wyckoff, 1925) to the metastable low-temperature modification (α) in space group $P4_12_12$ with a = 4.9709 Å and c = 6.9278 Å (Pluth *et al.*, 1985). This transformation is accompanied by a significant decrease in the cell volume which causes cracks in the final product (Schmahl, 1993).

The behavior of illite during brick burning processes depends on its variety in chemical composition. Generally, decomposition of illite starts at about 850° C, but illitic

compounds are detectable up to 1000° C (Kromer & Schüller, 1974). Due to its complex chemical composition, a wide variety of mineralizations based on illite is possible e.g. hematite, corundum, feldspar, leucite, spinel etc. (Jasmund & Lagaly, 1993). The presence of illite in raw clay material supports the formation of liquid phase during the annealing process (Salmang & Scholze, 1983). It is important for further reactions and improves properties and quality of the technical product.

Participation of quartz in reaction processes is expected at temperatures above 1000° C (Salmang & Scholze, 1983).

Generally, the high temperature reactions are considered for immobilization of heavy metal ions upon thermal treatment. Both mullite and cristobalite are supposed to incorporate foreign cations. Schneider (1990) describes the incorporation of transition metal ions in mullite. It occurs as substitution either of Al^{3+} in AlO_6-octahedra or AlO_4-tetrahedra, or Si^{4+} in SiO_4-tetrahedra. Additionally, incorporation is possible in structural channels and in structural voids (Schneider, 1990). Mullites incorporating metal ions are characterized by significant changes in their lattice constants. Cristobalite, on the other hand, does not only incorporate foreign cations: its formation is influenced by the presence of cationic impurities (Flörke, 1955). The incorporation of these impurities is based on the substitution of Si^{4+} by ions of lower valence, e.g. Al^{3+}. For charge compensation, the incorporation of additional cations e.g. Na^+ is necessary. These derivatives of silica structures are so-called "stuffed" derivatives of silica (Buerger 1948, 1954). Stuffed cristobalite shows no phase transition upon cooling: the cubic structure of the high-β-form is stable even at room temperature (Perrotta et al., 1989). The incorporation of foreign cations in the structure inhibits the phase transition and, in consequence, the contraction of the structure (Saltzberg et al., 1992). Therefore, the presence of stuffed cristobalite in ceramics may prevent fragmentation of the product during the cooling process.

Previous studies showed that heavy metal contaminated wastes like sewage sludge in Japan can substitute clay as raw material for brick manufacturing (Rosenwinkel, 1998). The final products satisfy the industrial standards and the physical properties of these bricks permit the utilization as construction material. Beside sewage sludge other heavy metal contaminated materials are suitable as additives in clay as well. Some manufacturers use incineration ashes, slags, contaminated soils (e.g. of former foundry sites), or muds from galvanizing, chemical, and metal industries. The more constituents occur in these waste mixtures, the more variations in the mineralizations during annealing processes are possible. The determination of heavy metal fixation is difficult in a multi-phase system with small concentrations of the single phases. Margane (1992) described the thermal treatment of contaminated soils up to 1000° C. He limited the determination of the mineral phases to the main components. Enrichment of accessory components would have been required for detailed investigation but it was not possible: due to the high density of the final products a separation of several constituents is not practicable. In this study, we reduced the investigated parameters by replacing the complex waste system by selected heavy metal compounds, like oxides or chromates which were added to the clay or the silica system. This way, the enrichment of one component is independent of accompanying phases and less difficult to monitor.

Bish, D. L., von Dreele, R. B. (1989): Rietveld refinement of non-hydrogen atomic positions in kaolinite. *Clays and Clay Minerals*, **37**, 289-296.

Brindley, G. W., Nakahira, M. (1959): The kaolinite-mullite reaction series: I. A survey of outstanding problems. II. Metakaolin. III. The high-temperature phases. *J. Am. Ceram. Soc.*, **42**, 311-342.

Buerger, M. J. (1948): Crystals based on the silica structures. *Am. Mineral.*, **33**, 751-752.

Buerger, M. J. (1954): The stuffed derivatives of the silica structures. *Am. Mineral.*, **39**, 600-614.

Flörke, O. W. (1955): Strukturanomalien bei Tridymit und Cristobalit. *Ber. Dtsch. Keram. Ges.*, **32**, 369-81.

Gualtieri, A., Bellotto, M. (1998): Modelling the structure of the metastable phases in the reaction sequence kaolinite-mullite by X-ray scattering experiments. *Phys. Chem. Minerals*, **25**, 442-452.

Jasmund, K., Lagaly, G. (eds.) (1993): Tonminerale und Tone: Struktur, Eigenschaften, Anwendungen und Einsatz in Industrie und Umwelt. Steinkopff Verlag, Darmstadt, 490 p.

Kromer, H., Schüller, K. H. (1974): Sintervorgänge bei Kaolinen und Tonen. *N. Jb. Min. Abh.*, **122**, 145-185.

Margane, J. (1992): Änderung der Schwermetallbindungsformen in thermisch behandeltem Bodenmaterial. Geologisches Institut der Universität zu Köln, Sonderveröffentlichungen Nr. 87.

Perrotta, A. J., Grubbs, D. K., Martin, E. S., Dando, N. R., McKinstry, H. A., Huang, C. Y. (1989): Chemical stabilization of β-cristobalite. *J. Am. Ceram. Soc.*, **72**, 441-447.

Pluth, J. J., Smith, J. V., Faber, J. Jr. (1985): Crystal structure of low cristobalite at 10, 293, and 473 K: Variation of framework geometry with temperature. *J. Appl. Phys.* **57**, 1045-1049.

Richardson, S. M., Richardson, J. W. Jr. (1982): Crystal structure of a pink muscovite from Archer's post Kenya: implications for reverse pleochroism in dioctahedral micas. *Am. Mineral.*, **67**, 69-75.

Rosenwinkel, K. H. (1998): BMBF Statusseminar: Stoffliche Verwertung von Klärschlämmen und Aschen aus der Klärschlammverbrennung als Baustoff. Veröffentlichungen des Institutes für Siedlungswasserwirtschaft und Abfalltechnik der Universität Hannover, Heft 107.

Salmang, H., Scholze, H. (1983): Keramik: Allgemeine Grundlagen und wichtige Eigenschaften. Springer Verlag, Berlin Heidelberg New York.

Saltzberg, M. A., Bors, S. L., Bergna, H., Winchester, S. C. (1992): Synthesis of chemically stabilized cristobalite. *J. Am. Ceram. Soc.*, **75**, 89-95.

Schmahl, W. (1993): A thermal transformation behaviour and thermal hysteresis at the SiO_2-α/β-cristobalite phase transition. *Eur. J. Mineral.*, **5**, 377-380.

Schneider, H. (1990) Transition metal distribution in mullite. *Ceram. Trans.* **6** (Mullite Mullite Matrix Compos.), 135-157.

Wyckoff, R. W. G. (1925): Die Kristallstruktur von beta-Cristobalit SiO_2. *Z. Krist.*, **62**, 189-200.

Zöller, M. H. (1994): Einkristalluntersuchungen an $1M$- und $2M_1$-Illiten durch konvergente Elektronenbeugung. PhD thesis, University of Bremen, Germany.

Part II Experimental and analyses

All brick burning experiments were performed with one kind of raw clay material which was provided by Ziegelwerk Grehl, Humlangen. Several clays were analyzed and one was selected which represented a common composition for brick manufacturing.

The clay was ground by hand in an agate mortar. Great care was bestowed on this process as clay minerals, e. g. kaolinite, are very sensitive to grinding. Kristóf et al. (1993) described altered behavior of mechanically treated kaolinite during annealing processes.

The raw clay material was mixed with several heavy metal compounds (for detailed description see *Publications*). First studies showed that a special oven and equipment is necessary for the annealing experiments. In a usual laboratory kiln the corundum furnishing is contaminated by volatile heavy metal compounds. In this study, a tube furnace was used instead. The corundum furnishing was protected by a silica glass tube. Silica glass boats containing the reactants were positioned in the glass tube (see Part III: *Publications: Phase reactions in the brick firing process of V-doped clay,* Fig. 2). The detailed reaction conditions are discussed in the "Experimental" sections of the publications (Part III).

X-ray powder diffraction patterns were recorded of all samples. The analysis of powder diffraction patterns yields detailed information on the phase composition of a sample. Furthermore, quantitative analyses in multi-phase systems are possible. In this study, the Rietveld method was used for refinement and quantification. For this purpose, XRD patterns are simulated based on crystal structure data. These calculated patterns are refined and fitted to measured data. However, determination and simulation of clay minerals remains difficult. Disordered structures, mixed layers and a small particle size cause anisotropic peak broadening in XRD patterns. These are difficult to fit even with excellent structure data. But,

furthermore, chemical and crystal structure models of clay minerals are often insufficient. Due to the great variety in chemical composition a standardized structure model cannot fit the varying appearance of a clay mineral, e.g. illite, in powder diffraction patterns. However, the refinements are sufficient for a semiquantitative description of the mineral composition in the raw material, and, following the aim of these studies, for the interpretation of the reaction sequences during heating.

Further data were obtained by chemical analyses using X-ray fluorescence spectroscopy (XRF). Infrared (IR) and Nuclear Magnetic Resonance (NMR) spectroscopy yielded informations on the incorporation of foreign cations in cristobalite. Analytical Transmission Electron Microscopy (ATEM) was performed to investigate the incorporation of foreign cations in mullite.

In completion of the experiments concerning the reaction sequence, leaching tests of the final products were performed. Deviating from the DEV S4 norm we tested leaching behavior under acidic, neutral, and alkaline pH conditions.

DEV S4 DIN 38414 Teil 4 (1984): Deutsche Einheitsverfahren zur Wasser-, Abwasser- und Schlammuntersuchung, Schlamm und Sedimente (Gruppe S), Bestimmung der Eluierbarkeit mit Wasser (S4), Beuth-Verlag Berlin.

Kristóf, E., Juhász, A. Z., Vassányi, I. (1993): The effect of mechanical treatment on the crystal structure and thermal behavior of kaolinite. *Clays and Clay Minerals*, **41**, 609-612.

Crystallization of cristobalite and tridymite in the presence of vanadium

Petra Bruhns and Reinhard X. Fischer

Fachbereich Geowissenschaften der Universität, Klagenfurter Straße,

D-28359 Bremen, Germany

Abstract

The formation of cristobalite and tridymite compounds is described in the system SiO_2-V_2O_5-M_2CO_3 (M=Na,K). A number of syntheses was performed with various vanadium concentrations at annealing temperatures between room temperature and 1000° C. The crystallization of cristobalite occurs at much lower temperatures (about 800° C) in the presence of vanadium than observed in the pure silica system which stays amorphous in this temperature range. With increasing amounts of vanadium, the crystallization of sodium or potassium vanadates is observed along with the formation of cristobalite and tridymite. XRD, IR, and NMR results indicate that cristobalite is formed by catalytic processes in presence of vanadium without V-substitutions in its structure. Variations in the thermal behavior of cristobalite are attributed to different states of crystallinity.

Keywords

Cristobalite, vanadium, tridymite, XRD, IR, NMR

Introduction

Preliminary investigations (Bruhns & Fischer, 1998) of brick stone burning processes from V-doped clay showed that the reaction paths differ significantly from the phase formations in undoped clays. Crystallization of cristobalite and mullite is observed at 800° C, far below their ususal formation in brick stones. Under normal conditions cristobalite, the high form of SiO_2, is stable between 1470° C and the melting point. It undergoes a phase transition in the range between 180° and 270° C from the high-β-form in space group $Fd\bar{3}m$ with unit cell parameter a = 7.12 Å (Wyckoff, 1925) to the metastable low-α-form in space group $P4_12_12$ with a = 4.9709 Å and c = 6.9278 Å at room temperature (Pluth *et al.*, 1985). This β→α phase transition is reversible and the exact temperature depends on the crystallinity of the sample (Perrotta *et al.* 1989). Well crystallized cristobalites show higher transition temperatures than poorly crystallized samples. Roy & Roy (1964) showed that additives in the synthesis of cristobalite, as e.g. $NaAlSiO_4$, lower the cristobalite inversion temperature and minimize the hysteresis effect between heating and cooling.

As described by Flörke (1955), cristobalite formation and its phase transition temperature are dependent on cationic impurities, especially alkali ions. Buerger (1948, 1954) defined the so-called "stuffed" derivatives of silica structures: a certain amount of Si^{4+} is replaced by atoms of lower valence, e. g. Al^{3+}. Charge compensation is achieved by incorporation of additional cations, e. g. Na^+.

Perrotta *et al.* (1989a, 1989b) synthesized β-cristobalite by stabilizing the structure with Na^+ and Ca^{2+} at temperatures between 850° C and 1400° C from sol-gel or zeolite precursors.

Saltzberg *et al.* (1992) describe the synthesis of chemically stabilized β-cristobalite (CSC) from a dried and calcined sol with chemical compositions $Si_{1-x}Al_x M^{n+}_{x/n} O_2$ with M = Na^+, K^+, Li^+, Mg^{2+}, Ca^{2+}, Sr^{2+},Ba^{2+}, Zn^{2+} and La^{3+}. It is shown that very low doping levels of Ca^{2+} ($x < 0.02$) form mixtures of quartz and α-cristobalite, x between about 0.02 and 0.04 yields pure CSC, and with higher amounts anorthite reflections are determined in the diffraction patterns. Experiments with other dopants show the relation between ionic radii and the formation of CSC: only in the systems containing Na^+, Ca^{2+}, and Sr^{2+} with ionic radii between 1.00 Å and 1.18 Å CSC is stabilized in significant amounts.

Thomas *et al.* (1994) used a gel-synthetic route according to Perrotta *et al.* (1989a) heating the samples between 900° C and 1200° C for 18 to 24 hours. Na^+, Ca^{2+}, Sr^{2+}, and Cu^{2+} are used as dopants. From ^{27}Al MAS NMR and ^{29}Si MAS NMR spectra of the Ca^{2+}-stabilized samples a random substitution of Al^{3+} for Si^{4+} with Ca^{2+} occupying adjacent cavities is considered.

Monrós *et al.* (1990b) investigated the system SiO_2-V_2O_5. All their samples were prepared by colloidal gel and ceramic methods. For the ceramic synthesis NH_4VO_3 and industrial-quality quartz were milled and fired in alumina crucibles at temperatures between 650° C and 1300° C. The first appearance of a cristobalite phase, identified as low-cristobalite, is determined at a temperature of 900° C after 3 days, completely crystallized at about 1100° C after 12 h. In samples prepared by gel synthesis the first appearance of cristobalite can be observed at 800° C and 12 h heating time. Infrared spectra showed no evidence of Si-O-V bonds, though semi-quantitative analyses (EDXA) detected cristobalite crystals containing vanadium, possibly as a solid solution.

Cristobalite is known to contain tridymitic stacking faults. In powder diffraction

patterns a broad "hump" is observed at about 20.7° 2θ. The formation of tridymite depends on incorporation of impurities (Flörke, 1955) and it exhibits several phase transitions (Wennemer & Thompson, 1984; Pryde & Dove, 1998). Three phases are stable at room temperature: A monoclinic form, space group *Cc* (Dollase & Baur, 1976), a second monoclinic, so-called MX-1 with incommensurate superstructure (Graetsch & Topalovic-Dierdorf, 1996), and a triclinic one, space group *F1*, described by Konnert & Appleman (1978).

The aim of this work is the description of cristobalite and tridymite formation upon addition of V_2O_5. In order to reduce the parameters influencing the complex phase formations in the clay system, we have performed experiments with synthetic precursor materials.

Experimental

(1) Syntheses:

In order to check whether vanadium is directly incorporated into the structure of cristobalite, various syntheses are performed. Precursor phases are selected based on the assumption that V either replaces Si in the framework charge compensated by alkaline ions or it provides charge compensation for Al^{3+} substituting Si^{4+}.

The first batch (I) contains SiO_2 (Aerosil, Degussa), V_2O_5 (Merck), and $Al(OH)_3$ (Fluka). According to the composition $Si_{1-x}Al_x V^{n+}_{x/n} O_2$ based on the hypothesis that silicon may be replaced by aluminum with vanadium cations for charge compensation. Another system (II) containing SiO_2, V_2O_5, and K_2CO_3 (Riedel-de Haën) is synthesized following the stoichiometry $Si_{1-x}V_xK_xO_2$. It is based on the assumption that silicon is replaced by vanadium with potassium cations for charge compensation. Vanadium needs to change its valence during the reaction process from V^{5+} to V^{3+}. A third system (III) with a composition

according to $Si_{1-x}V_xNa_xO_2$ was studied as well.

Syntheses were performed with various fractions in the interval $0.01 \leq x \leq 0.05$. Additional samples were prepared with vanadium excess according to the composition $Si_{0.85}V_{0.15}Na_{0.15}O_2$.

The starting materials were mixed and homogenized in an agate mortar. The mixtures were pressed to pellets of 13 mm diameter for the annealing experiments. The pellets were heated between 200° and 1000° C with a heating rate of 200° C/h in a tube furnace. The corundum material of the furnace is protected by a quartz glass tube from contamination with vanadium.

(2) X-ray powder diffraction (XRD)

XRD patterns were recorded with a Philips PW 3050 powder diffractometer with $CuK_{\alpha 1}$ radiation from a primary monochromator. Data were collected at room temperature with fixed slit configuration in the range between 5° and 120° 2θ with steps of 0.02° 2θ. All refinements and quantitative analyses were performed with the Philips PC-Rietveld plus program package (Fischer *et al.*, 1993).

(3) X-ray fluorescence spectroscopy (XRF)

Chemical analyses were performed using a Philips 1404 X-ray fluorescence spectrometer at the institute of mineralogy, university of Mainz. It was calibrated with SiO_2 (quartz), V_2O_5, Al_2O_3, and Na_2CO_3 standards.

(4) Magic angle spinning nuclear magnetic resonance spectrometry (MAS NMR)

^{23}Na and ^{51}V MAS NMR spectra were carried out on a Bruker spectrometer CXP-300 upgraded with a TECMAG pulse programmer and data acquisition system at the university of

Münster. The resonance frequencies for ^{51}V and ^{23}Na were 78.9 and 79.4 MHz, respectively. Spectra were recorded at a spinning speed of 15 KHz with pulse length 0.5 μs and relaxation delay of 0.2 s for ^{51}V MAS NMR. Acquisition parameters for ^{23}Na MAS NMR were pulse length 1 μs and relaxation delay 0.2 s.

(5) Infrared spectroscopy (IR)

IR spectra were recorded with a Biorad STS 60 A spectrometer at the institute of physical chemistry, university of Bremen. An amount of 1 mg of the sample was homogeneously mixed with 200 mg KBr and pressed to a pellet. A pure KBr pellet was prepared as standard. Spectra were compared with pure cristobalites synthesized and provided by W. Schmahl, university of Tübingen.

(6) Differential thermal analysis (DTA) and thermogravimetry (TG)

Differential thermal analyses were performed using a Netzsch Simultan Thermo Analyse Modell 429. Samples were heated with 1° C/min and cooled with the same rate. Al_2O_3 was used as reference material.

Results

Samples admixed with the alkalis react to form cristobalite, well crystallized at 800° C (Fig. 1). Upon increasing amounts of vanadium, the formation of additional phases is observed.

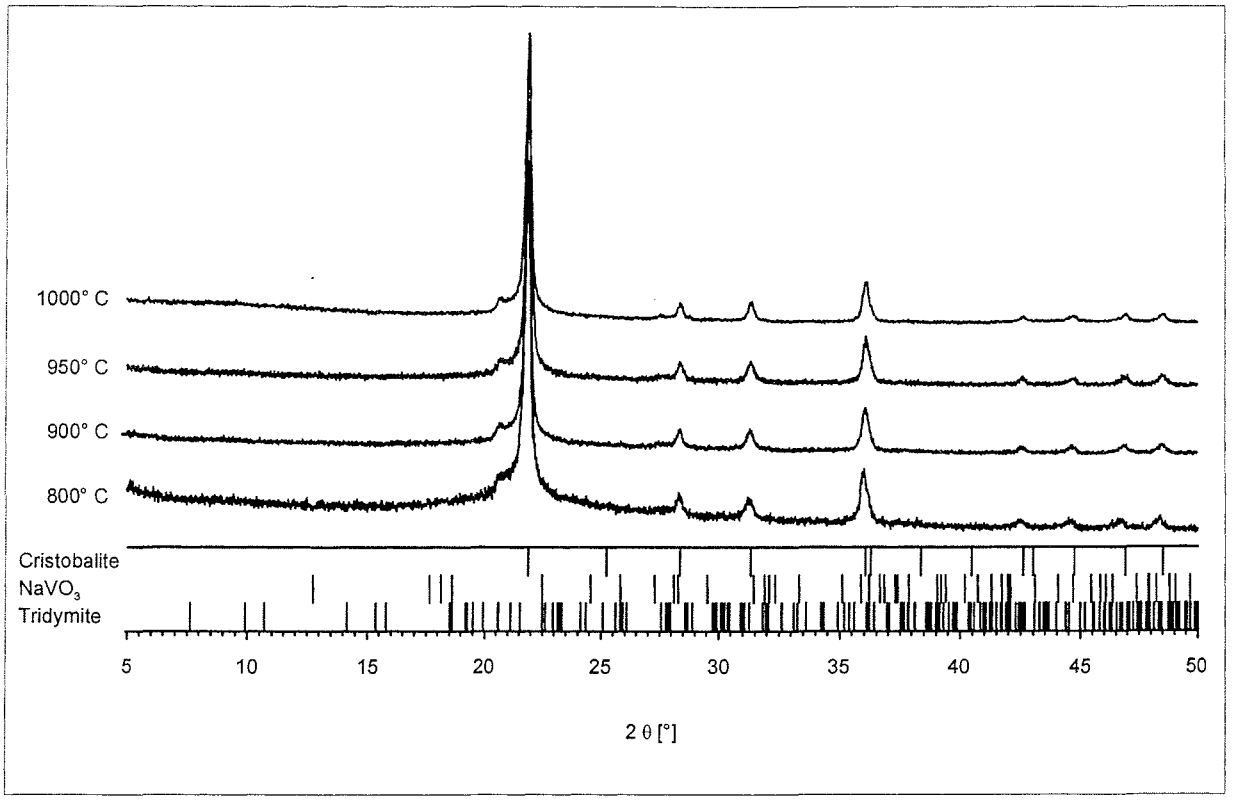

Fig. 1: Powder diffraction patterns of the sample $Si_{0.99}V_{0.01}Na_{0.01}O_2$ in the temperature range between 800° and 1000° C

The first series of samples (I) with varying amounts of potassium in the compositional range $Si_{1-x}V_xK_xO_2$ ($0.01 \leq x \leq 0.05$) was annealed at 1000° C. The phase formations are shown in Fig. 2. Cristobalite is observed as the main component. The shoulder at the low 2θ side of the main cristobalite peak is assigned to a tridymite phase. At higher potassium concentrations, additional tridymite peaks are observed at 23.7° and 27.2° 2θ. The assignment was confirmed by Rietveld simulations based on the triclinic structure in space group *F1* (Konnert & Appleman, 1978). Additional peaks in the powder diagrams of samples with higher amounts of potassium are assigned to $K_3V_5O_{14}$ (Bystroem & Evans, 1959).

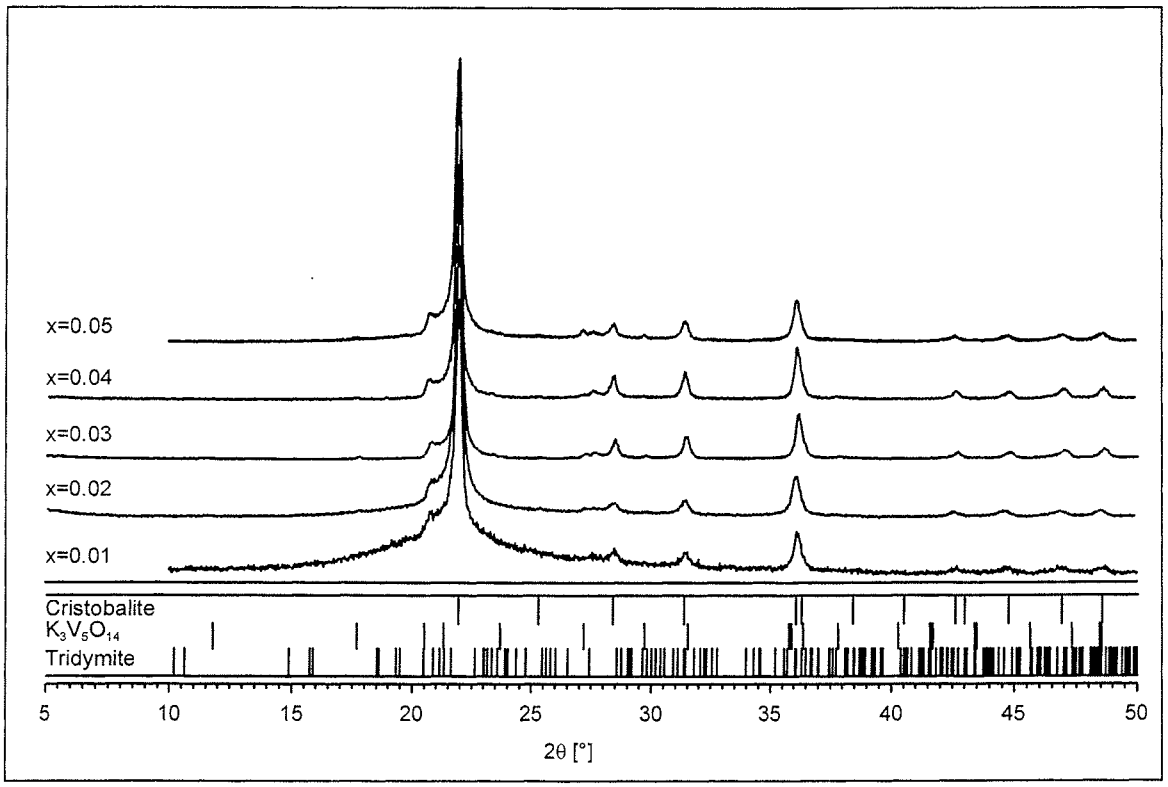

Fig. 2: Powder diffraction patterns of the sample $Si_{1-x}V_xK_xO_2$ with $0.01 \leq x \leq 0.05$ annealed at 1000° C

Similar experiments were performed with the sodium containing samples (II) corresponding to the bulk chemical composition of $Si_{1-x}V_xNa_xO_2$ with $0.01 \leq x \leq 0.05$. Fig. 3 shows the powder diagrams with varying amounts of sodium annealed at 1000° C. The main component consists of cristobalite. Towards higher Na concentrations, additional peaks are observed assigned to tridymite and $NaVO_3$. All phases exhibit higher crystallinities than the corresponding potassium samples as expressed by the relatively sharp peaks even for tridymite. Recalling that the aim of this study is to provide data for the interpretation of the complex reactions of V-doped clay, it is a crucial point to characterize the crystal chemical behavior of vanadium. Especially the occurrence of $NaVO_3$ which is soluble in water indicates that vanadium would not be immobilized under normal environmental conditions for brick stones. The question remains whether cristobalite is chemically stabilized by V incorporation or if its crystallization is just catalytically supported.

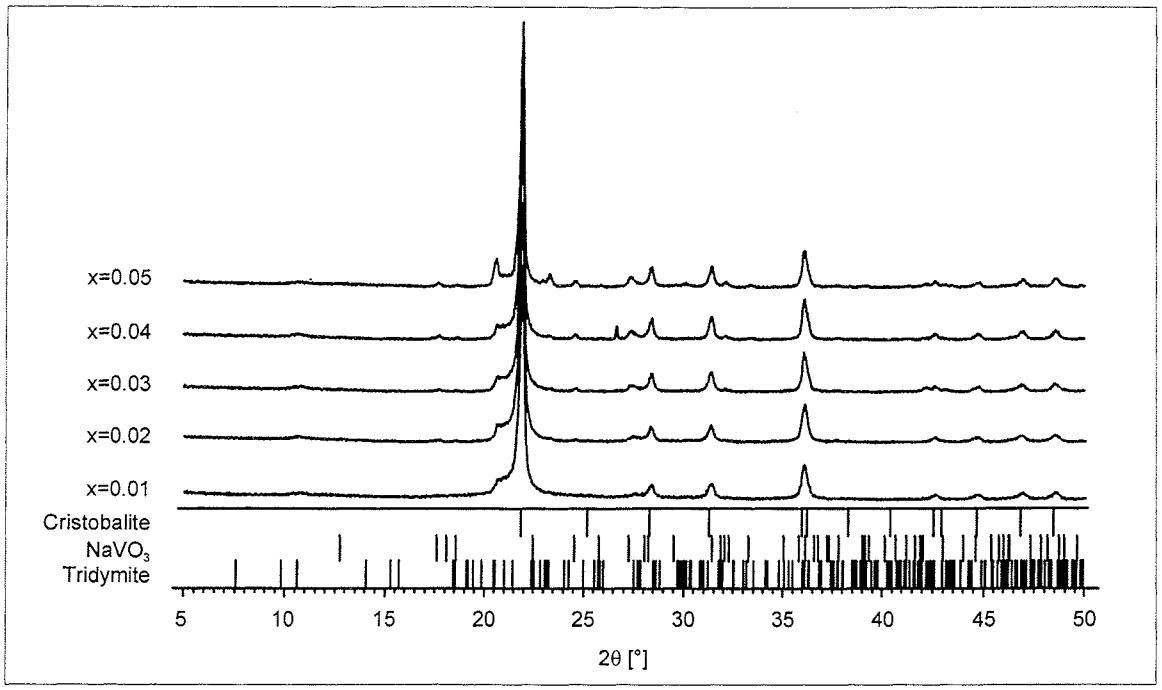

Fig. 3: Powder diffraction patterns of the sample $Si_{1-x}V_xNa_xO_2$ with $0.01 \leq x \leq 0.05$ annealed at 1000° C

DTA, IR, and NMR experiments were performed to yield some clues to this point. The results were compared with reference samples of cristobalite obtained from W. Schmahl (Tübingen) and $NaVO_3$ synthesized in the present work.

Lattice constant refinements for cristobalite did not show significant deviations from expected values. However, the quality of the X-ray diffraction data might not be sufficient to imply that vanadium has not entered the cristobalite structure. IR spectroscopy is less affected by crystallinity effects. In Fig. 4, the IR spectrum of the vanadium doped sample with bulk chemical composition $Si_{0.99}V_{0.01}Na_{0.01}O_2$ is compared with the spectrum of the reference cristobalite. Both spectra agree with values given by Farmer (1974) for pure cristobalite. The characteristic bands at 490, 515, 623, 795, 1095, 1160, and 1202 cm^{-1} are observed without significant shifts.

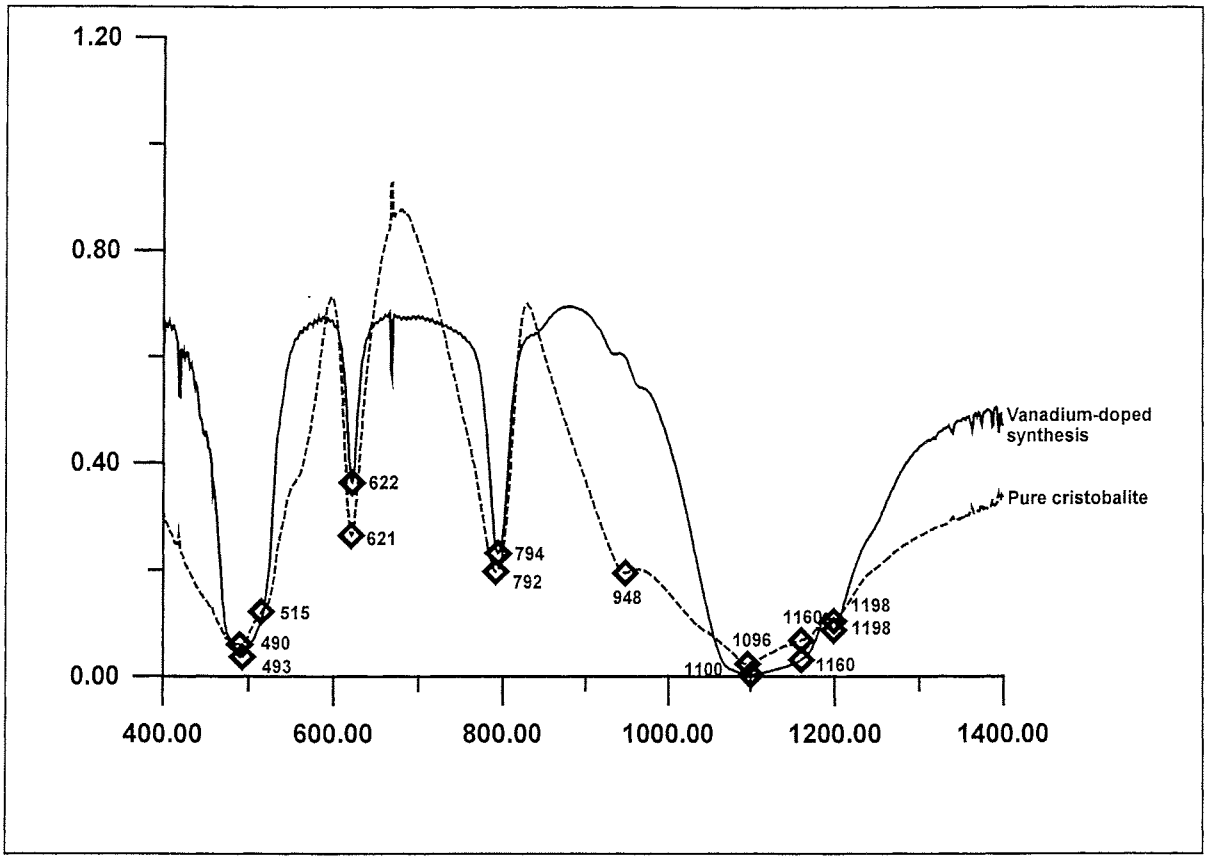

Fig. 4: Infrared spectrum of the sample $Si_{0.99}V_{0.01}Na_{0.01}O_2$ annealed at 1000° C in comparison with the spectrum of pure cristobalite

In addition to these characteristic bands the spectra of samples containing vanadium and sodium show additional bands at 693, 839, 912, 937, and 962 cm^{-1}. These bands can be assigned to $NaVO_3$ as derived from Fig. 5 which shows the two spectra of the vanadium doped sample and the synthetic $NaVO_3$.

The ^{23}Na and ^{51}V MAS NMR results indicate that the crystallization of $NaVO_3$ starts already at low vanadium concentrations not observable in the X-ray diagrams. The NMR analysis yields signals which are characteristic for the sodium vanadate without any indication for Si-V^{5+} interactions. ESR studies showed that vanadium in its V^{4+} valence is not present. However, V^{3+} is not active in NMR and, consequently, a V^{3+} incorporation in cristobalite could not be analyzed.

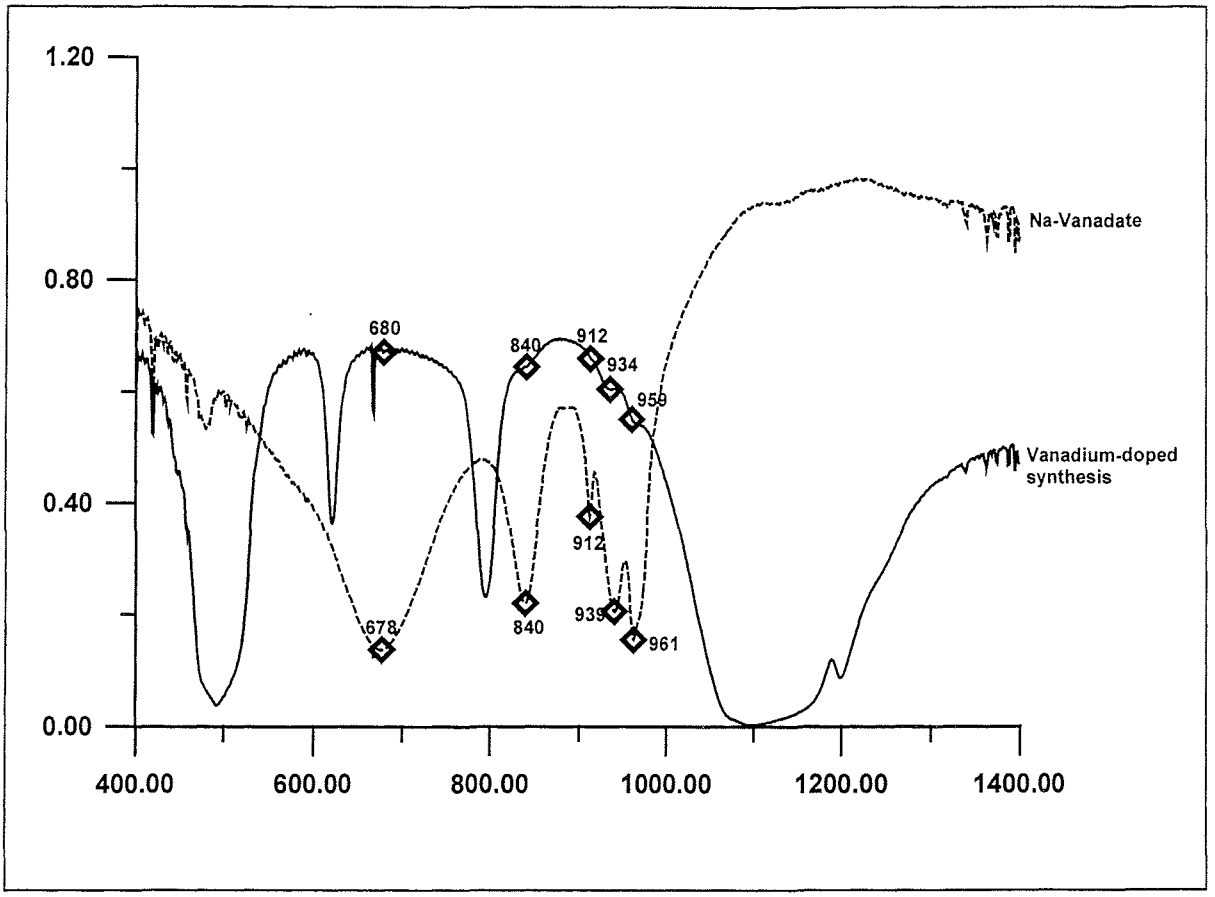

Fig. 5: Infrared spectrum of the sample $Si_{0.99}V_{0.01}Na_{0.01}O_2$ annealed at 1000° C in comparison with the spectrum of sodium-vanadate

DTA is an additional method for material characterization. Analysis of the reference cristobalite yielded the transition point at 250° C upon heating and 232° C upon cooling as commonly observed (Schmahl, 1993; Schmahl *et al.*, 1992). In contrast to that, a transition temperature of 207° C without hysteresis between heating and cooling can be inferred from the DTA studies of the V-doped sample (Tab. 1). The exact temperature of the α-β transition of cristobalite depends on the crystallinity of the sample. Well-ordered material transforms at higher temperatures than less-ordered specimens (Flörke, 1956; Leadbetter & Wright, 1976).

	Transition temperature [° C]	
	Heating	Cooling
Cristobalite (provided by W. Schmahl)	250	232
$Si_{0.85}V_{0.15}Na_{0.15}O_2$ (white)	246	230
$Si_{0.85}V_{0.15}Na_{0.15}O_2$ (brown)	245	232
$Si_{0.99}V_{0.01}Na_{0.01}O_2$	207	207

Tab. 1: Transition temperatures of cristobalite syntheses

Flörke (1955) and Roy & Roy (1964) point out that impurities in cristobalite lower the α-β transition temperatures and reduce the hysteresis effects. We observe that the thermal effects change upon increasing vanadium concentration until they adapt more or less the thermal parameters observed for pure cristobalites. However, since there is no indication for a chemical stabilization of cristobalite from the XRD, IR, and NMR results, we assume that the changes in the thermal behavior are caused by crystallinity effects and not by the formation of a V-doped cristobalite.

Samples (III) with high amounts of vanadium corresponding to bulk chemical composition $Si_{0.85}V_{0.15}Na_{0.15}O_2$ conform to this observation. The α-β transition is detected at about 246° C upon heating and the reverse transformation at about 231° C upon cooling (Tab. 1). We assume that vanadium is not incorporated in the structure, but acts as a catalyst to yield a cristobalite phase of better crystallinity. However, the annealed sample consists of two clearly separated parts distinguished by their white and brown colors.

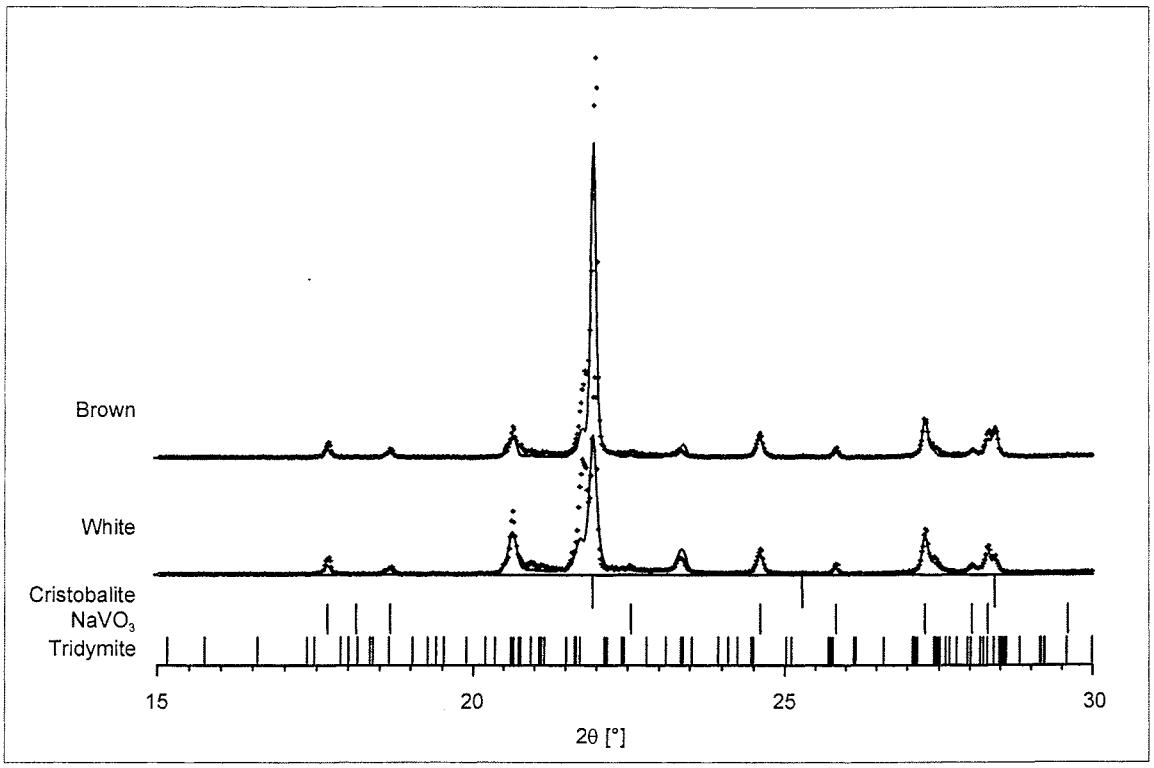

Fig. 6: Powder diffraction patterns of the brown and white parts of the sample $Si_{0.85}V_{0.15}Na_{0.15}O_2$ annealed at 1000° C

The white and brown bodies were investigated separately. X-ray diffraction analyses reveal two main peaks at d = 4.076 Å and d = 4.046 Å which correspond to values observed by Butler & Dyson (1997) for two different forms of cristobalites in devitrified aluminosilicate ceramic fibres. They assume that the peak at the higher angle belongs to the pure α-cristobalite and the low angle peak to an α'-form representing a defect form or a cation substituted form of cristobalite. Similar effects are described by Madsen *et al.* (1991) who observed the simultaneous formation of three cristobalite forms in brick stones. They propose that one phase is formed from quartz and the other one crystallizes from kaolin, presumably with cation substitutions. Since we do not observe further peaks in the X-ray patterns (Fig. 6) at d = 2.506 Å, d = 2.494 Å, and d = 2.038 Å as found by Butler & Dyson, the formation of an α'-cristobalite in our samples is rather unlikely. Furthermore, the IR-spectra (Fig. 7) of the differently colored parts of our sample do not deviate from typical spectra of pure SiO_2 cristobalites.

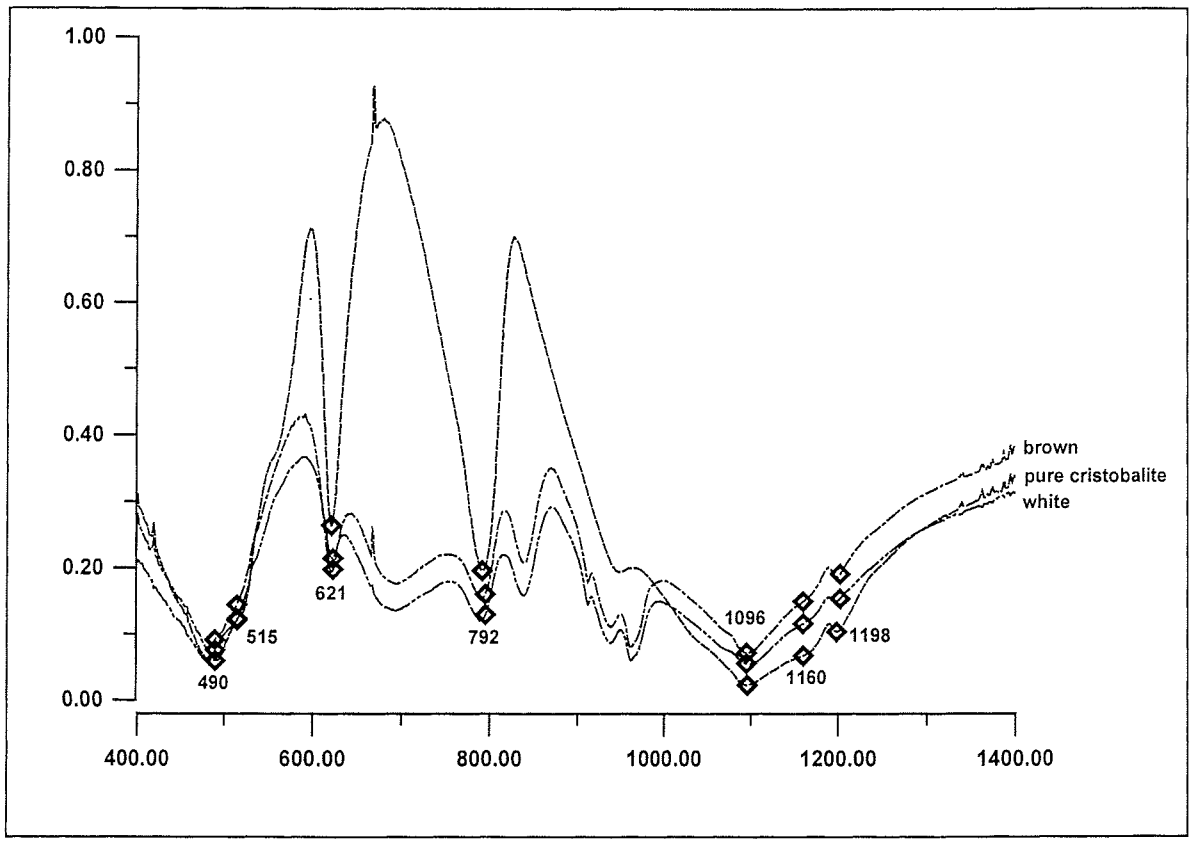

Fig. 7: Infrared spectrum of the brown and white bodies in sample $Si_{0.85}V_{0.15}Na_{0.15}O_2$ annealed at 1000° C in comparison with the spectrum of pure cristobalite

As Butler & Dyson (1997) observe just one transition point upon heating at 220° C and no effect upon cooling, this cristobalite phase differs significantly from the one synthesized in our samples.

Powder diffraction patterns (Fig. 6) of the V-doped samples studied here show additional strong peaks at d = 4.30 Å and 3.81 Å which could be assigned to tridymite although the intensity of the strongest reflection is calculated too low in the Rietveld refinement. However a tridymite formation is still the best interpretation of the powder diffraction patterns most pronounced in the white part of the sample. All remaining peaks can be assigned to $NaVO_3$.

Conclusion

The crucial point in this study is the interpretation of the cristobalite formation which could be attributed to vanadium incorporation in its structure forming a substituted or stuffed derivative of SiO_2, or it could be described by a catalytically supported reaction in the presence of vanadium. The lattice constants determined in the XRD analyses do not differ from values of pure SiO_2, the IR spectra are nearly identical with the spectra of pure cristobalite, and NMR spectra do not give any indication for V substitutions in cristobalite. Just the thermal behavior of cristobalite in some of the samples deviates from the thermal properties of well crystallized and pure cristobalites. We infer from these results that cristobalite crystallizes in various states of crystallinity without direct participation of vanadium as a substituent. However, tridymite could be chemically stabilized by vanadium or alkaline cations. Its occurrence is directly related to the amount of vanadium and sodium with highest fractions in the sample with the high V/Na concentration. Vanadium, added as V_2O_5, reacts to $NaVO_3$ and $K_3V_5O_{14}$. Small amounts of the sodium vanadate are already detected by NMR analyses in samples which do not show corresponding peaks in their XRD patterns. We propose that the formation of alkali vanadates is favored over a silicatic immobilization in the SiO_2 phases.

Acknowledgements

Financial support is gratefully acknowledged from the Zentrale Kommission des Akademischen Senats für Forschungsplanung und wissenschaftlichen Nachwuchs (FNK). Pure cristobalite specimens were kindly provided by W. Schmahl (Bochum). H. Eckert, M.

Hengelbrock and L. van Wüllen (Münster) are acknowledged for performing and discussing the MAS NMR measurements, and N. Groschopf (Mainz) for XRF analyses. We thank the Institute of Physical Chemistry (Bremen) for providing access to the infrared spectrometer.

References

Alcalá, M. D., Real, C., Criado, J.M. (1996): A new "incipient-wetness" method for the synthesis of chemically stabilized β-cristobalite. *J. Am. Ceram. Soc.*, **79**, 1681-1684.

Barth, T. F. W., Posnjak, E. (1932): Silicate structures of the cristobalite type: I. The crystal structure of α-carnegieite ($NaAlSiO_4$). *Z. Krist.*, **81**, 135-141.

Barth, T. F. W., Posnjak, E. (1932): Silicate structures of the cristobalite type: II. The crystal structure of Na_2CaSiO_4. *Z. Krist.*, **81**,370-375.

Barth, T. F. W., Posnjak, E. (1932): Silicate structures of the cristobalite type: III. Structural relationship of high-cristobalite, α-carnegieite, and Na_2CaSiO_4. *Z. Krist.*, **81**,376-385.

Bruhns, P., Fischer, R. X. (1998): Die Bildung von V-stabilisierten SiO_2-Phasen beim Ziegelbrand von Tonen. Tagungsband 3. Symposium Technische und Angewandte Mineralogie.

Buerger, M. J. (1948): Crystals based on the silica structures. *Am. Min.*, **33**, 751-752.

Buerger, M. J. (1954): The stuffed derivatives of the silica structures. *Am. Min.*, **39**, 600-614.

Butler, M. A., Dyson, D. J. (1997): The quantification of different forms of cristobalite in devitrified alumino-silicate ceramic fibres. *J. Appl. Cryst.*, **30**, 467-475.

Bystroem, A. M., Evans, H. T. (1959): The crystal structure of $K_3V_5O_{14}$. *Acta Chem. Scan.*, **13**, 377-394.

Dollase, W. A. (1965): Reinvestigation of the structure of low cristobalite. *Z. Krist.*, **121**, 369-377.

Dollase, W. A., Baur, W. H. (1976): The superstructure of meteoritic low tridymite solved by

computer simulation. *Am. Min.*, **61**, 971-978.

Downs, R. T., Palmer, D. C. (1994): The pressure behaviour of a α cristobalite. *Am. Min.*, **79**, 9-14.

Fischer, R. X., Lengauer, C., Tillmanns, E., Ensink, R. J., Reiss, C. A., Fantner, E. J. (1993): PC-Rietveld Plus, a comprehensive Rietveld analysis package for PC. *Mater. Sci. Forum*, **133-136**, 287-292.

Flörke, O. W. (1955): Strukturanomalien bei Tridymit und Cristobalit. *Ber. deut. keram. Ges.*, **32**, 369-81.

Flörke, O. W. (1957): X-ray mineral analysis and thermal expansion behavior of cristoblite and tridymite and the composition of silica materials. *Ber. Dtsch. Keram. Ges.*, **34**, 343.

Flörke, O. W. (1961): A discussion of the tridymite-cristobalite problem. *Silic. Ind.*, **26**, 415.

Graetsch, H., Topalovic-Dierdorf, I. (1996): ^{29}Si MAS NMR spectrum and superstructure of modulated tridymite L3-T_O(MX-1). *Eur. J. Mineral.*, **8**, 103-113.

Hatch, D. M., Ghose, S. (1991): The α-β phase transition in cristobalite, SiO_2: Symmetry analysis, domain structure, and the dynamical nature of the β-phase. *Phys. Chem. Miner.*, **17**, 554-562.

Heaney, P. J. (1994): Structure and chemistry of the low-pressure silica polymorphs. *Rev. Mineral.*, **29** (SILICA), 1-40.

Hill, V. G., Roy, R. (1958): Silica structure studies: V, the variable inversion in cristobalite. *J. Am. Ceram. Soc.*, **41**, 532-537.

Hua, G. L., Welberry, T. R., Withers, R. L., Thompson, J. G. (1988): An electron diffraction and lattice-dynamical study of the diffuse scattering in β-cristobalite, SiO_2. *J. Appl. Cryst.*, **21**, 458-465

Kato, K., Takayama, E. (1984): Das Entwässerungsverhalten des

Natriummetavanadatdihydrats und die Kristallstruktur des β-Natriummetavanadats. *Acta Cryst.*, **B 40**, 102-105.

Konnert, J. H., Appleman, D. E. (1978): The crystal structure of low tridymite. *Acta Cryst.*, **B34**, 391-403.

Kosten, K., Arnold, H. (1980): The III-V analogues of SiO_2. *Z. Krist.*, **152**, 119-123.

Leadbetter, A. J., Wright, A. F. (1976): The α-β transition in the cristobalite phases of SiO_2 and $AlPO_4$. I. X-ray studies. *Phil. Mag.*, **33**, 105-112.

Leadbetter, A. J., Wright, A. F. (1976): The α-β transition in the cristobalite phases of SiO_2 and $AlPO_4$. II. Calorimetric studies. *Phil. Mag.*, **33**, 113-119.

Limin, Q. I., Jiming, M. A., Humin, C., Zhenguo, Z. (1996): Crystallization of sol-gel derived $PbTiO_3$-SiO_2 glass ceramics. *J. Mat. Sci. Lett.*, **15**, 1074-1076.

Madsen, I. C., Finney, R. J., Flann, R. C. A., Frost, M. T., Wilson, B. W. (1991): Quantitative analysis of high-alumina refractories using X-ray powder diffraction data and the Rietveld method. *J. Am. Ceram. Soc.*, **74**, 619-624.

Marumo, F., Isobe, M., Iwai, S. (1974): α form of sodium metavanadate. *Acta Cryst.*, **B 30**, 1628-1630.

Monrós, G., Carda, J., Escribano, P., Alarcón, J. (1990): Synthesis of V-$ZrSiO_4$ solid solutions. *J. Mat. Sci. Letters*, **9**, 184-186.

Monròs, G., Carda, J., Tena, M. A., Escribano, P., Alarcón, J. (1990): Synthesis and reactivity of cristobalite obtained from the SiO_2-V_2O_5 system. *J. Mat. Sci. Letters*, **9**, 484-488.

Nieuwenkamp, W. (1935): Die Kristallstruktur des Tief-Cristobalits SiO_2. *Z. Krist.*, **92**, 82-88.

Nieuwenkamp, W. (1937): Über die Struktur von Hoch-Cristobalit. *Z. Krist.*, **96**, 454-458.

O'Keefe, M., Hyde, B. G. (1976): Cristobalites and topologically-related structures. *Acta Cryst.*, **B32**, 2923-2936.

Palmer, D. C. (1994): Stuffed derivatives of the silica polymorphs. *Rev. Mineral.*, **29**, 83-122.

Palmer, D. C., Finger, L. W. (1994): Pressure-induced phase transition in cristobalite: An X-ray powder diffraction study to 4.4 GPa. *Am. Min.*, **79**, 1-8.

Parise, J. B., Yeganeh-Haeri, A., Weidner, D. J., Jorgensen, J. D., Saltzberg, M. A. (1994): Pressure-induced phase transition and pressure dependence of crystal structure in low (α) and Ca/Al-doped cristobalite. *J. Appl. Phys.*, **75**, 1361-1367.

Peacor, D. R. (1973): High-temperature single-crystal study of the cristobalite inversion. *Z. Krist.*, **138**, 274-298.

Perrotta, A. J., Grubbs, D. K., Martin, E. S., Dando, N. R., McKinstry, H. A., Huang, C. Y. (1989): Chemical stabilization of β-cristobalite. *J. Am. Ceram. Soc.*, **72**, 441-447.

Perrotta, A. J., Grubbs, D. K., Martin, E. S. (1989): Process for preparing stabilized high cristobalite. U.S. Pat. No. 4818729, April 4 1989.

Pryde, A. K. A., Dove, M. T. (1998): On the sequence of phase transitions in tridymite. *Phys. Chem. Miner.*, **26**, 171-179.

Rey, T. (1966): Infrared absorption of $AlPO_4$ and SiO_2 as a function of disorder and temperature. *Z. Krist.*, **123**, 253-314.

Roy, D. M., Roy, R. (1964): Tridymite-cristobalite relations and stable solid solutions. *Am. Min.*, **49**, 952-962.

Saltzberg, M. A., Bors, S. L., Bergna, H., Winchester, S. C. (1992): Synthesis of chemically stabilized cristobalite. *J. Am. Ceram. Soc.*, **75**, 89-95.

Schmahl, W. (1993): A thermal transformation behaviour and thermal hysteresis at the SiO_2-α/β-cristobalite phase transition. *Eur. J. Mineral.*, **5**, 377-380.

Schmahl, W., Swainson, M. T. D., Graeme-Barber, A. (1992): Landau free energy and order parameter behaviour of the α/β phase transition in cristobalite. *Z. Krist.*, **201**, 125-145.

Schneider, H., Flörke, W. O. (1986): High-temperature transformation of tridymite single crystals to cristobalite. *Z. Krist.*, **175**, 165-176.

Spearing, D. R., Farnan, I., Stebbins, J. F. (1992): Dynamics of the α-β phase transitions in quartz and cristobalite as observed by in-situ high temperature ^{29}Si and ^{17}O NMR. *Phys. Chem. Miner.*, **19**, 307-321.

Thomas, E. S., Thompson, J. G., Withers, R. L., Sterns, M., Xiao, Y., Kirkpatrick, R. J. (1994): Further investigation of the stabilization of β-cristobalite. *J. Am. Ceram. Soc.*, **77**, 49-56.

Welberry, T. R., Hua, G. L., Withers, R. L. (1989): An optical transform and Monte Carlo study of the disorder in β-cristobalite SiO_2. *J. Appl. Cryst.*, **22**, 87-95.

Wilson, M. J., Russell, J. D., Tait, J. M. (1974): A new interpretation of the structure of disordered α-cristobalite. *Contrib. Mineral. Petrol.*, **47**, 1.

Withers, R. L., Thompson, J. G., Welberry, T. R. (1989): The structure and microstructure of α-cristobalite and its relationship to β-cristobalite. *Phys. Chem. Miner.*, **16**, 517-523.

Wright, A. F., Leadbetter, A. J. (1975): The structures of the β-cristobalite phases of SiO_2 and $AlPO_4$. *Phil. Mag.*, **31**, 1391-1401.

Wyckoff, R. W. G. (1925): Die Kristallstruktur von beta-Cristobalit SiO_2. *Z. Krist.*, **62**, 189-200.

Phase reactions in the brick firing process of V doped clay

Petra Bruhns and Reinhard X. Fischer

Fachbereich Geowissenschaften der Universität, Klagenfurter Straße,

D-28359 Bremen, Germany

Abstract

The phase reactions of V-doped clays in brick burning processes are studied to evaluate the utilization of V-containing wastes in brickworks. V_2O_5 was admixed to clay and annealed at temperatures between 200° and 1000° C. The formation of mullite, cristobalite, and a pseudobrookite compound is observed between 700° and 800° C. These phases do not occur in pure clay annealed in the corresponding temperature range. The samples were investigated with X-ray powder diffraction methods, quantitative analyses were performed with the Rietveld method and chemical analyses with X-ray fluorescence spectroscopy. Analytical transmission electron microscopy showed incorporation of vanadium and iron in mullite.

Keywords

Brick burning, heavy metal contaminated waste, vanadium, cristobalite, mullite, X-ray powder diffraction (XRD), Rietveld analysis, Analytical Transmission Electron Microscopy (ATEM)

Introduction

Deposition of heavy metal contaminated wastes (e.g. sewage sludge, waste incinerator ashes etc.) could be avoided by immobilization of the heavy metals as constituents in mineral phases. The immobilization can be achieved by thermal treatment as described by Förstner (1995) and discussed by Margane (1992). A possible procedure would be the utilization of clay – waste mixtures in brick burning processes typically at temperatures around 1000°C . Meanwhile, the process of manufacturing bricks doped with heavy metals is already established, e.g. at Grehl brickworks in Humlangen, southern Germany. However, the formation of phases and the details of heavy metal incorporation are not known. Some indication of the brick's solubility behavior is achieved by leaching tests according to DEV S4 DIN 38414 (1984). But these tests do not explain the long term properties of the material, especially under non standard conditions in acidic or basic environments. Dondi *et al.* (1997) describe the mobilization of vanadates and chromates during firing processes. The vanadates migrate to the surface of ceramic materials in the presence of water resulting in efflorescences which affect the long term properties of the ceramic product. The solubility of vanadium increases with increasing annealing temperature.

A comprehensive crystal chemical description of the phase formations and reactions during

brick burning in the presence of heavy metals is needed for an extensive and more reliable interpretation of the complex processes. It is compared with the corresponding processes during annealing of natural clay without additives. Salmang & Scholze (1983) describe the processes of brick burning using pure clays consisting of clay minerals, feldspar and quartz. At temperatures between 500° and 700° C the dehydroxylation of the clay minerals, especially kaolinite, is observed (Bellotto *et al.*, 1995). Kaolinite transforms to metakaolinite. Last traces of -OH groups are removed and the sheet structure collapses between 800° and 950° C. Cristobalite and mullite are formed upon further heating between 1100° and 1400° (Brindley & Nakahira, 1959; Gualtieri *et al.*, 1995), according to the transformation:

$$3\ Al_2(Si_2O_5)(OH)_4 \rightarrow 3\ Al_2O_3 \cdot 2SiO_2 + 4\ SiO_2 + 6\ H_2O.$$

The formation of cristobalite upon addition of V_2O_5 is described by Bruhns & Fischer (2000). In the system SiO_2-V_2O_5-M_2CO_3 (M = Na, K), the crystallization of a cristobalite like phase starts at about 800° C. With increasing amounts of vanadium, the formation of alkali vanadates is observed. Phase diagrams of the systems SiO_2-V_2O_5 indicate partial melting at temperatures above 661° C and for Al_2O_3-V_2O_5 above 658° C (Gravette *et al.*, 1966; Barham, 1965). In the presence of a liquid phase, a higher reactivity of the system is expected and formation of cristobalite occurs in lower temperature regions.

Decomposition of illite starts at about 850° C but traces of illite are still observed up to 1000° C (Kromer & Schüller, 1974). Depending on the chemical composition of illite, a wide variety of resulting phases is possible in clay systems, e. g. hematite, corundum, feldspar, leucite, spinel etc (Jasmund & Lagaly, 1993). Mazzucato *et al.* (1999) describe the high temperature dehydroxylation of muscovite which is the K-rich mica structurally closely related to illite. A dehydroxylated phase is observed between 700° and 1000° C transforming to mullite at higher temperatures. In brick burning processes, illite acts as a flux (Salmang &

Scholze, 1983). The presence of liquid phase is important for further reactions and influences properties and quality of the burned brick. Quartz is expected to participate only in the reactions at temperatures above 1000° C.

The aim of this work is to determine the influence of vanadium on the phase reactions in brick burning processes of V-doped clay.

Experimental

(1) Sample treatment and calcination

The raw clay material used for the syntheses was provided by Ziegelwerk Grehl, Humlangen, Germany. It consists of quartz, kaolinite, illite, minor amounts of rutile and hematite, and about 17 wt.-% of amorphous phases (Figure 1) as determined by Rietveld analyses using an internal standard.

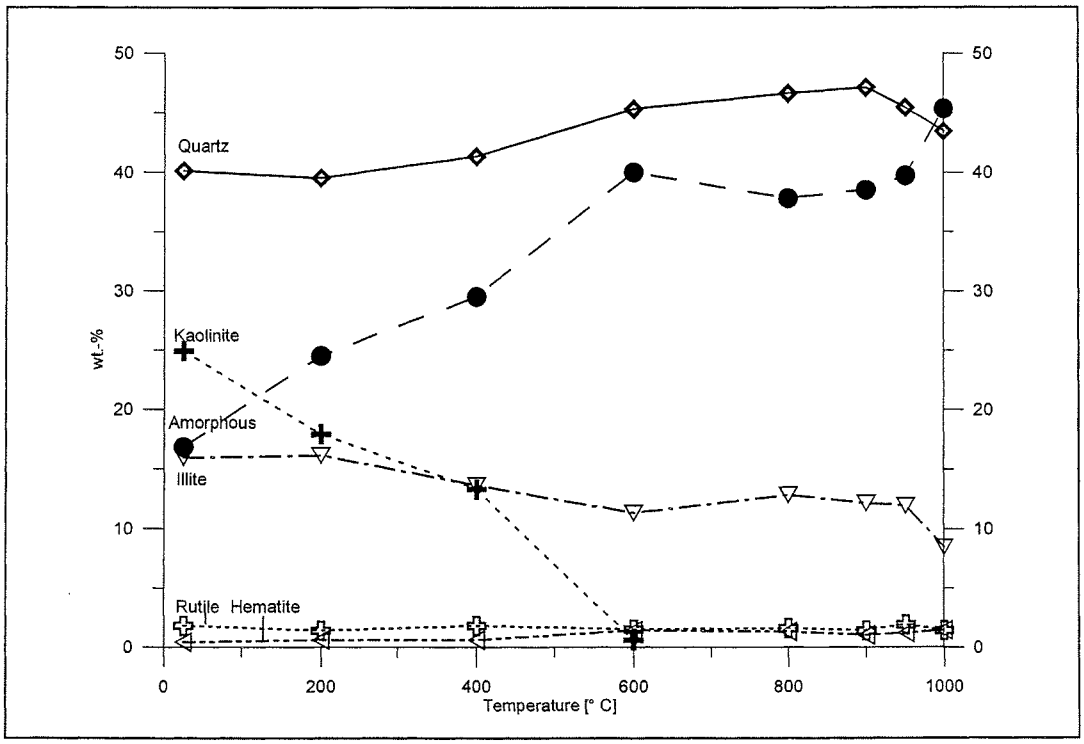

Fig. 1: Reaction sequence of pure clay; quantitative data obtained from Rietveld refinements

It was homogenized in an agate mortar and pressed to pellets of 13 mm diameter for the annealing experiments. Kaolinite is very sensitive to mechanical treatment. A destruction of the crystal structure could be caused by grinding or pressing. Kristóf *et al.* (1993) showed the influence of the amorphization of kaolinite on its thermal behavior and the formation of mullite. In this work great care was bestowed to avoid these effects as far as possible. Hand grinding up to 15 min. did not show any significant effect in powder diffraction patterns of either the raw or the annealed material.

In addition to the pure clay samples, further batches were mixed with 1, 2, and 5 wt.-% V_2O_5 and treated similarly. The experiments with addition of 5 wt.-% V_2O_5 showed the most evident mineralization effects so they are compared in the following with the pure clay samples.

For the thermal treatment of samples containing volatile vanadium compounds, special care was taken to avoid contamination of the furnace environment. Since corundum tubes and crucibles are permeable to vanadium, they are not suitable as containers for the calcination experiments. A silica glass tube (Figure 2) was used to protect the furnace from contamination. The tapering ends of the synthesis pipe allow a definite gas flow and the

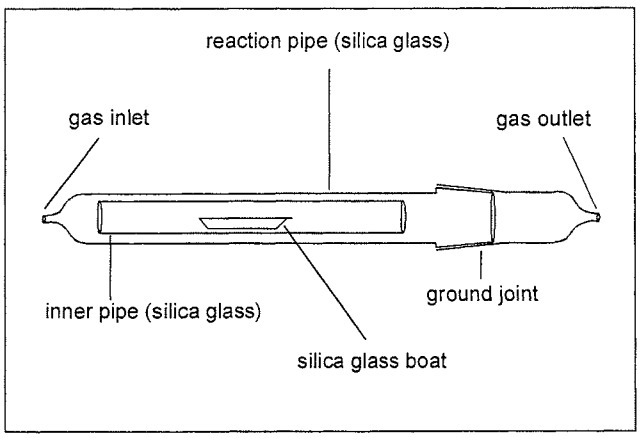

Fig. 2: Reaction tube for the syntheses. The sample is placed in a silica glass boat, within an inner glass tube. The assemblage is protected by an outer reaction pipe with gas in- and outlets. All parts are made of silica glass due its impermeability for vanadium.

adjustment of different reaction atmospheres. The following syntheses were performed under oxidizing conditions with air. The samples were prepared in silica glass boats. All samples were annealed in the range between 200° C to 1000° C for 17 h with a heating rate of 200° C/h. In the temperature range around 500° C (decomposition of kaolinite) syntheses were performed in steps of 50° C. Additionally, the specimens containing vanadium were annealed in steps of 50° C up to 800° C to describe the reaction sequence.

(2) X-ray fluorescence spectroscopy (XRF)

Chemical analyses were performed using a Philips 1404 X-ray fluorescence spectrometer at the Institute of Mineralogy, University of Mainz. The XRF analysis of the pure clay yielded weight fractions of 67.48% SiO_2, 18.84% Al_2O_3, 3.17% Fe_2O_3, 1.37% TiO_2, 0.16% CaO, 0.4 % MgO, 0.15% Na_2O, 1.72% K_2O, and 0.03% P_2O_5. The deviation to 100% was determined as weight loss due to dehydroxylation and water desorption.

(3) X-ray powder diffraction (XRD)

XRD patterns were recorded using a Philips PW 1050 powder diffractometer with secondary monochromator and a Philips PW 3050 powder diffractometer with primary monochromator. Data were collected using Cu$K_{\alpha 1}$ radiation at room temperature in the range between 5° and 120° 2θ and steps of 0.02° 2θ. All refinements were performed with the Philips PC-Rietveld plus program package (Fischer *et al.*, 1993), background values were set by hand. Quantitative analyses were performed using the scale factors from the Rietveld refinements. Amorphous fractions were determined with ZnO as internal standard. The following structure models were used for the simulation of the powder patterns: quartz by

Will *et al.* (1988), cristobalite by Pluth *et al.* (1985), kaolinite by Bish & von Dreele (1989), mullite by Ban & Okada (1992), hematite by Blake *et al.* (1966), rutile by Abrahams & Bernstein (1971), ZnO by Kisi & Elcombe (1989), V_2O_5 by Ketelaar (1936), pseudobrookite by Hamelin (1958). Input parameters for the simulation of the illite structure were taken from muscovite data determined by Richardson & Richardson (1982) which showed the best fit with the illite among all available data on muscovites. Zöller (1994) demonstrated that the structural parameters of muscovite, adapted to the illite cation distribution and optimized by distance least squares refinements, closely resembles the illite structure as analysed by electron diffraction.

Reliable structural data do not exist for illite due to its bad crystallinity and variable chemical composition in natural clay. Using data for illite based on the muscovite model recently published by Gualtieri (2000) did not improve the refinements in this work.

(4) Analytical Transmission Electron Microscopy (ATEM)

Analytical Transmission Electron Microscopy was performed at the Deutsches Zentrum für Luft- und Raumfahrt (DLR) in Köln using a Philips EM 430 analytical microscope (300 kV accelerating voltage, LaB_6 filament) equipped with a Tracor system for energy-dispersive X-ray spectroscopy.

Further studies of thin sections using a petrographic microscope failed as well as additional analyses with an electron beam microprobe. The crystallites formed in the annealing process were too small and could not be resolved by these microscopic methods.

Results

The XRD pattern of the raw clay material (Figure 3) shows a composition of quartz, rutile, hematite, kaolinite, and illite. Illite was identified as $2M_1$ polytype by its characteristic reflections at 25.3° and 27.9° 2θ which match the $(11\bar{4})$ and (114) peaks of the $2M_1$ modification (Moore and Reynolds, 1989). Weight fractions of the crystalline phases and the amorphous compound are plotted in Figure 1.

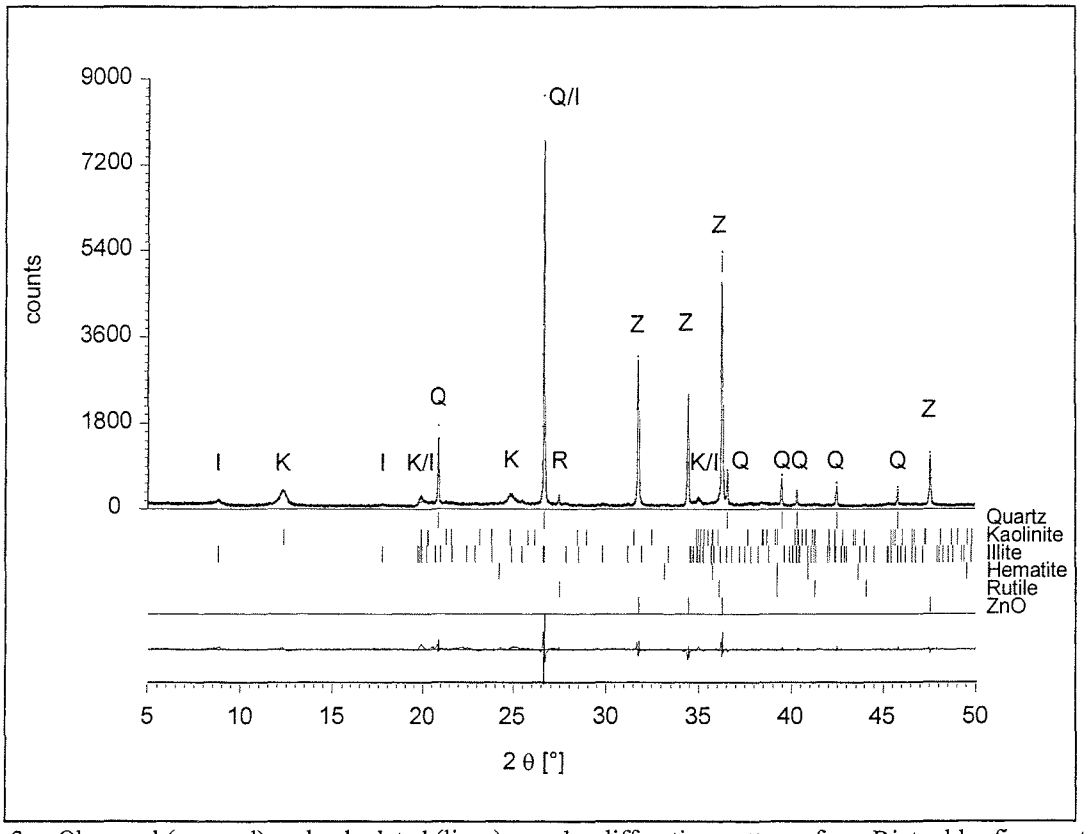

Fig. 3: Observed (crossed) and calculated (lines) powder diffraction patterns from Rietveld refinements of raw clay. Q: quartz, Z: ZnO, H: hematite, R: rutile, I: illite, K: kaolinite.

Quantification is a crucial point in multi phase analyses, especially when clay minerals are present. Possible sources of errors in quantitative Rietveld analyses are anisotropic peak broadening caused by disordered structures, incorrectly determined chemical compositions, and insufficient crystal structure models. It is expected that the effect is most pronounced for

illite and kaolinite which undergo continuous changes in the annealing process. In order to get a rough estimate of the errors, the chemical composition of muscovite, used to simulate the powder diffraction pattern of illite, has been varied between typical illite and muscovite compositions. The resulting weight fractions differed by less than 2 wt.-%, which indicates that the quantitative analyses are not much affected by using muscovite data for the simulation in lack of reliable structure models of illite. The phase formations in the pure clay material between 200° and 1000° C are shown in Figure 4 and the corresponding weight fractions of the single phases are plotted in Figure 1.

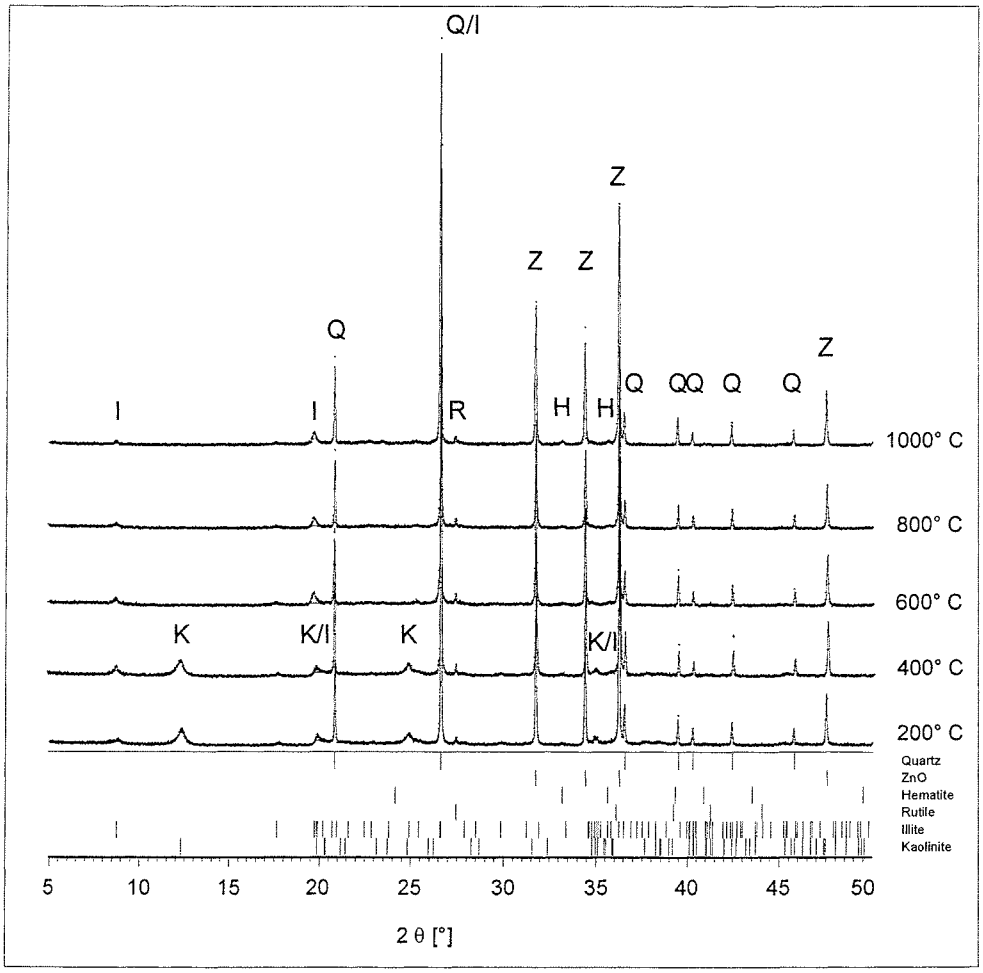

Fig. 4: Observed (crosses) and calculated (lines) powder diffraction patterns from Rietveld refinements of pure clay annealed between 200° and 1000° C. Q: quartz, Z: ZnO, H: hematite, R: rutile, I: illite, K: kaolinite.

Samples of clay mixed with V_2O_5 (5 wt-%) and heated in the range 200° C to 1000° C show different phase compositions (Figure 5).

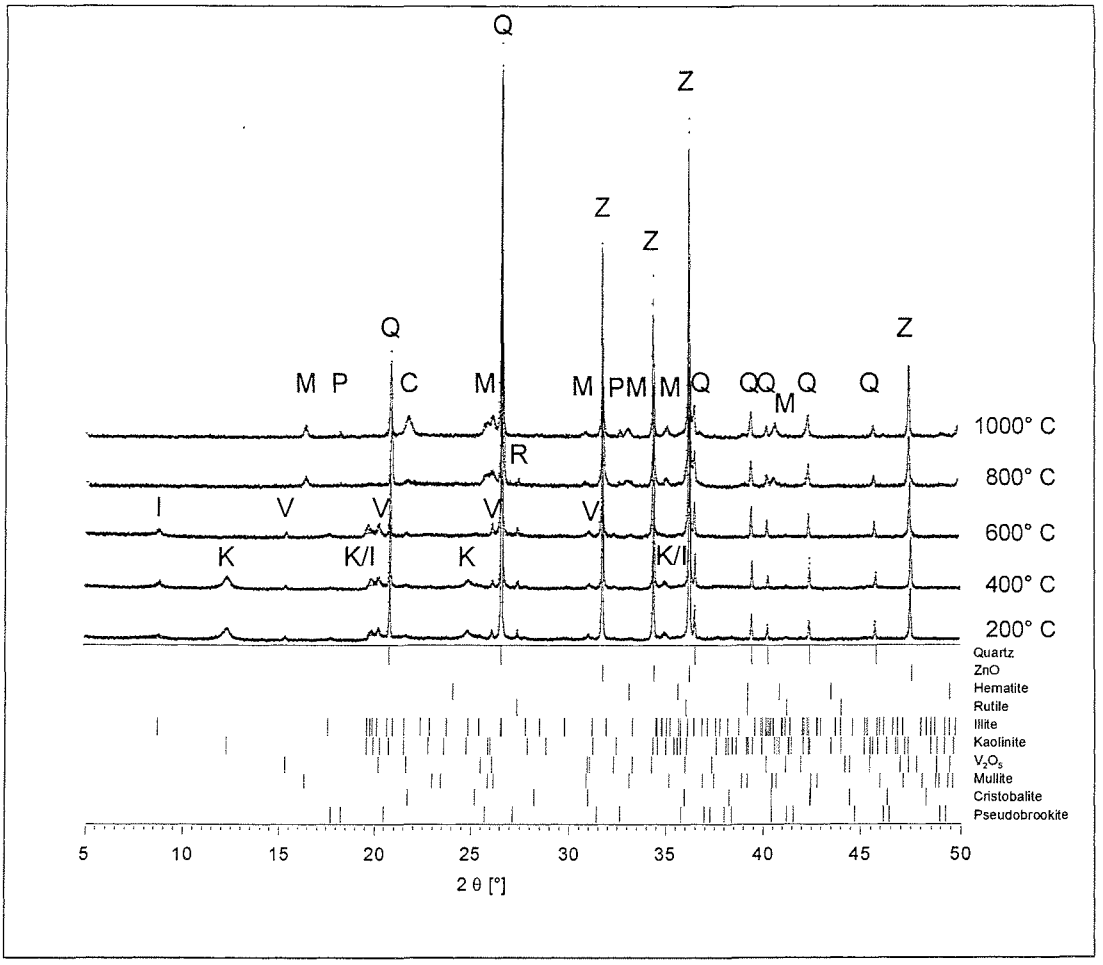

Fig. 5: Observed (crosses) and calculated (lines) powder diffraction patterns from Rietveld refinements of clay admixed with 5 wt.-% V_2O_5 annealed between 200° and 1000° C. Q: quartz, Z: ZnO, R: rutile, I: illite, K: kaolinite, V: V_2O_5, M: mullite, C: cristobalite, P: pseudobrookite.

Weight fractions of the crystalline phases and amorphous compounds as derived from the Rietveld analyses are given in Figure 6. XRF analyses proved that there is no loss of vanadium content during burning processes.

The reaction sequence up to about 700° C is similar in pure clay and in vanadium containing samples: kaolinite decomposes and then disappears above 650° C. Syntheses performed at higher temperatures reveal remarkable differences. While the mineral content in the pure clay samples remains qualitatively and quantitatively more or less stable except the decomposition

of kaolinite, it changes significantly in the V-doped samples. First traces of mullite are detected at 750° C with increasing content towards higher annealing temperatures. At 1000° C, an amount of about 26 wt.-% is determined (Figure 6).

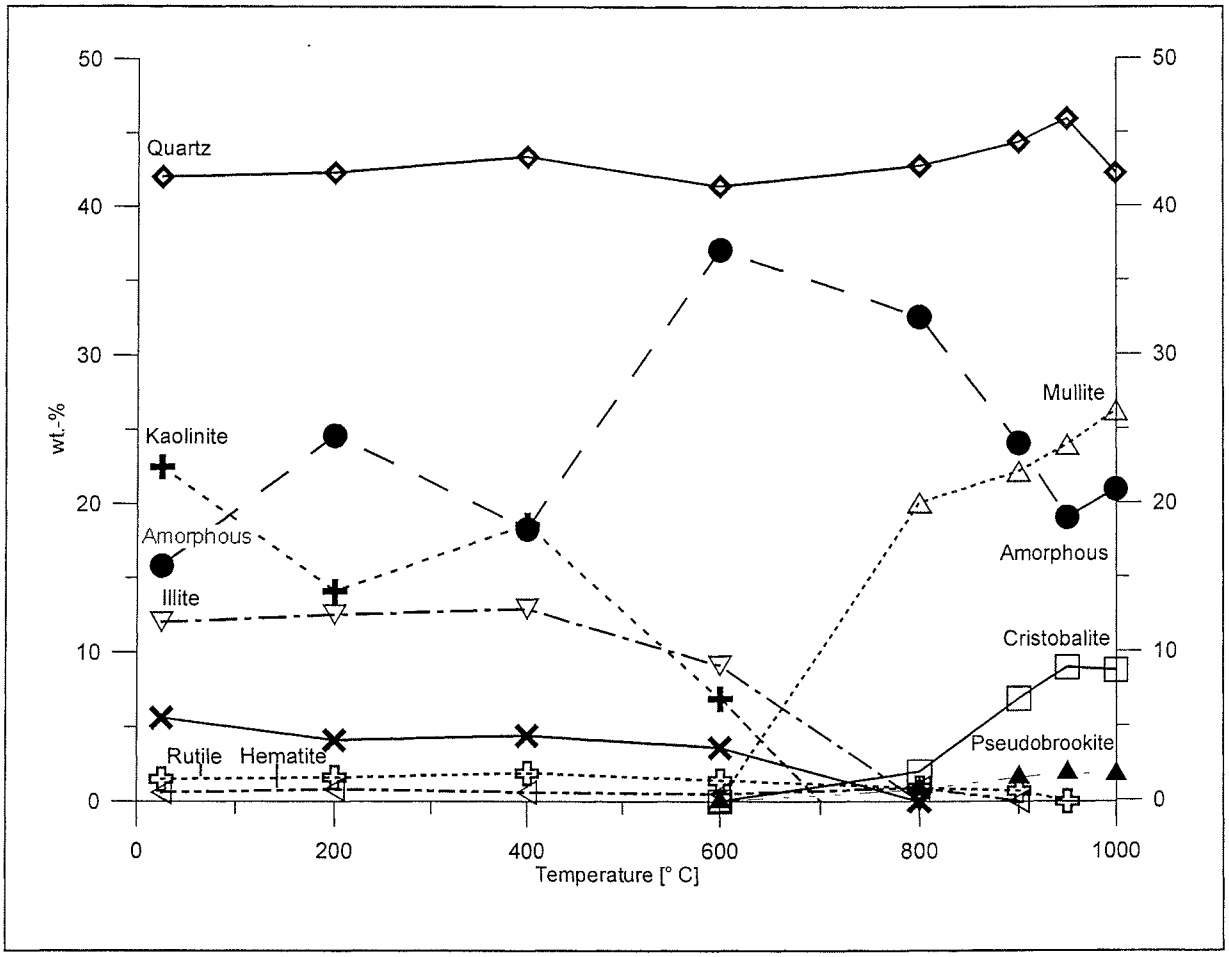

Fig. 6: Reaction sequence of clay admixed with 5 wt.-% V_2O_5; quantitative data obtained from Rietveld refinements.

The refined lattice constants of this mullite phase, derived by Rietveld refinement, show remarkable deviations from the starting parameters given by Ban & Okada (1992) (Table 1). Fischer *et al.* (1996) plotted several mullite lattice constants and showed the relationship between the cell parameters and the molar content of Al_2O_3. These curves are plotted in Figure 7. The shaded areas indicate the range of lattice constants determined from the four mullites from our studies annealed at different temperatures (Table 1). Usually, the chemical composition of mullite is determined by its *a* cell constant which is linearly related to the

molar Al_2O_3 content of mullite. The lattice constants determined here clearly deviate from this relationship since the *b* and *c* parameters do not match with the curves at the positions of any of the observed *a* constants.

		a [Å]	b[Å]	c[Å]
Ban & Okada (1992)	Pure mullite (3:2)	7.5459(2)	7.6937(2)	2.88346(7)
Schneider (1990)	Mullite (8.7 wt.-% V_2O_3)	7.555(2)	7.711(3)	2.8995(9)
	Mullite (10.3 wt.-% Fe_2O_3)	7.574(1)	7.726(1)	2.9004(5)
Schneider & Rager (1986)	Mullite (3.64 wt.-% Fe_2O_3)	7.5507(5)	7.7000(6)	2.8883(2)
	Mullite (11.1 wt.-% Fe_2O_3)	7.571(1)	7.725(1)	2.9001(5)
This study	800° C	7.604(2)	7.741(2)	2.8987(5)
	900° C	7.5953(6)	7.7037(6)	2.8986(2)
	950° C	7.589(1)	7.723(1)	2.8957(3)
	1000° C	7.582(1)	7.723(1)	2.8958(4)

Table 1: Lattice constants of pure and transition metal doped mullites

Further investigations of 50 x 20 nm crystals of mullite with Analytical Transmission Electron Microscopy (ATEM) yielded an amount of 3.2 mole-% vanadium and 3.8 mole-% iron in mullite of the sample synthesized at 1000° C which explains the observed deviations. Further cell parameters of vanadium and iron doped mullite described by Schneider & Rager (1986) and Schneider (1990) (Table 1) are plotted in Figure 7. The *b* and *c* lattice constants, especially of the iron doped samples, correlate with the shaded zones. The syntheses temperatures are significantly higher (> 1300° C) than the temperature range used in our study. We observe an expansion of the cell parameters of mullite already at 800° C. Obviously, the addition of vanadium oxide promotes the formation of mullite in a clay system. Transformation of kaolinite to metakaolinite yields the precursor and vanadium is incorporated in the structure.

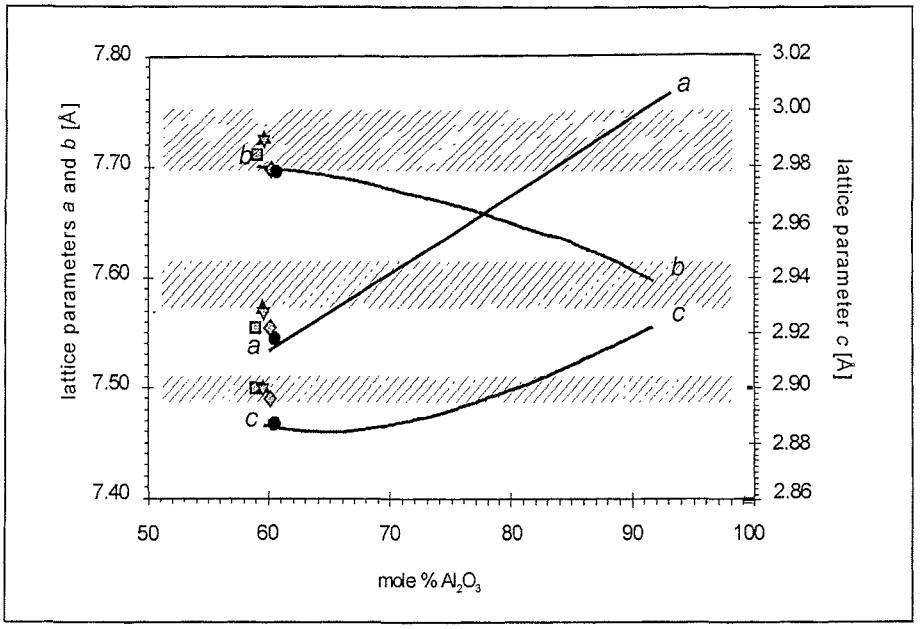

Fig. 7: Lattice constants vs. Al_2O_3 content of pure and transition metal doped mullite samples: ● pure mullite (3:2), Ban & Okada (1992); ▩ mullite with 8.7 wt.-% V_2O_3, Schneider (1990); ▲ mullite with 10.3 wt.-% Fe_2O_3, Schneider (1990); ◆ mullite with 3.64 wt.-% Fe_2O_3, Schneider & Rager (1986); ▼ mullite with 11.1 wt.-% Fe_2O_3, Schneider & Rager (1986). Continuous lines show cell parameters in mullite compositions without heavy metal addition (Fischer *et al.*, 1996), shaded areas mark the region of cell parameters obtained in this study.

Furtheron, the crystallization of α-cristobalite starts at 800° C as well. Just as mullite, cristobalite is not formed in the pure clay samples in the temperature range up to 1000° C. The reaction influenced by vanadium was determined by Bruhns and Fischer (2000): we observed cristobalite formation in the system SiO_2-V_2O_5-M_2CO_3 (M = Na, K) in the same temperature range. The reduction of the complex clay system to a composition of only three components allowed the syntheses and detailed determination of cristobalite. Experiments with XRD, IR, DTA, and MAS NMR were performed. We did not find any indication for V-incorporation in the cristobalite structure. Clay syntheses containing vanadium yield an additional mineral phase which is not detected in pure clays. At 800° C, a pseudobrookite compound (Fe_2TiO_5) crystallizes. Its content increases with increasing annealing temperature while rutile and hematite decrease simultaneously. Above 900° C, neither rutile nor hematite are detected in X-ray patterns. Formation of pseudobrookite influenced by V_2O_5 was simulated in a system containing TiO_2, Fe_2O_3, and V_2O_5. The oxides were admixed according to the stoichiometric

composition of pseudobrookite. These batches were annealed under the same conditions (1000° C, oxidic atmosphere) as the clay samples. The amount of Fe_2TiO_5 increases significantly with the addition of vanadium. Additionally, an iron-vanadate compound ($FeVO_4$) occurs which incorporates vanadium. The powder patterns of this pseudobrookite did not provide any indication for a chemically modified phase. However, it cannot be ruled out that some V has entered the structure which does not show in the X-ray pattern. Chemical analysis was not possible due to the extremely small crystals.

As mentioned above, syntheses in pure clay systems did not show any formation of new mineral phases in the temperature range between 800° and 1000° C. After decomposition of kaolinite, an increase in the amorphous amount up to about 45 wt.-% at 1000° C is observed (Figure 1). The contents of rutile and hematite are approximately constant.

In pure clay samples, illite is not completely decomposed during heating . It is detected up to 1000° C, although in very poor crystallinity. The beginning destruction of the structure is evident in the Rietveld refinement. At temperatures above 600° C a peak broadening is observed and the intensities decrease. Only the intensity of the peak at 19.7° 2θ remains more or less constant. While transformation processes and high-temperature phases are described for muscovites, a corresponding model for illite is not available so far. The formation of a second high-temperature phase, similar to muscovite described by Mazzucato *et al.* (1999) or Gualtieri *et al.* (1994), is not observed in our samples. The situation in vanadium doped clay is different: we observe a decrease of the illite content with complete decomposition below 800° C (Figure 6).

If we assume that quartz does not participate in the reactions, and consequently should not change its quantities, the variations in the weight fractions shown in Figures 1 and 6 reflect the possible range of errors in these determinations. The deviation from mean values is

about ± 3 wt.-% in both determinations. It is not clear whether the continuous reduction of kaolinite in the pure clay system (Figure 1) between room temperature and 400° C is caused by a systematic error in the determination. The decomposition and transition to metakaolinite is expected to occur above 400° C. This is also expressed by the decrease and subsequent increase in the amount of kaolinite in the V-doped clay below 400° C which is reversed for the amorphous quantities.

However, absolute errors of about 3 to 5 wt.-% on the high quantities of quartz, kaolinite, mullite, and the amorphous compound, and errors between 0.2 and 3 wt.-% on the smaller fractions of the other compounds do not affect the general interpretation of the reaction paths determined here: A (V, Fe)-doped mullite is formed above 600° C along with cristobalite and pseudobrookite if vanadium is admixed with clay in brick burning processes.

Conclusion

The reaction sequence shows the evident influence of addition of vanadium on the phase formation in clay systems. Several compounds as illite, hematite, and rutile decompose or react to form new phases not observed in the pure clay systems. The formation of mullite and cristobalite is observed in a temperature range much below their expected fields of stability. With the increasing amount of mullite and cristobalite the amorphous content, mainly metakaolinite, decreases. V_2O_5 supports the reaction and some of the vanadium together with iron from Fe_2O_3 participates in the crystallization of mullite.

We assume that vanadium is not incorporated, or only in very small traces, into the structure of cristobalite as discussed by Bruhns & Fischer (2000). Similar reasoning applies to pseudobrookite which crystallizes in the presence of vanadium without a distinct indication of

V incorporation. The vanadium, added as V_2O_5 to the sample, is not completely exhausted by the V-mullite which incorporates only a small fraction of the initial amount of vanadium. The remaining quantity cannot be assigned to an identified mineral phase. We assume that additional vanadate compounds crystallize as well, in quantities below the detection limits of our analytical methods. Former investigations (Bruhns & Fischer, 2000) showed the formation of alkali-vanadates during cristobalite syntheses in the presence of vanadium and alkali metals. The syntheses of pseudobrookite, separately performed in this work, yielded an iron-vanadate phase.

These results show that the concept of cation immobilization in the brick burning process is very limited for V-containing materials. It is assumed that only part of the vanadium is bound in silicates (here: mullite) and the rest is expected to form vanadates mainly with alkalis and iron. Since some of these vanadates are soluble in water, its utilization in building materials should be carefully evaluated.

Acknowledgements

Financial support is gratefully acknowledged from the Zentrale Kommission des Akademischen Senats für Forschungsplanung und wissenschaftlichen Nachwuchs (FNK). We thank M. Schmücker (Köln) for performing and discussing the Analytical Transmission Electron Microscopy (ATEM), and N. Groschopf (Mainz) for the XRF analyses.

References

Abrahams, S.C., Bernstein, J.L. (1971): Rutile: normal probability plot analysis and accurate measurement of crystal structure. *J. Chem. Phys.*, **55**, 3206- 3211.

Ban, T., Okada, K. (1992): Structure refinement of mullite by the Rietveld method and a new method for estimation of chemical composition. *J. Am. Ceram. Soc.*, **75**, 227-230.

Barham, D. (1965): An investigation of the system V_2O_5-Al_2O_3. *Trans. Brit. Ceram. Soc.*, **64**, 371-375.

Bellotto, M., Gualtieri, A., Artioli, G., Clark, S. M. (1995): Kinetic study of the kaolinite-mullite reaction sequence. Part I: Kaolinite dehydroxylation. *Phys. Chem. Miner.*, **22**, 207-214.

Bish, D. L., von Dreele, R. B. (1989): Rietveld refinement of non-hydrogen atomic positions in kaolinite. *Clays and Clay Minerals*, **37**, 289-296.

Blake, R. L., Hessevick, R. E., Zoltai, T., Finger, L. W. (1966): Refinement of the hematite structure. *Am. Mineral.*, **51**, 123-129.

Brindley, G. W., Nakahira, M. (1959): The kaolinite-mullite reaction series:

I. A survey of outstanding problems.

II. Metakaolin.

III. The high-temperature phases. *J. Am. Ceram. Soc.*, **42**, 311-342.

Bruhns, P., Fischer, R. X. (2000): Crystallization of cristobalite and tridymite in the presence of vanadium. *Eur. J. Mineral.*, **12**, 615-624.

DEV S4 DIN 38414 Teil 4 (1984): Deutsche Einheitsverfahren zur Wasser-, Abwasser- und Schlammuntersuchung, Schlamm und Sedimente (Gruppe S), Bestimmung der Eluierbarkeit mit Wasser (S4), Beuth-Verlag Berlin.

Dondi, M., Fabbri, B., Mingazzini, C. (1997): Mobilization of chromium and vanadium during firing of structural clay products. *Ziegelindustrie*, **10**, 685-696.

Fischer, R. X., Lengauer, C., Tillmanns, E., Ensink, R. J., Reiss, C. A., Fantner, E. J. (1993): PC-Rietveld Plus, a comprehensive Rietveld analysis package for PC. *Mater. Sci. Forum*, **133-136**, 287-292.

Fischer, R. X., Schneider, H., Voll, D. (1996): Formation of aluminium rich 9:1 mullite and its transformation to low alumina mullite upon heating. *J. Eur. Ceram. Soc.*, **16**, 109-113.

Förstner, U. (1995): Umweltschutztechnik: eine Einführung. Springer Verlag, Berlin Heidelberg New York.

Gravette, N.C., Barham, D. Barrett, L. R. (1966): An investigation of the system V_2O_5-SiO_2. *Trans. Brit. Ceram. Soc.*, **65**, 199-206.

Gualtieri, A., Artioli, G., Bellotto, M., Clark, S. M., Palosz, B. (1994): High temperature phase transition of muscovite-2M_1: angle and energy dispersive powder diffraction studies. *Mater. Sci. Forum*, **166-169**, 547-552.

Gualtieri, A., Bellotto, M., Artioli, G., Clark, S. M. (1995): Kinetic study of the kaolinite-mullite reaction sequence. Part II: Mullite formation. *Phys. Chem. Miner.*, **22**, 215-222.

Gualtieri, A. F. (2000): Accuracy of XRPD QPA using the combined Rietveld-RIR method. *J. Appl. Cryst.*, **33**, 267-278.

Hamelin, M. (1958): The structure of the composition TiO_2-Al_2O_3, in comparison with pseudobrookite. *Bull. Soc. Chim. France*, **1958**, 1559-1566.

Jasmund, K., Lagaly, G. (eds.) (1993): Tonminerale und Tone: Struktur, Eigenschaften, Anwendungen und Einsatz in Industrie und Umwelt. Steinkopff Verlag,

Darmstadt, 490 p.

Ketelaar, J. A. A. (1936): Die Kristallstruktur des Vanadinpentoxids. *Z. Krist.*, **95**, 9-27.

Kisi, E. H., Elcombe, M. M. (1989): U parameters for the wurtzite structure of ZnS and ZnO using powder neutron diffraction. *Acta Cryst.*, **C45**, 1867-1870.

Kristóf, E., Juhász, A. Z., Vassányi, I. (1993): The effect of mechanical treatment on the crystal structure and thermal behavior of kaolinite. *Clays and Clay Minerals*, **41**, 609-612.

Kromer, H., Schüller, K. H. (1974): Sintervorgänge bei Kaolinen und Tonen. *N. Jb. Min. Abh.*, **122**, 145-185.

Margane, J. (1992): Änderung der Schwermetallbindungsformen in thermisch behandeltem Bodenmaterial. Geologisches Institut der Universität zu Köln, Sonderveröffentlichungen Nr. 87.

Mazzucato, E., Artioli, G., Gualtieri, A. (1999): High temperature dehydroxylation of muscovite-2M_1: a kinetic study by in situ XRPD. *Phys. Chem. Miner.*, **26**, 375-381.

Moore, D. M., Reynolds, R. C. Jr. (1989): X-ray diffraction and the identification and analysis of clay minerals. Oxford University Press, Oxford, New York, 332 p.

Pluth, J. J., Smith, J. V., Faber, J. Jr (1985): Crystal structure of low cristobalite at 10, 293, and 473 K: Variation of framework geometry with temperature. *J. Appl. Phys.*, **57**, 1045-1049.

Richardson, S. M., Richardson, J. W. Jr. (1982): Crystal structure of a pink muscovite from Archer's post Kenya: implications for reverse pleochroism in dioctahedral micas. *Am. Mineral.*, **67**, 69-75.

Salmang, H., Scholze, H. (1983): Keramik: Allgemeine Grundlagen und wichtige

Eigenschaften. Springer Verlag, Berlin Heidelberg New York.

Schneider, H. (1990): Transition metal distribution in mullite. *Ceram. Trans.* **6** (Mullite Mullite Matrix Compos.), 135-157.

Schneider, H., Rager, H. (1986): Iron incorporation in mullite. *Ceram. Int.*, **12**, 117-125.

Will, G., Bellotto, M., Parrish, W., Hart, M. (1988): Crystal structures of quartz and magnesium germanate by profile analysis of synchrotron-radiation high-resolution powder data. *J. Appl. Cryst.*, **21**, 182-191.

Zöller, M. H. (1994): Einkristalluntersuchungen an 1*M*- und $2M_1$-Illiten durch konvergente Elektronenbeugung. PhD thesis, University of Bremen, Germany.

Phase reactions in the brick firing process of clay in the presence of Cr, Cu, and Pb

Petra Bruhns and Reinhard X. Fischer

Fachbereich Geowissenschaften der Universität, Klagenfurter Straße,

D-28359 Bremen, Germany

Abstract

The phase reactions of clays in brick burning processes upon addition of heavy metal compounds are studied to evaluate the utilization of contaminated wastes in brickworks. The oxides (PbO, CuO, and Cr_2O_3) and chromates (Na_2CrO_3 and $K_2Cr_2O_7$) were admixed to clay and annealed at temperatures between 200° and 1000° C. The reaction sequences differ from those in pure clay annealed in the corresponding temperature range. The addition of PbO yields a lead feldspar and in CuO-doped clays mullite is formed. Cr_2O_3 remains inert during annealing processes whereas the addition of chromates yields kalsilite, nosean, and nepheline like phases. The samples were investigated by X-ray powder diffraction methods. Quantitative analyses were performed with the Rietveld method and chemical analyses with X-ray fluorescence spectroscopy.

Introduction

The deposition of heavy metal contaminated wastes like incineration ashes or sewage sludges could be avoided by proper utilization of these materials ensuring that the metal ions are not released to the environment. A possible method to immobilize the heavy metals is a thermal treatment as described by Förstner (1995) and Margane (1992). The brick burning process with a mixture of raw clay and heavy metal contaminated material is a promising approach expecting an incorporation of metal ions in the brick mineral phases. However, there is only scarce knowledge on the phase formations in clay annealed with metal compounds. Since the phase formations are very important for the materials' properties it is desirable to analyze the complete reaction path. The strength of the incorporation of heavy metals is normally determined by leaching tests. Previous studies show the mineralization processes dependant on the thermal treatment of natural clay upon addition of vanadium oxide (Bruhns and Fischer, 2001). A significant influence on the phase reactions was observed, e.g. the formation of mullite and cristobalite at rather low temperatures (800° C). In this paper, the reaction sequences during annealing processes of natural clay upon addition of copper, chromium, and lead bearing compounds are described. The mineralizations are compared with the processes in natural clay annealed without additives.

Natural clay is a composition of various mineral phases. Our investigations are based on a clay containing kaolinite, illite, quartz, rutile, and hematite as crystalline components. The dehydroxylation of kaolinite occurs in a temperature range between 500° and 700° C (Bellotto et al. 1995) yielding metakaolinite. Brindley and Nakahira (1959) describe the formation of mullite and cristobalite at temperatures above 1050° to 1100° C.

The high temperature reactions of illite depend on its chemical composition; decomposition may start at 850° C but some samples show illite up to 1000° C, as described by Kromer and Schüller (1974). The crystal structure and the chemical composition of illite

are closely related to muscovite. During annealing processes of muscovite a dehydroxylated phase is observed between 700° and 1000° C transforming to mullite at higher temperatures (Mazzucato et al. 1999). Quartz is not expected to participate in reactions below 1000° C.

During brick burning the formation of a liquid phase is important for the mineralizations and, in consequence, the stability of the final product. For systems consisting of SiO_2 and metal oxides like CuO and PbO, phase diagrams indicate partial melting at temperatures of about 1050° C (CuO) and 730° C (PbO) which may influence the reactions in the natural clay system (Levin et al. 1969). As the natural clay system is very complex, the influence of a single compound is not predictable in detail.

The aim of this work is to describe the reaction sequences in clay during annealing processes upon addition of heavy metal compounds.

Experimental

(1) Sample treatment and calcination

For the syntheses the same raw clay material was used as in the former investigations of vanadium clay reactions by Bruhns and Fischer (2001). It was provided by Ziegelwerk Grehl (Humlangen, Germany).

Mixtures of the raw clay material and heavy metal compounds were homogenized in an agate mortar and pressed to pellets of 13 mm in diameter. The samples were annealed in a tube furnace. To protect the furnace from contamination caused by volatile heavy metal compounds, the experiments were performed in a silica glass tube which was placed in the furnace tube. All specimens were annealed for 17 h up to 1000° C, representing the temperature range typical for brick burning. The heating rate was 200° C/h as was the cooling rate. The syntheses containing heavy metal compounds were compared with a pure clay

sample annealed in the same temperature range.

(1.1) Syntheses with lead

The samples were prepared by mixing pure clay with 5 wt.-% PbO. The reaction sequence was determined between 400° and 1000° C in steps of 100° C.

(1.2) Syntheses with copper

The mixtures consisted of pure clay and 5 wt.-% CuO annealed between 400° and 1000° C.

(1.3) Syntheses with chromium

As chromium oxide is a rather unreactive compound, further chromium compounds were admixed to pure clay. Three batches were prepared. The first one contained clay with 5 wt.-% Cr_2O_3. The second was a mixture of clay and Na_2CrO_4 with the sodium-chromate content varying from 5 wt.-% to 10 wt.-% and 20 wt.-%. To determine the influence of sodium on the system, a third batch containing clay and $K_2Cr_2O_7$ (10 and 20 wt.-%) was tempered.

(2) Analytical

All samples were analysed by X-ray powder diffraction to identify and quantify the phases. A Philips PW 3050 powder diffractometer with primary monochromator was used. Data were collected using Cu$K_{\alpha 1}$ radiation at room temperature in the range between 5° (or 10°) and 120° 2θ with steps of 0.02 2θ. All refinements and quantifications were performed with the Philips PC-Rietveld plus program package by Fischer et al. (1993). The simulations are based on the structure models of quartz (Will et al. 1988), kaolinite (Bish and von Dreele 1989), hematite (Blake et al. 1966), rutile (Abrahams and Bernstein 1971), PbO (Hill 1985),

$PbAl_2Si_2O_8$ (Benna et al. 1996), CuO (Brese et al. 1990), mullite (Ban and Okada 1992), Cr_2O_3 (Newnham and de Haan 1962), nepheline (Dollase 1970), nosean (Schulz 1970), $KAlSiO_4$ (Perrotta et al. 1965), and ZnO (Kisi and Elcombe 1989). There is no structure model for illite available so far. Since the structure and composition of illite are closely related to muscovite the structure model determined by Richardson and Richardson (1982) is used for refinements in this work

Chemical analysis of pure clay was performed using a Philips 1404 X-ray fluorescence spectrometer at the Institute of Mineralogy, University of Mainz.

Results

Pure clay

The XRF analysis of the raw clay yielded weight fractions of 67.48% SiO_2, 18.84% Al_2O_3, 3.17% Fe_2O_3, 1.37% TiO_2, 0.16% CaO, 0.4 % MgO, 0.15% Na_2O, 1.72% K_2O, and 0.03% P_2O_5. The deviation to 100% was determined as weight loss due to dehydroxylation and water desorption.

The powder diffraction pattern in Figure 1 shows the reaction sequence of pure clay samples from room temperature up to 1000° C. Raw clay material consists of quartz, kaolinite, illite, and minor amounts of rutile and hematite. After dehydroxylation, kaolinite is decomposed between 500° and 600° C. No formation of high temperature phases (e.g. mullite or cristobalite) is observed during the annealing process up to 1000° C. The Rietveld refinement of illite is aggravated by the poor quality of the diffraction data upon increasing temperature. The characteristic peaks at 10.01° and 4.99° 2θ disappear whereas the intensity of the peak at 4.47° 2θ remains as the structure decomposes. Although illite is closely related to muscovite,

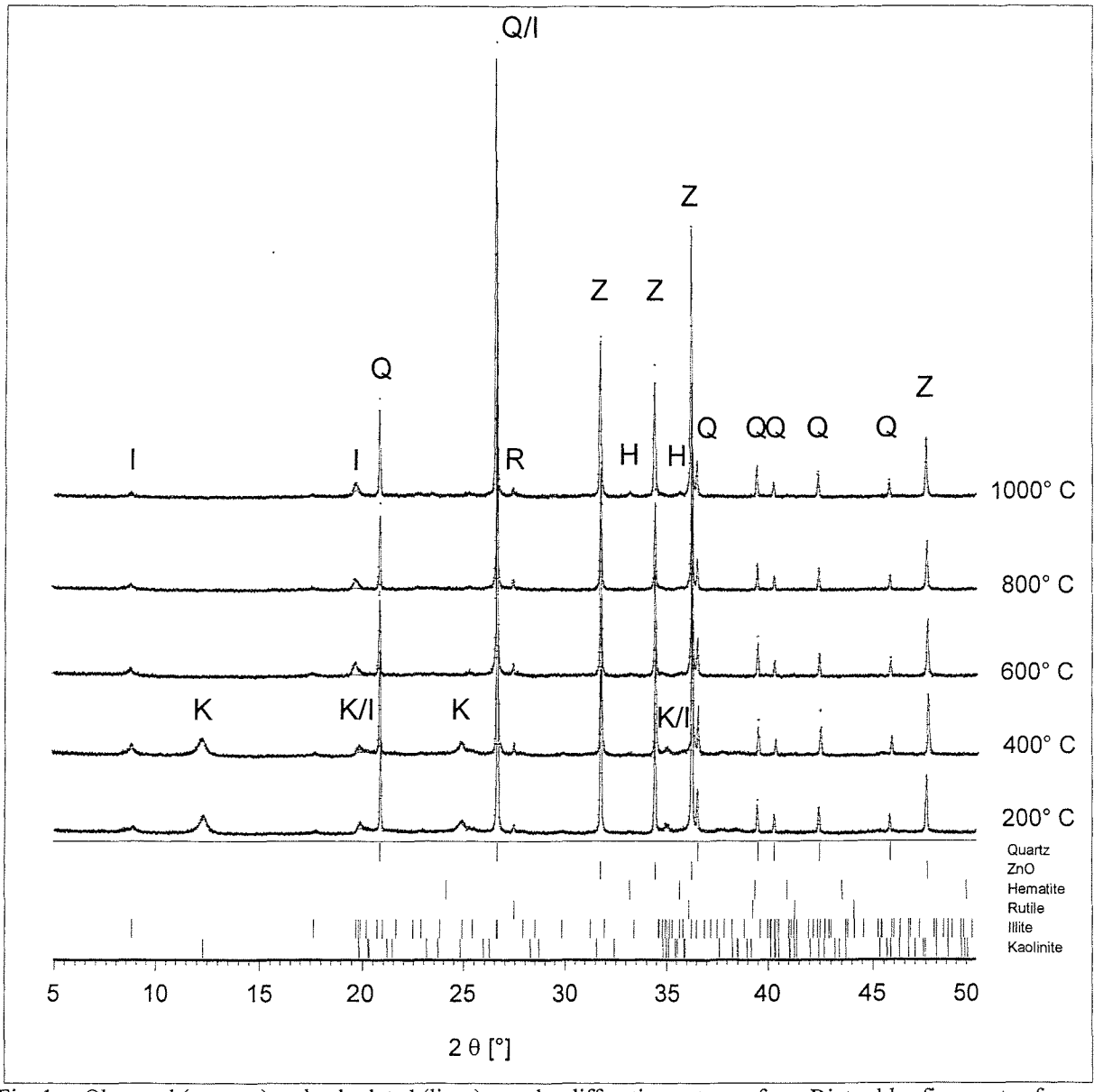

Fig. 1: Observed (crosses) and calculated (lines) powder diffraction patterns from Rietveld refinements of pure clay between room temperature and 1000° C. Q: quartz, Z: ZnO, H: hematite, R: rutile, I: illite, K: kaolinite.

no transformation to a high temperature phase corresponding to muscovite, as described by Mazzucato et al. (1999), is observed.

Mineral phase [wt%]	Raw clay material	Clay annealed at [°C]										
		200	400	500	550	600	650	700	800	900	950	1000
Quartz	40.1	39.5	41.3	41.9	45.9	45.3	44.6	48.4	46.6	47.1	45.4	43.4
Kaolinite	24.9	17.9	13.3	14.3	12.8	0.6	5.9	-	-	-	-	-
Illitic components	15.9	16.1	13.6	12.8	13.4	11.3	8.2	10.9	12.8	12.1	11.9	8.4
Rutile	1.8	1.4	1.8	1.5	1.6	1.5	1.3	1.1	1.6	1.4	1.9	1.4
Hematite	0.4	0.6	0.6	0.6	1.0	1.4	0.6	1.0	1.3	1.0	1.2	1.4
Amorphous	16.8	24.5	29.5	28.9	25.3	40.0	39.4	38.5	37.8	38.5	39.7	45.3

Tab. 1: Weight fractions of pure clay annealed in the range between room temperature and 1000° C

The results of the quantitative analysis of the mineral phases are given in Table 1. The data are based on Rietveld refinements with ZnO as internal standard.

Syntheses with lead

The reaction sequence of clay mixed and annealed with 5 wt.-% PbO is shown in Figure 2. Similar to pure clay, kaolinite is decomposed at temperatures above 500° C. The

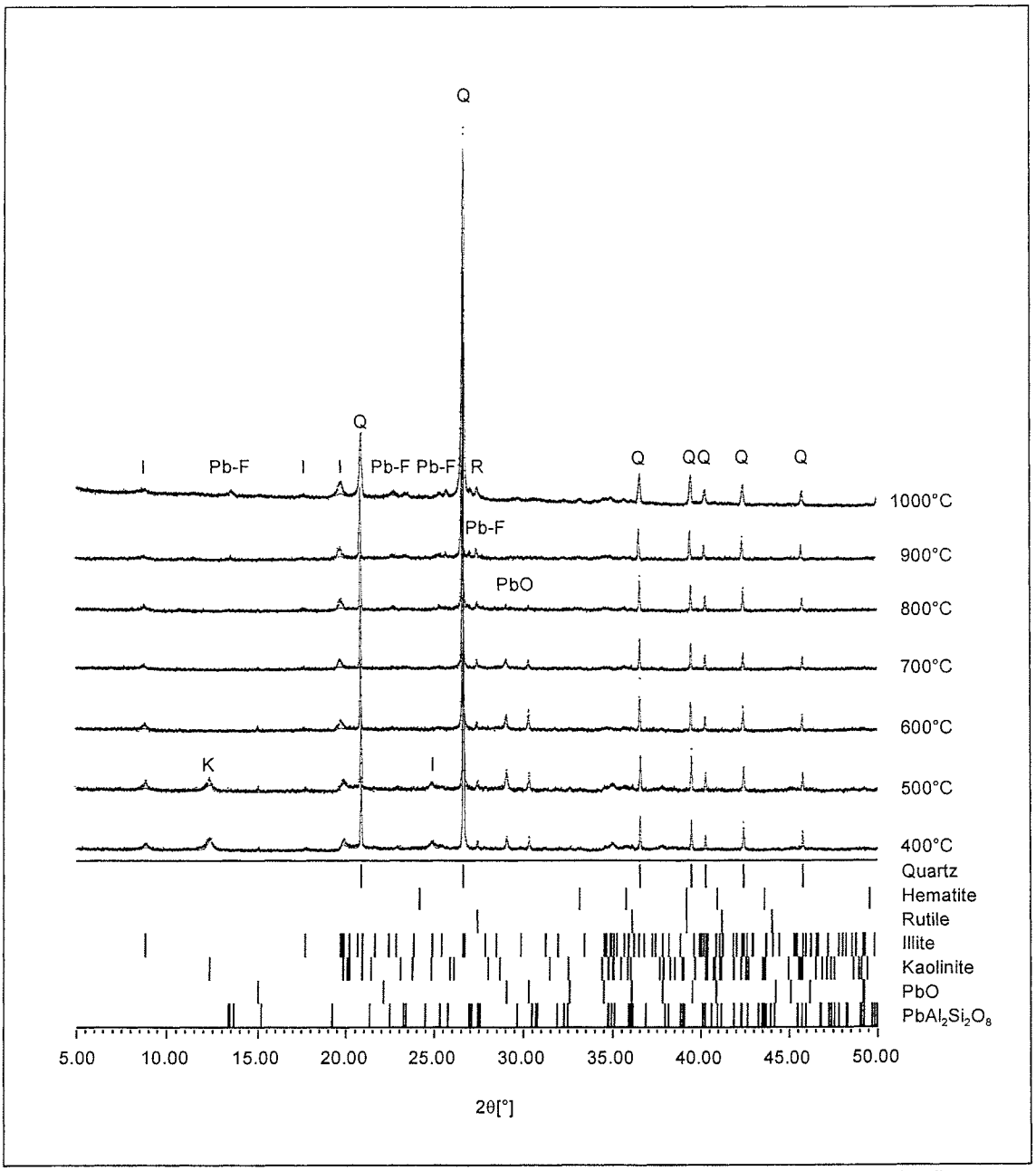

Fig. 2: Observed (crosses) and calculated (lines) powder diffraction patterns from Rietveld refinements of clay admixed with 5 wt.-% PbO annealed between 400° and 1000° C. Q: quartz, I: illite, K: kaolinite, R: rutile, PbO: PbO, Pb-F: lead feldspar.

amount of PbO decreases above 500°C and a lead bearing feldspar is observed. Its content increases with higher temperatures. Ordered and disordered modifications of lead feldspar are described by Benna et al. (1996, 1999). Powder diffraction patterns of the samples studied here agree with the disordered structure model in space group *C* 2/*m*. A detailed quantitative description of the samples is problematic as the refinement of clay minerals suffers from anisotropic peak broadening caused by disordered structures, incorrectly determined chemical compositions, and insufficient crystal structure models. Especially quantitative analysis is problematic when strong absorbers like PbO are mixed with weekly absorbing materials (Brindley 1945) due to microabsorption effects. Resulting weight fractions deviate significantly from the true contents even if these effects are corrected. Any error in the determination of the particle size has an influence on the results. Since we are mainly interested in the qualitative description of the reaction sequences we abstained from listing the weight fractions as determined in the Rietveld analysis. However, reactions and relative changes in the phase content as a function of the annealing temperature is described properly.

Syntheses with copper

Powder diffraction patterns of the samples admixed and annealed with CuO are shown in Figure 3. Quantitative data from Rietveld refinements are given in Table 2.

Clay + 5% CuO, annealed at [°C]	Quartz [wt%]	Hematite [wt%]	Rutile [wt%]	Illite [wt%]	Kaolinite [wt%]	CuO [wt%]	Mullite [wt%]
400	56.0	1.3	1.8	16.8	18.2	5.9	-
600	71.1	1.5	1.8	19.1	-	6.5	-
800	74.1	1.9	1.6	18.2	-	4.3	-
900	70.5	2.5	1.9	15.8	-	3.0	6.3
950	75.6	2.5	1.9	-	-	1.3	18.6
1000	78.3	2.2	2.2	-	-	1.2	16.1

Tab. 2: Weight fractions of clay with 5 wt.-% CuO annealed in the range between 400° and 1000° C

In the temperature range below 900° C the mixture shows a reaction sequence similar to pure clay. Above 900° C different reactions occur. The content of illite decreases and the formation

of mullite is observed. Since quartz is considered to remain stable in the annealing process, it was used as an internal standard for the quantitative determinations. An amount of 44 wt.-%

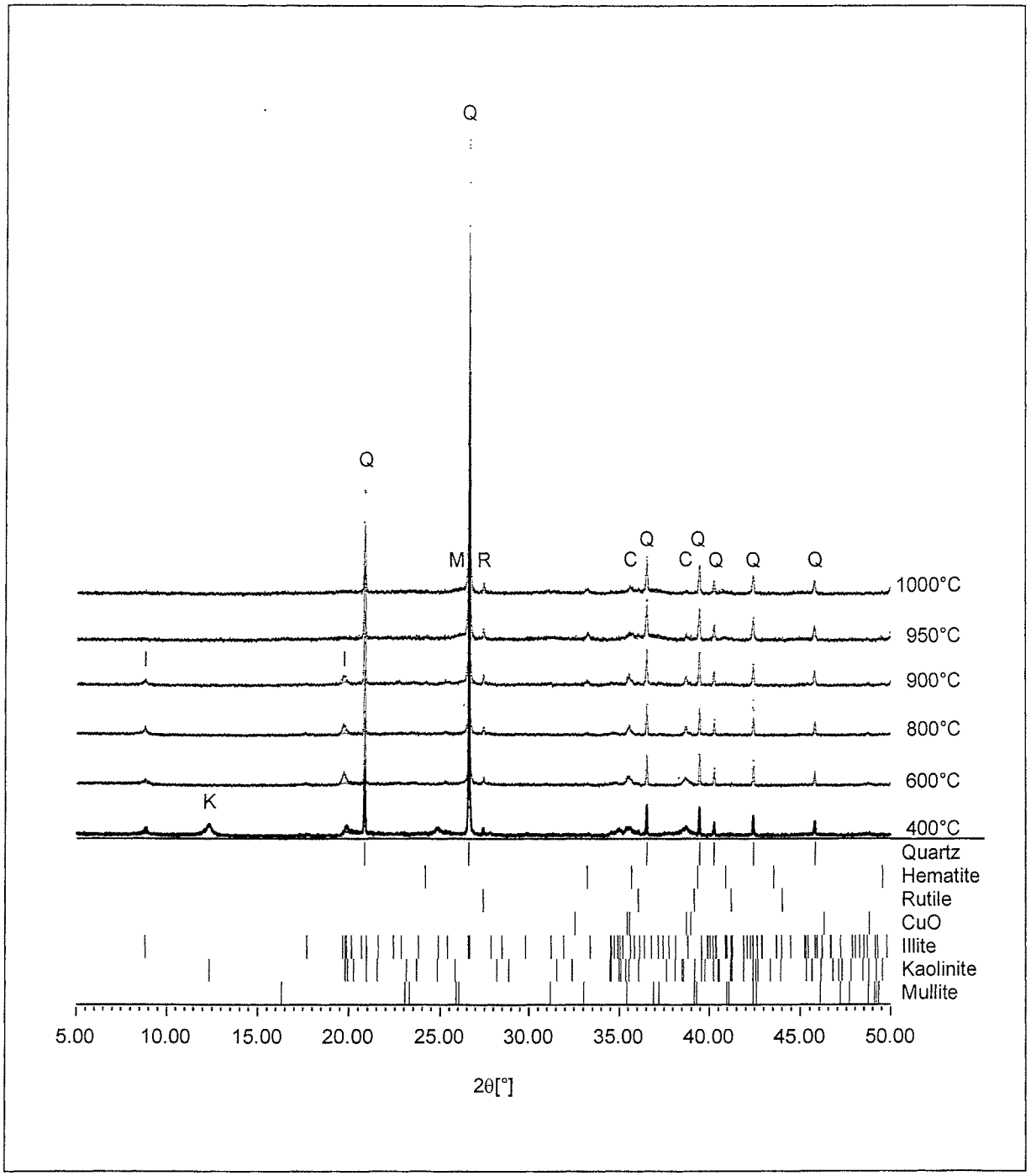

Fig. 3: Observed (crosses) and calculated (lines) powder diffraction patterns from Rietveld refinements of clay admixed with 5 wt.-% CuO annealed between 400° and 1000° C. Q: quartz, I: illite, K: kaolinite, R: rutile, M: mullite, C: CuO.

was determined as a mean value. Figure 4 shows the quantification of the phases based on the standardization of quartz to 44 wt.-%. At temperatures above 900° C illite is decomposed

completely whereas the amount of mullite increases. A similar reaction sequence was observed upon addition of vanadium oxide to clay during former studies by Bruhns and

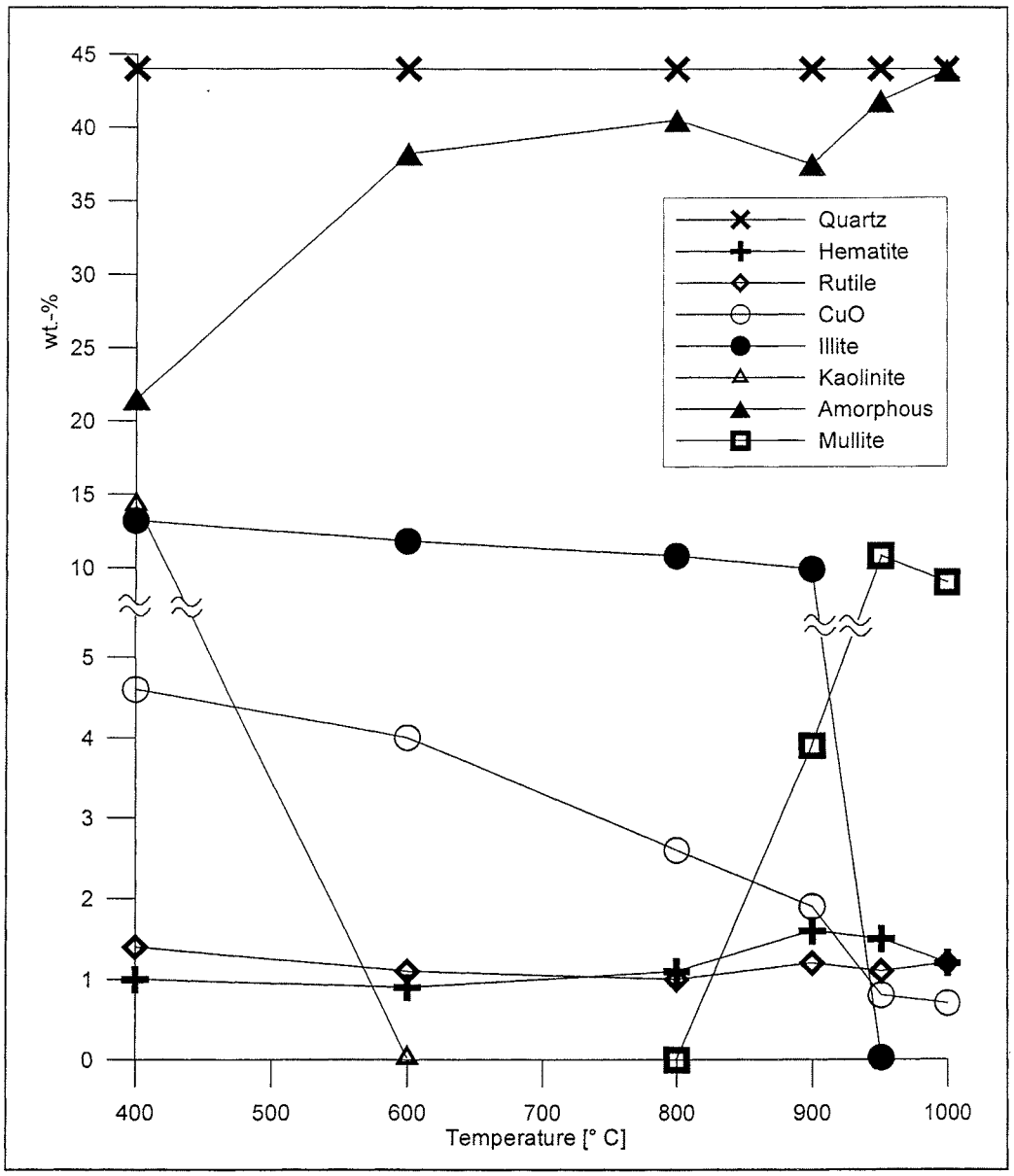

Fig. 4: Reaction sequence of clay admixed with 5 wt.-% CuO; quantitative data obtained from Rietveld refinements and standardized to a fix quartz content.

Fischer (2001). In contrast to the syntheses containing copper, the mullite formation in the presence of vanadium starts at lower temperatures (700° C) and, additionally, cristobalite is observed. Upon addition of copper, no cristobalite is observed during the annealing process up to 1000° C. Furthermore, the crystallization of mullite is rather poor and a refinement of the lattice constants is questionable. Consequently, the analysis does not yield direct clues on

the incorporation of Cu in mullite. However, the formation of mullite at rather low temperatures could be explained by a stabilization with Cu analogously to the V-doped mullite described by Bruhns and Fischer (2001).

Syntheses with chromium

X-ray powder diffraction patterns of samples containing Cr_2O_3 are shown in Figure 5. The phase composition of the annealed sample is not influenced by Cr_2O_3. Similar to pure

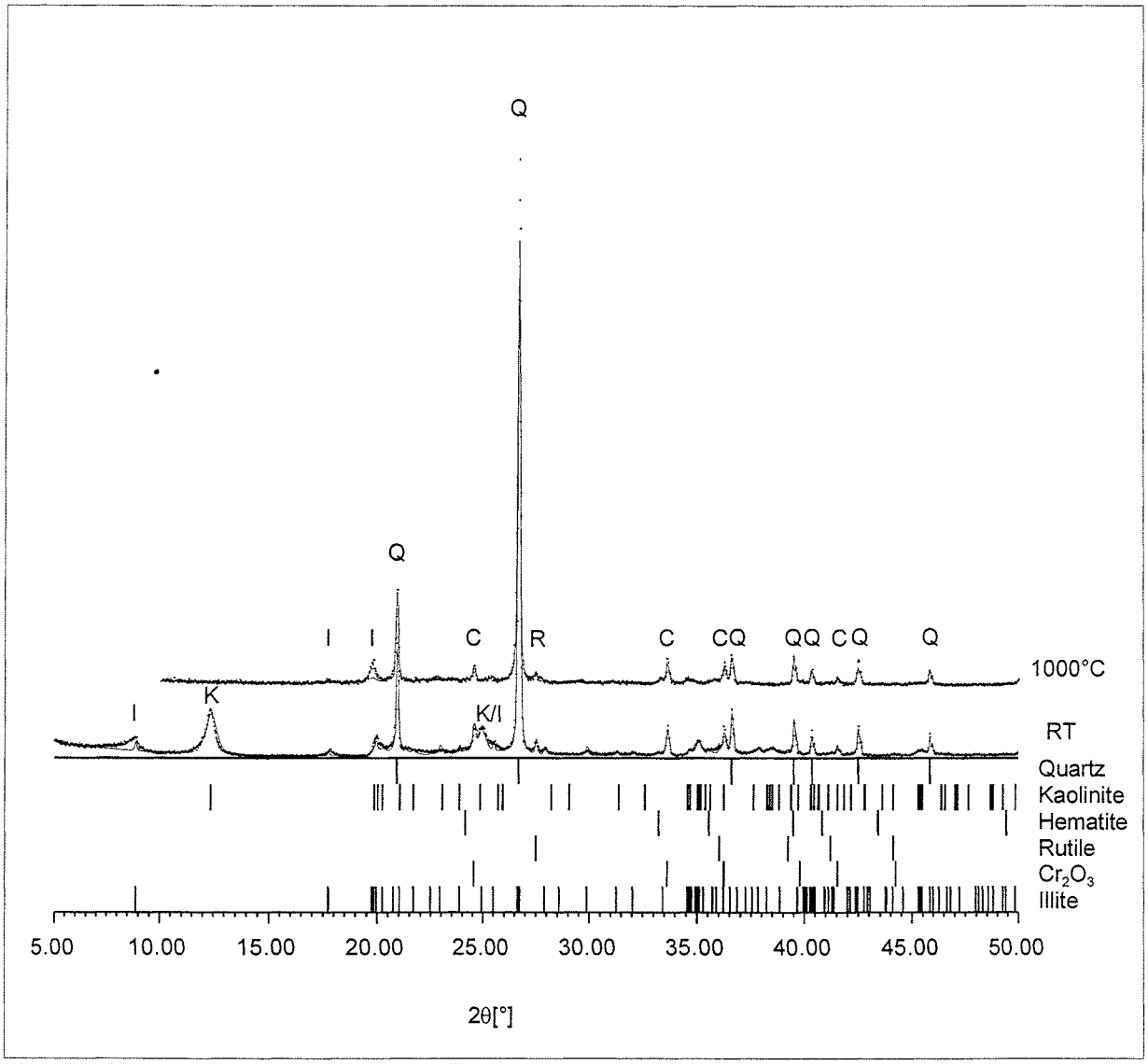

Fig. 5: Observed (crosses) and calculated (lines) powder diffraction patterns from Rietveld refinements of clay admixed with 5 wt.-% Cr_2O_3 at room temperature and annealed at 1000° C. Q: quartz, I: illite, K: kaolinite, R: rutile, C: Cr_2O_3.

clay at 1000° C, quartz, hematite, rutile, and illite are observed. Quantification with Rietveld refinements yields equivalent ratios of the phase contents in the raw sample as well as in the annealed sample showing that Cr_2O_3 did not react with any of the compounds.

Different reactions are observed for the other batches synthesized with Na_2CrO_4 and $K_2Cr_2O_7$. Powder diffraction patterns in Figure 6 show the phase composition for clay with varying sodium chromate contents annealed at 1000° C.

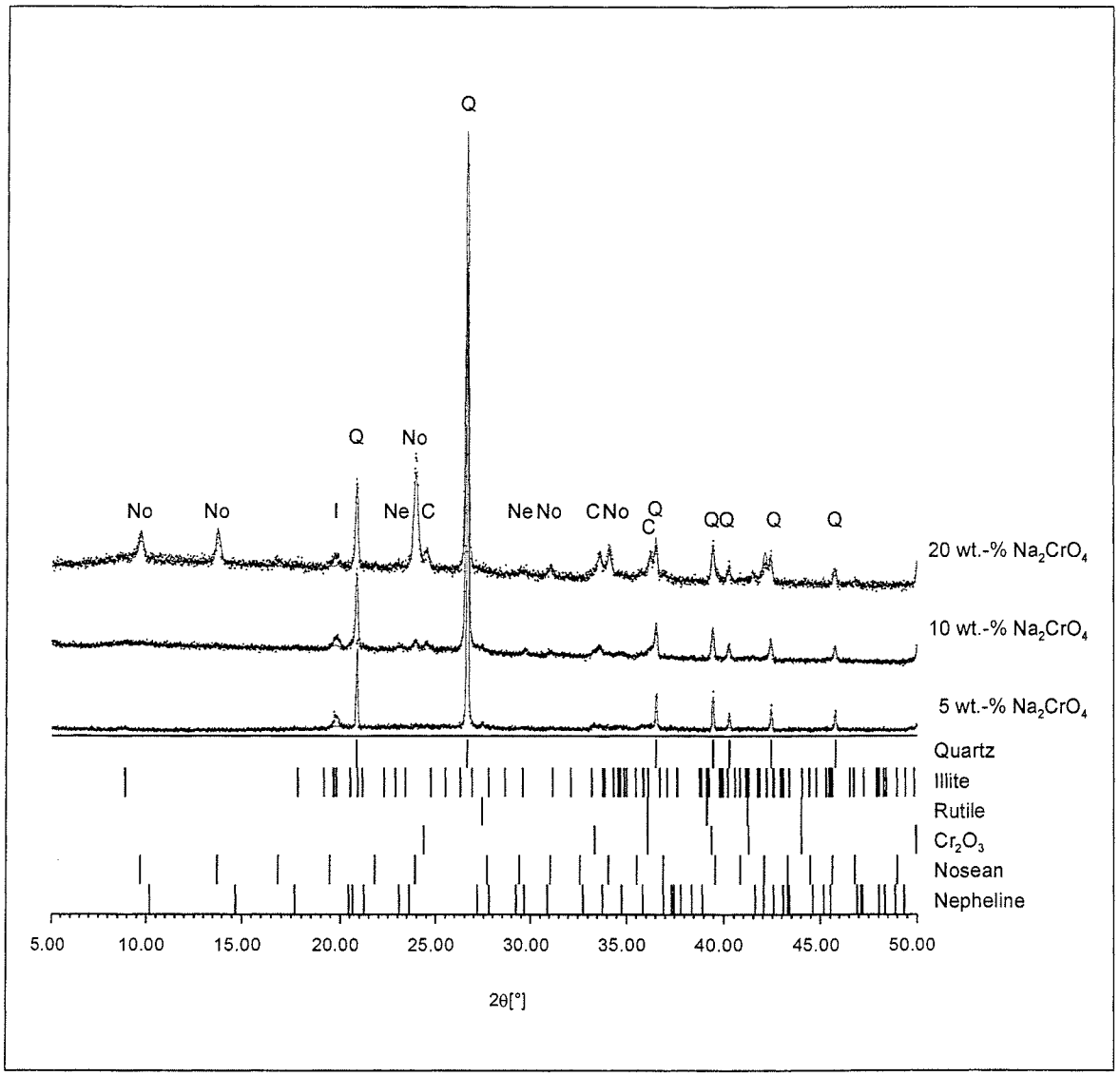

Fig. 6: Observed (crosses) and calculated (lines) powder diffraction patterns from Rietveld refinements of clay admixed with 5, 10, and 20 wt.-% Na_2CrO_4 at 1000° C. Q: quartz, No: nosean, Ne: nepheline, C: Cr_2O_3.

In samples containing 5 wt.-% Na_2CrO_4, Cr_2O_3 is formed during the annealing process. Illite is observed up to 1000° C. With increasing sodium chromate content, further mineralizations

occur: the addition of 10 wt.-% Na_2CrO_4 yields a nepheline and a nosean compound. Simultaneously, the illite content decreases whereas Cr_2O_3 increases. In samples synthesized with 20 wt.-% Na_2CrO_4, the amount of illite is further reduced while the contents of nepheline and Cr_2O_3 increase. Syntheses with $K_2Cr_2O_7$ were performed under similar conditions. Upon annealing to 1000° C, samples containing 10 wt.-% $K_2Cr_2O_7$ yield a phase composition of quartz, Cr_2O_3, rutile, hematite, and illite. With increasing amount of $K_2Cr_2O_7$ (20 wt.-%) the formation of a potassium-alumino-silicate phase is observed (Figure 7), as described by a kalsilite model (Perrotta et al. 1965). Since the refinement of the kalsilite like phase yields rather poor results, the quantification of the samples is not very reliable.

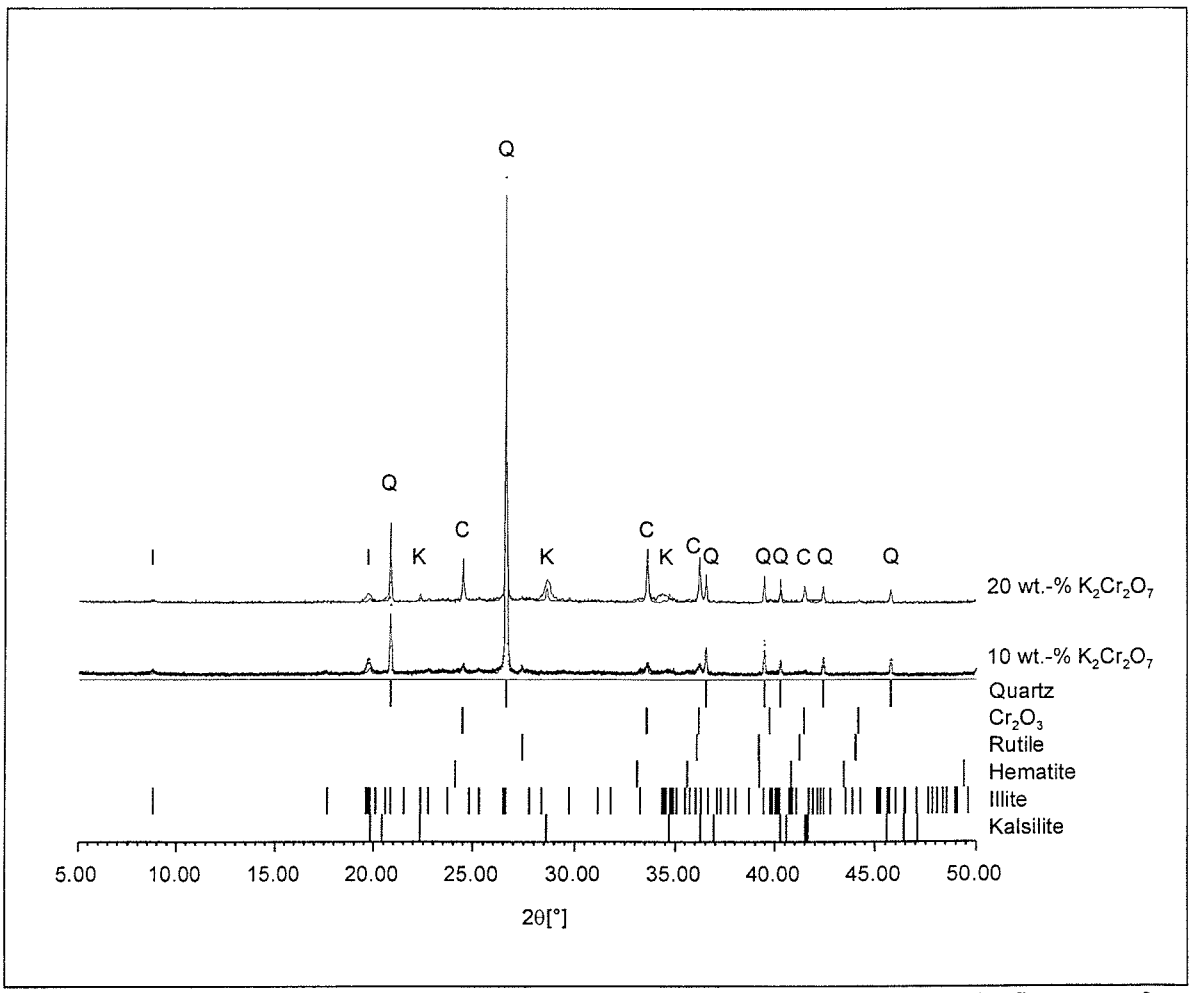

Fig. 7: Observed (crosses) and calculated (lines) powder diffraction patterns from Rietveld refinements of clay admixed with 10 and 20 wt.-% $K_2Cr_2O_7$ at 1000° C. Q: quartz, I: illite, K: kalsilite, C: Cr_2O_3.

Discussion

The results presented here show that the addition of heavy metal compounds influences the reaction sequences of clay during the annealing process.

Upon addition of PbO a lead feldspar phase is formed. According to the phase diagram of SiO_2 and PbO, a partial melting at about 730° C is observed (Levin et al. 1969). This temperature coincides with the range where the decomposition of PbO and formation of $PbAl_2Si_2O_8$ occur in our samples. The phase diagram of PbO and Al_2O_3 shows partial melting at about 1000° C. Due to the decomposition of clay minerals, SiO_2 and Al_2O_3 are quantitatively the main components which participate in the reaction sequence and therefore these systems are considered. The presence of a liquid phase triggers mineralization processes, but simultaneously the liquid phase is consumed to form lead feldspar. Obviously, the phase diagrams of the oxides represent a limitation of the actual composition of the clay and can only give a hint for the interpretation.

Samples synthesized upon addition of CuO yield a mullite phase at about 900° C. As no specific Cu-phase is observed, we assume that Cu is present in the liquid phase supporting mullite formation in this temperature range. Upon addition of CuO mullite occurs at significantly higher temperatures than in syntheses of V-doped clay where it is observed at about 750° C (Bruhns and Fischer, 2001). In the system V_2O_5-SiO_2 the formation of liquid phase is expected at about 661° C whereas the phase diagram CuO-SiO_2 shows partitial melting at about 1050° C (Levin et al. 1969). As mentioned above, the clay used here contains additional compounds like Fe_2O_3 or TiO_2 which probably influence the thermodynamic behavior. It is remarkable that either mullite (clay with V_2O_5 or CuO), or a specific mineral phase (like Pb-feldspar) which incorporates and immobilizes the metal ions, is formed. We assume that in the former compositions the heavy metal oxides participate in partial melting which triggers mullite formation. When the metal ions are incorporated in other phases, liquid

phase is consumed and mullite formation in rather low temperature ranges is not possible any more. Reactions in natural clay are very complex and the discussion of binary phase diagrams is insufficient to explain all processes. However, it gives some indication for possible reactions.

In contrast to the syntheses containing PbO and CuO, samples annealed with Cr_2O_3 show no deviations from the reaction path of pure clay. Cr_2O_3 remains admixed and no further mineralization is observed. Considering the phase diagrams of Cr_2O_3 and SiO_2, and Cr_2O_3 and Al_2O_3, mineralizations are not expected in a temperature range below 1723° and 2045° C, respectively (Levin et al. 1969). Syntheses with chromates as more reactive compounds yield different results which depend significantly on the cation Na^+ or K^+. However, all syntheses containing chromium yield Cr_2O_3 during annealing processes.

Acknowledgements

Financial support is gratefully acknowledged from the Zentrale Kommission des Akademischen Senats für Forschungsplanung und wissenschaftlichen Nachwuchs (FNK). We thank Nora Groschopf (University of Mainz) for XRF analyses and Emma Eades (University of Bremen) for her comments on the manuscript.

References

Abrahams, S.C., and Bernstein, J.L. (1971) Rutile: normal probability plot analysis and accurate measurement of crystal structure. Journal of Chemical Physics, 55, 3206-3211.

Ban, T., and Okada, K. (1992) Structure refinement of mullite by the rietveld method and a new method for estimation of chemical composition. Journal of the American Ceramic Society, 75, 227-230.

Bellotto, M., Gualtieri, A., Artioli, G., and Clark, S. M. (1995) Kinetic study of the kaolinite-mullite reaction sequence. Part I: Kaolinite dehydroxylation. Physics and Chemistry of Minerals, 22, 207-214.

Benna, P., Tribaudino, M., and Bruno, E. (1996) The structure of ordered and disordered lead feldspar ($PbAl_2Si_2O_8$). American Mineralogist, 81, 1337-1343.

Benna, P., Tribaudino, M., and Bruno, E. (1999) High-temperature in situ structural investigation on lead feldspar. American Mineralogist, 84, 120-129.

Bish, D. L., and von Dreele, R. B. (1989) Rietveld refinement of non-hydrogen atomic positions in kaolinite. Clays and Clay Minerals, 37, 289-296.

Blake, R. L., Hessevick, R. E., Zoltai, T., and Finger, L. W. (1966) Refinement of the hematite structure. American Mineralogist, 51, 123-129.

Brese, N. E., O'Keeffe, M., Ramakrishna, B. L., and von Dreele, R. B. (1990) Low-temperature structures of CuO and AgO and their relationships to those of MgO and PdO. Journal of Solid State Chemistry, 89, 184-190.

Brindley, G. W. (1945) The effect of grain or particle size on X-ray reflections from mixed powders or alloys. Philosophical Magazine 36, 347-369.

Brindley, G. W., and Nakahira, M. (1959) The kaolinite-mullite reaction series:

I. A survey of outstanding problems.

II. Metakaolin.

III. The high-temperature phases. Journal of the American Ceramic Society, 42, 311-342.

Bruhns, P., and Fischer, R. X. (2001) Phase reactions in the brick firing process of V-doped clay. European Journal of Mineralogy, in press.

Dollase, W. A. (1970) Least-squares refinement of the structure of a plutonic nepheline. Zeitschrift für Kristallographie, 132, 27-44.

Fischer, R. X., Lengauer, C., Tillmanns, E., Ensink, R. J., Reiss, C. A., and Fantner, E. J. (1993) PC-Rietveld Plus, a comprehensive Rietveld analysis package for PC. Materials Science Forum, 133-136, 287-292.

Förstner, U. (1995) Umweltschutztechnik: eine Einführung. Springer Verlag, Berlin Heidelberg New York.

Hill, R. J. (1985) Refinement of the structure of orthorhombic PbO (massicot) by Rietveld analysis of neutron powder diffraction data. Acta Crystallographica C41, 1281-1284.

Kisi, E. H., and Elcombe, M. M. (1989) U parameters for the wurtzite structure of ZnS and ZnO using powder neutron diffraction. Acta Crystallographica, C45, 1867-1870.

Kromer, H., and Schüller, K. H. (1974) Sintervorgänge bei Kaolinen und Tonen. Neues Jahrbuch Mineralogie Abhandlungen, 122, 145-185.

Levin, E. M., Robbins, C. R., and McMurdie, H. F. (1969) Phase Diagrams for Ceramists. The American Ceramic Society, Columbus, Ohio.

Margane, J. (1992) Änderung der Schwermetallbindungsformen in thermisch behandeltem Bodenmaterial. Geologisches Institut der Universität zu Köln, Sonderveröffentlichungen Nr. 87.

Mazzucato, E., Artioli, G., and Gualtieri, A. (1999) High temperature dehydroxylation of

muscovite-2M_1: a kinetic study by in situ XRPD. Physics and Chemistry of Minerals, 26, 375-381.

Newnham, R. E., and de Haan, Y. M. (1962) Refinement of the Al_2O_3-alpha, Ti_2O_3, V_2O_3, and Cr_2O_3 structures. Zeitschrift für Kristallographie, 117, 235-237.

Perrotta, A. J., Smith, S. M., and Smith, J. V. (1965) The crystal structure of kalsilite, $KAlSiO_4$. Mineralogical Magazine, 35, 588-617.

Richardson, S. M., and Richardson, J. W. Jr. (1982) Crystal structure of a pink muscovite from Archer's post Kenya: implications for reverse pleochroism in dioctahedral micas. American Mineralogist, 67, 69-75.

Schulz, H. (1970) Struktur- und Ueberstrukturuntersuchungen an Nosean-Einkristallen. Zeitschrift für Kristallographie, 131, 114-138.

Will, G., Bellotto, M., Parrish, W., and Hart, M. (1988) Crystal structures of quartz and magnesium germanate by profile analysis of synchrotron-radiation high-resolution powder data. Journal of Applied Crystallography, 21, 182-191.

Incorporation and leaching of heavy metals in clay annealed with Pb, Cu and V

Volker Karius, Petra Bruhns, Kay Hamer, and Reinhard X. Fischer

Universität Bremen, Fachbereich Geowissenschaften der Universität, Klagenfurter Straße, D-28359 Bremen, Germany

Abstract

The leaching characteristics of annealed clay enriched with heavy metals (5 wt.-% PbO, CuO, V_2O_5) were compared with the mineral phase composition. X-ray powder diffraction analyses of the products at different annealing temperatures (up to 1000° C) revealed that Pb is incorporated in a lead feldspar whereas Cu and V are mainly incorporated in the amorphous component. The phases incorporating Pb, Cu, or V were investigated by thermodynamic calculations to confirm consistency to the observed solubility behaviour in pH-static experiments at pH 4, 7 and 11. Mobilization data indicate that Pb and Cu are sufficiently immobilized during annealing processes whereas the high mobility of V strongly depends on the annealing temperature.

Keywords

pH-static, heavy metals, leaching, XRD, brick, immobilization, Rietveld analysis

Introduction

The utilization of heavy metal contaminated wastes as additives in brick manufacturing gets more and more established. Waste materials like dredged harbour sediments, steel dust, sewage-sludge incinerator ash, coal fly-ash and slag are used as substitutes for natural clay in the brick industry (Karius and others 1999, Domínguez & Ullmann 1996, Wiebusch & Seyfried 1997, Güler and others 1995, Freidin & Erell 1995). Even natural clays contain quantities of vanadium and chromium which form vanadates and chromates during brick burning processes. Apart from the environmental risks of heavy metal leaching the durability of the products may be reduced as well due to the efflorescence of these compounds on the surfaces of ceramic products (Dondi and others 1997).

In addition to economic aspects thermal treatment is employed to destroy organic contaminants and to immobilize heavy metals as constituents in newly built mineral phases or in the glass matrix of the bricks. The incorporation of heavy metals in mineral phases like mullite or spinell is assumed (Margane 1992). However, the details of heavy metal incorporation in a brick's matrix are not known.

Several methods are suitable to yield information about these processes. Leaching tests are commonly used to characterize the leaching behaviour of a material in order to conform to environmental standards (e.g. van der Sloot 1998). In this study the observed leaching properties of an annealed clay doped with Pb, Cu and V are correlated with the known solubility behaviour of possible host minerals based on thermodynamic calculations. Mineral phase formations during annealing processes are characterized by X-ray powder diffraction

methods. These data yield initial information on the complex phase compositions in clay systems. Former studies were performed on mixtures of clay and various heavy metal compounds like V_2O_5, PbO, CuO, Cr_2O_3 and sodium and potassium chromates. Detailed descriptions of the mineralizations during annealing processes up to 1000° C in these systems are given (Bruhns & Fischer 2001, Bruhns & Fischer submitted).

Materials and Methods

(1) Phase analyses

The raw clay material used for the annealing experiments was kindly provided by the brickwork Grehl, Humlangen, Germany. Chemical analyses were performed using a Philips 1404 X-ray fluorescence (XRF) spectrometer at the Institute of Mineralogy, University of Mainz. Phase analyses and quantification are performed with Rietveld refinements based on X-ray powder diffraction (XRD) data. Data were collected using a Philips PW 3050 powder diffractometer with Cu$K_{\alpha 1}$ radiation and primary monochromator in the range between 5° and 120° 2θ and steps of 0.02° 2θ. All refinements were performed using the Philips PC-Rietveld plus program package (Fischer and others 1993). Quantitative analyses and determination of the amorphous content of the samples were performed using ZnO as internal standard.
Three batches of clay were mixed with 5 wt.-% of PbO, CuO, and V_2O_5, respectively. The mixtures were homogenized in an agate mortar and pressed to pellets of 13 mm diameter for the annealing experiments in a tube furnace. To protect the furnace from contamination caused by volatile heavy metal compounds, the experiments were performed in a silica glass tube inside the furnace ceramic tube. Maximum temperature was 1000° C, held for 17 h, representing the temperature range typical for brick burning. The heating rate was 200° C/h, just as the cooling rate. The annealed samples were crushed and finally ground in an agate mortar.

(2) Leaching tests

The pH-static experiments at pH 4, 7, and 11 were performed to examine the leachability of Pb, Cu, V and the major elements after annealing the three finely ground batches at 1000° C. In order to investigate the leachability as a function of the annealing temperature the batch containing vanadium was annealed in a temperature range between 700° and 1000° C. For leaching experiments at pH 4 finely ground samples were used, too.

The pH-static experiments were performed on the basis of the method developed by Obermann & Cremer (1991). Each sample was leached for 24 h in three parallel experiments. As the available sample amounts were rather small only 0.1 - 0.5 g were used in the pH-static experiment. A liquid-to-solid ratio (L/S) of 1000 [ml/g] was chosen in order to ensure proper stirring and titrating conditions and to get sufficient amounts of leachants. De-ionized water with an electric conductivity of <0.0055 mS/m was used in the leaching experiments. The pH-value was held constant on a pre-set value using a pH-static controller and an autoburette titrating HNO_3 or NaOH, respectively. The samples were suspended with a PTFE-propeller inserted from above into a glassbeaker. The leachates were 0.45 µm filtered and acidified with HNO_3. The residue was analyzed by XRD.

All materials in contact with the leachant were precleaned with 0.3 N HNO_3 for 24 h and subsequently rinsed with de-ionized water. The reagents used were all suprapur® grade.

All leachates were analyzed with a Finnigan Mat Sola ICP-MS (Cu, Pb, V) and a Perkin Elmer Optima 3300 RL ICP-AES (Al, Ca, Fe, K, Mg, Na, S as SO_4, Si). The elements Na and K are strongly influenced by the leaching method. For pH 7 and 11 pH-static experiments were performed using NaOH as titrant. The pH-probe used during leaching tests had a double junction and contained KNO_3 as outer electrolyte which is enriched in all leachants by diffusion.

(3) Thermodynamic calculations

Thermodynamic calculations are used to explain the results of leaching experiments. The dissolution of minerals dependent on the pH-conditions are investigated and compared with the observed results of leaching experiments. For this purpose the saturation indices of several mineral phases were calculated in the leachants.

Thermodynamic calculations were performed with the program PHREEQC (Version 2) using the dataset Minteq (Parkhurst & Appelo 1999). PHREEQC is a geochemical model capable to calculate saturation indices (SI) and the distribution of aqueous species as well as batch-reaction calculation and surface-complexation reactions. The definition of the SI is given in Appelo & Postma (1993):

$$SI = \log (IAP/K)$$

with

IAP : Ion activity product [-]

K : Solubility product [-]

Two types of calculations were performed. First the saturation indices were calculated of compounds incorporating the heavy metals Pb, Cu, or V upon the different conditions of pH 4, 7, and 11. Input concentrations for main components and trace elements were taken as measured in the leaching experiments presented in the results section. In the second calculation, constant concentrations for the constituents of the particular phases were taken and the SI was calculated at pH 4, 7, and 11. The first method yields information on the actual state of saturation in the leaching solutions. The second provides qualitative information on the relative solubility of a mineral as a function of pH. With a higher degree of subsaturation the amount of leachable constituents gets larger at a specific pH-value. Both calculations yield similar results if the investigated elements are related to a single phase and a single process (e.g. dissolution). They will differ if more than one phase is involved or if more than one

process (e.g. dissolution and sorption) occurs.

Results

(1) Chemical and phase analyses

The XRF analysis of the raw clay yielded weight fractions of 67.5% SiO_2, 18.8% Al_2O_3, 3.2% Fe_2O_3, 1.4% TiO_2, 0.2% CaO, 0.4% MgO, 0.2% Na_2O, 1.7% K_2O, and 0.03% P_2O_5. The deviation from 100% was determined as weight loss due to dehydroxylation and water desorption.

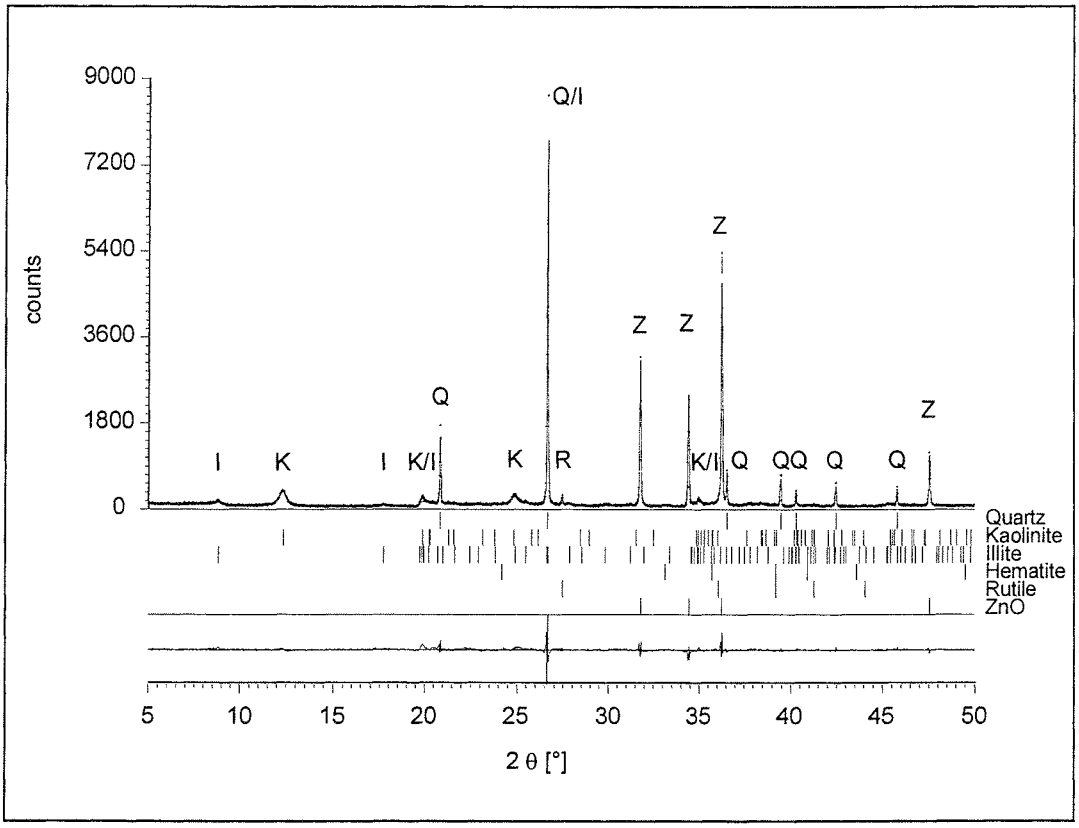

Fig. 1: Observed (crosses) and calculated (lines) powder diffraction patterns from Rietveld refinements of raw clay. Q: quartz, K: kaolinite, I: illite, R: rutile, Z: ZnO.

Figure 1 shows the powder diffraction pattern of pure clay with ZnO admixed as internal standard for quantification. Multi-phase Rietveld analysis yielded the composition shown in Table 1. Additionally, the composition of pure clay annealed at 1000° C is listed. Weight fractions are given with the first digit after the decimal point to include fractions <1 wt.-%.

	Quartz	Kaolinite	Illite	Rutile	Hematite	Amorphous
Clay at room temperature	40.1	24.9	15.9	1.8	0.4	16.8
Clay at 1000° C	43.4	-	8.4	1.4	1.4	45.3

Tab. 1: Phase composition of pure clay at room temperature and annealed at 1000° C, weight fractions in [%]

However, the relative error is about 5-10% (~ 3% absolute) for high contents and 20-50% (~ 0.3% absolute) for low contents. For pure clay we observed a typical composition of quartz, kaolinite, illite, hematite, rutile and an amorphous component. The annealing process up to 1000° C yields a composition of quartz, rutile, hematite, traces of illite, and an amorphous phase. The amorphous content increases significantly during annealing processes due to transformation of kaolinite to metakaolinite. Further increase of the annealing temperature leads to the formation of mullite (Brindley & Nakahira 1959).

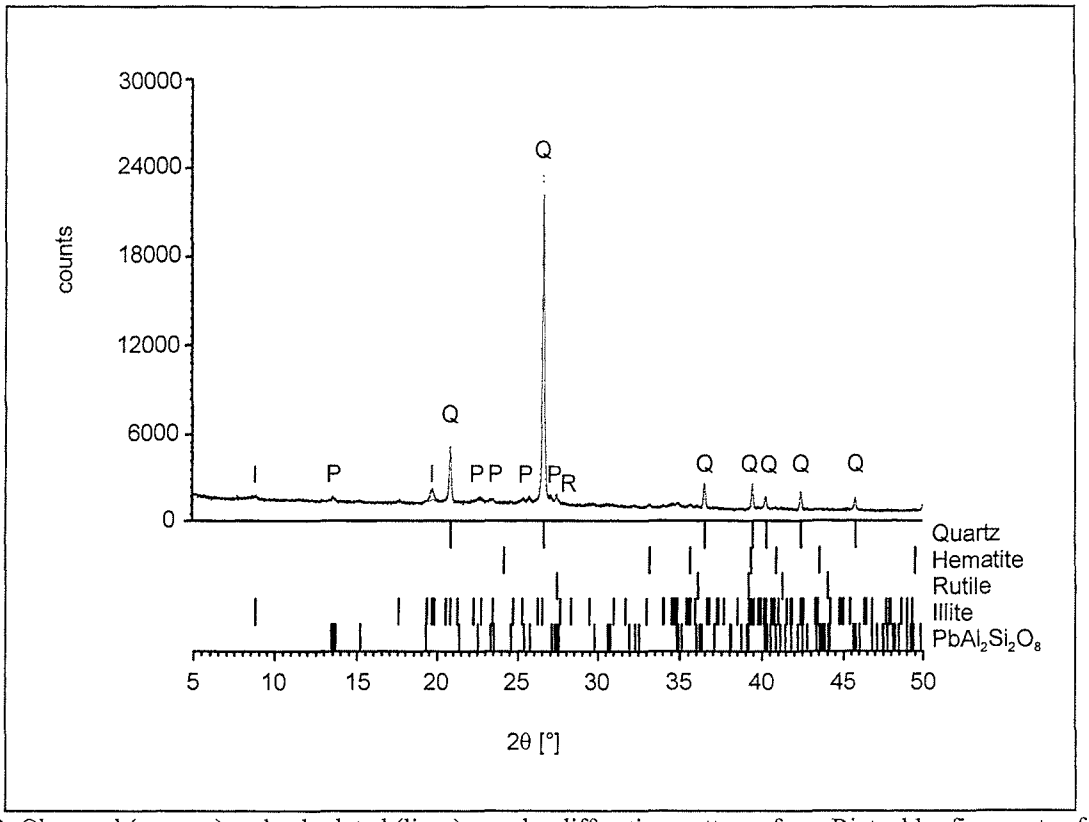

Fig. 2: Observed (crosses) and calculated (lines) powder diffraction patterns from Rietveld refinements of clay admixed with 5 wt.-% PbO annealed at 1000° C. Q: quartz, I: illite, R: rutile, P: $PbAl_2Si_2O_8$.

The powder diffraction pattern of clay with 5 wt.-% PbO annealed at 1000° C is shown in Figure 2.

The phase composition differs from pure clay as the formation of a lead feldspar occurs. PbO is not observed anymore in this temperature region. Apart from that, no mineralizations deviating from pure clay are observed.

In syntheses performed with clay and 5 wt.-% CuO at 1000° C newly built copper-bearing phases do not occur. A reduced amount of CuO remains in the sample. The formation of mullite in this temperature region is remarkable (Figure 3). It was not observed either in pure clay samples or in syntheses containing PbO.

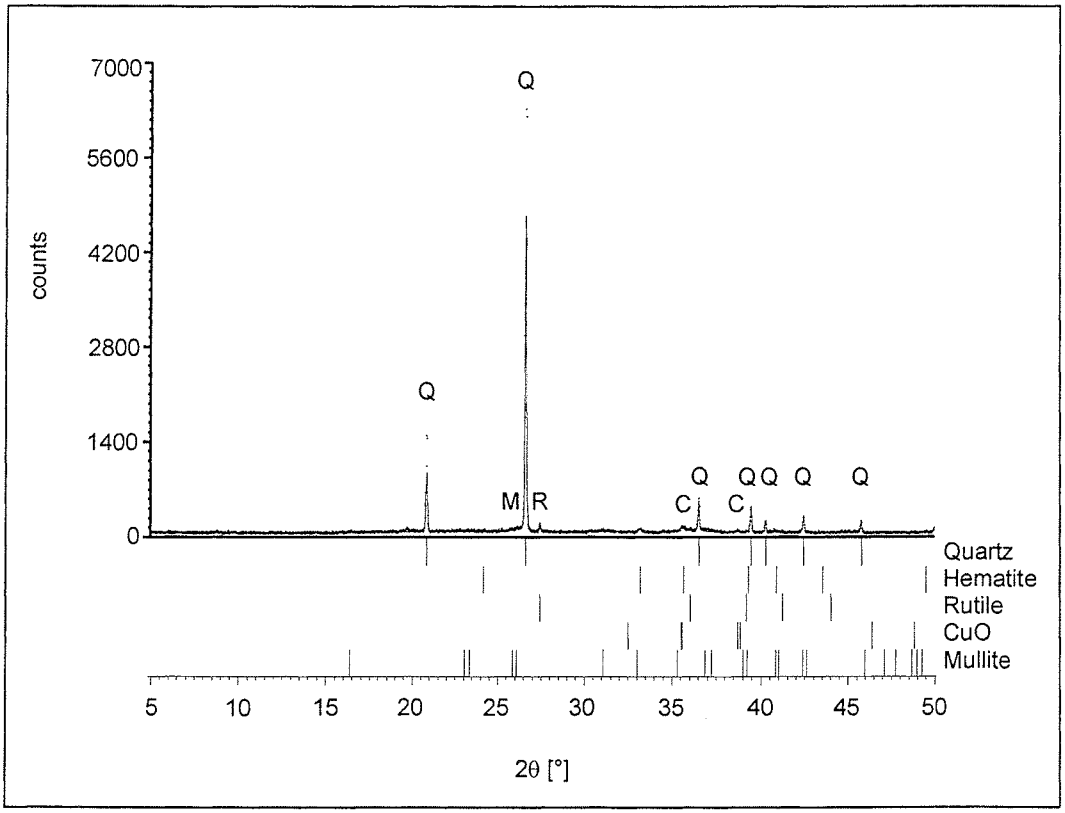

Fig. 3: Observed (crosses) and calculated (lines) powder diffraction patterns from Rietveld refinements of clay admixed with 5 wt.-% CuO annealed at 1000° C. Q: quartz, M: mullite, R: rutile, C: CuO.

The third batch containing 5 wt.-% V_2O_5 shows a significantly altered phase composition. The formation of mullite occurs at 750° C and, additionally, cristobalite is observed above 800° C. V_2O_5 is decomposed in the temperature range between 700° and 800° C. Powder diffraction patterns of the significant steps are shown in Figure 4.

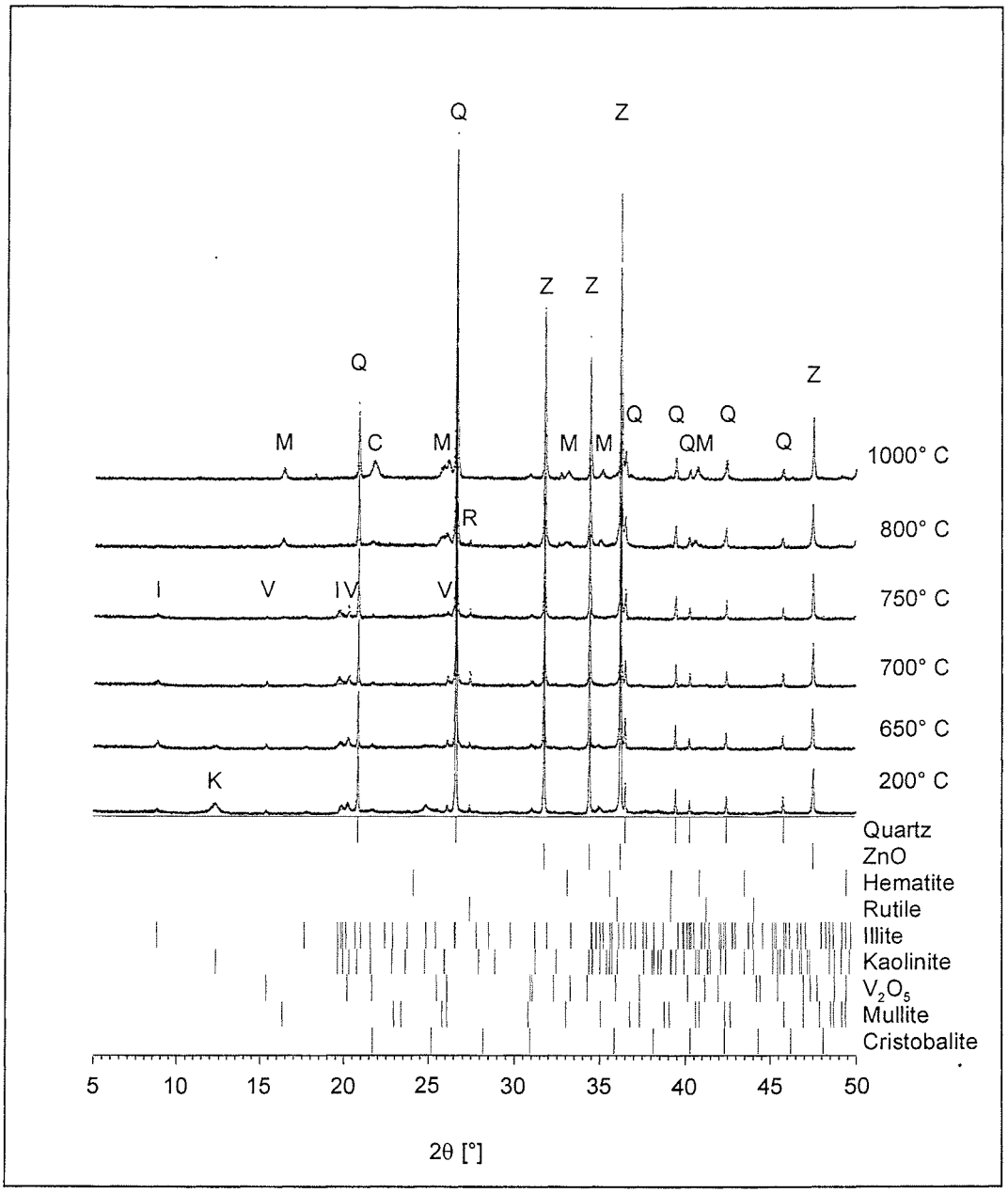

Fig. 4: Observed (crosses) and calculated (lines) powder diffraction patterns from Rietveld refinements of clay admixed with 5 wt.-% V_2O_5 annealed between 200° and 1000° C. Q: quartz, K: kaolinite, I: illite, V: V_2O_5, R: rutile, M: mullite, C: cristobalite, Z: ZnO.

The results of the quantitative analysis are given in Table 2. At 1000° C, 26.3 wt.-% mullite are detected in the sample. Further investigation of the mullite phase yielded lattice parameters which show remarkable deviations from data given by Ban & Okada (1992). Analyses with Analytical Transmission Electron Microscopy (ATEM) yielded 5.66 wt.-% vanadium incorporated in the mullite phase (Bruhns & Fischer 2001). The cristobalite structure is not supposed to incorporate vanadium (Bruhns & Fischer 2000).

	Clay with 5 wt.-% V_2O_5 annealed at [°C]												
	room temp.	200	400	500	550	600	650	700	750	800	900	950	1000
Quartz	42.0	42.3	43.4	43.9	45.2	41.4	44.8	47.2	46.3	42.8	44.4	46.0	42.3
Kaolinite	22.5	14.1	18.6	25.5	17.6	6.9	12.5	-	-	-	-	-	-
Illitic components	12.0	12.5	12.9	11.9	13.0	9.1	6.5	13.4	10.8	-	-	-	-
Mullite	-	-	-	-	-	-	-	-	3.5	20.1	22.2	24.0	26.3
Cristobalite	-	-	-	-	-	-	-	-	-	2.0	6.9	9.0	8.8
Rutile	1.5	1.6	1.9	1.4	1.3	1.4	1.1	1.9	1.0	0.9	0.7	-	-
Hematite	0.6	0.8	0.6	0.6	0.4	0.5	0.3	1.0	1.5	0.9	-	-	-
Pseudo-brookite	-	-	-	-	-	-	-	-	-	0.8	1.6	1.9	1.8
V_2O_5	5.6	4.1	4.4	5.2	5.0	3.6	4.9	5.0	2.1	-	-	-	-
Amorphous	15.8	24.6	18.3	11.6	17.5	37.1	30.0	31.6	34.7	32.6	24.1	19.1	21.0

Tab. 2: Phase composition of annealed clay admixed with 5 wt.-% V_2O_5, weight fractions in [%]

(2) Leaching tests

The leachability of major elements in the three batches is shown in Table 3. Obviously, the leachability of most elements differs significantly between the batches. As described by X-ray analyses the phase compositions of the batches differ dependent on the admixed heavy metal compound.

Clay + V_2O_5									
pH	Al	Ca	Fe	K	Mg	Na	SO_4	Si	V
4	985	568	29	16338	345	269	<500	524	8772
7	105	663	<5	15013	378	4516	<500	728	11623
11	1456	443	7	16141	28	74339	<500	2471	13260

Clay + CuO									
pH	Al	Ca	Fe	K	Mg	Na	SO_4	Si	Cu
4	787	76	10	11006	56	139	<500	516	1198
7	<100	<50	<5	8739	<10	2646	<500	302	21
11	605	<50	6	11040	<10	157400	<500	2934	49

Clay + PbO									
pH	Al	Ca	Fe	K	Mg	Na	SO_4	Si	Pb
4	738	84	105	10076	36	329	<500	2018	446
7	<100	<50	<5	10760	<10	2481	<500	270	1.3
11	2000	<50	37	7848	<10	124788	<500	4615	60

Tab. 3: Leachability in [mg/kg] of elements in clay admixed with 5 wt.-% PbO, CuO, V_2O_5 annealed at 1000°C

The mobility of Ca, K, and Mg in the batch containing vanadium oxide is significantly higher than in the batches containing lead or copper compounds. Additionally, the mobility of K is influenced by the electrolyte of the pH-probe.

Figure 5 shows the dependence of the pH-values on the investigated heavy metals. Cu and Pb show a similar behaviour.

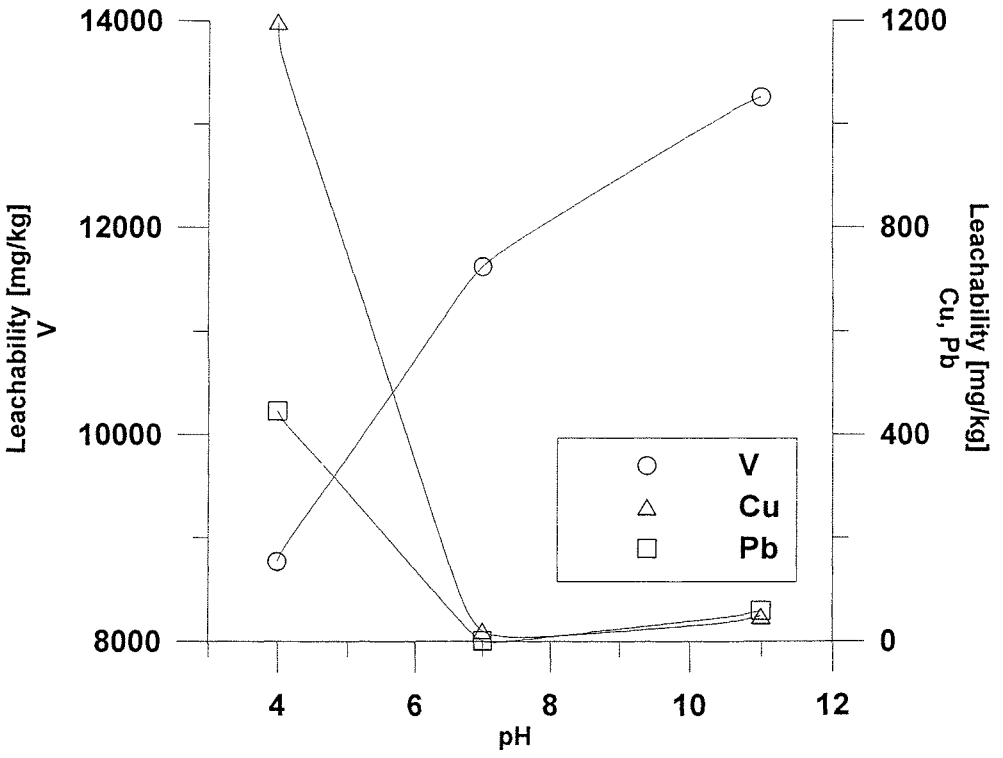

Fig. 5: Leachability of Pb, Cu, and V in clay admixed with 5 wt.-% PbO, CuO, V_2O_5 annealed at 1000°C

Highest leachability is observed at pH 4 whereas leachability remains low at neutral pH and increases slightly at pH 11. In contrast, V shows increasing leachability at increasing pH-values. The behaviour of Cu and Pb is in good agreement with investigations on a brick manufactured from dredged harbour sediments while pH-dependence of V is reverse (Karius and others 1999).

The pH-static tests of the V enriched batch annealed at different temperatures revealed that the leachability of V is influenced significantly by the annealing temperature (Figure 6).

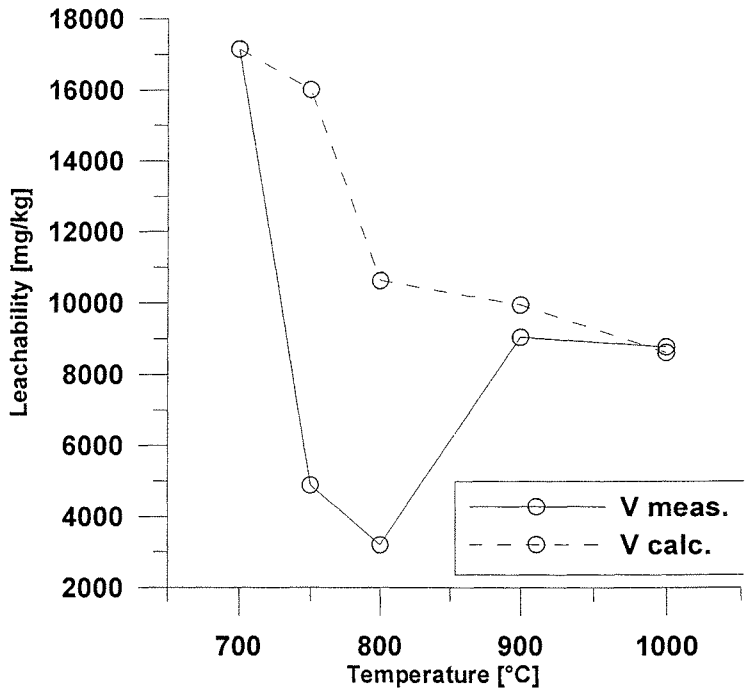

Fig. 6: Leachability (pH 4) of V in Clay admixed with 5 wt.-% V_2O_5 at different annealing temperatures

Leachability is high at 700 °C and decreases towards higher temperatures with a minimum at 800 °C. Further increasing of temperature yields an increasing leachability, too. A maximum is reached at 900 °C, the sample at 1000 °C shows a slightly lower leachability.

Mobilization of the examined elements by leaching in regard to the total content is given in Table 4 for the different batches at pH 4.

Batch	Clay + 5% V_2O_5	Clay + 5% CuO	Clay + 5% PbO
Na	24	12	29
Mg	14	2.3	1.5
Al	0.97	0.78	0.73
Si	0.16	0.16	0.63
K	113	76	70
Ca	49	6.6	7.2
Fe	0.13	0.047	0.47
V	29	-	-
Cu	-	2.8	-
Pb	-	-	0.90

Tab. 4: Mobilization in [%] of elements by leaching at pH 4 with regard to the total content

The powder diffraction pattern of the residues of the leached samples were compared with those recorded before the leaching tests. No alteration of the mineral composition was observed during leaching processes.

(3) Thermodynamic calculations

Related to the investigated heavy metals Figures 7-9 show the saturation indices of the minerals which were detected by XRD analyses or which showed a similar relative solubility with regard to Pb, Cu, and V as it was examined in the leaching tests. Two different calculations are given for each mineral. The open symbols represent the actual saturation index in the leachate (Calc.1). The closed symbols indicate the relative solubility of the mineral as a function of the pH-value qualitatively (Calc.2).

In XRD patterns of the batch containing Pb, lead feldspar is observed. Due to the lack of thermodynamic data of lead feldspar anorthite was investigated instead. Subsaturated conditions for anorthite were found at all investigated pH-values. Anorthite showed an increasing SI towards higher pH-values (Calc.1). Solubility of anorthite showed a minimum at pH 7 increasing towards acidic as well as alkaline pH-conditions (Calc.2) (Figure 7).

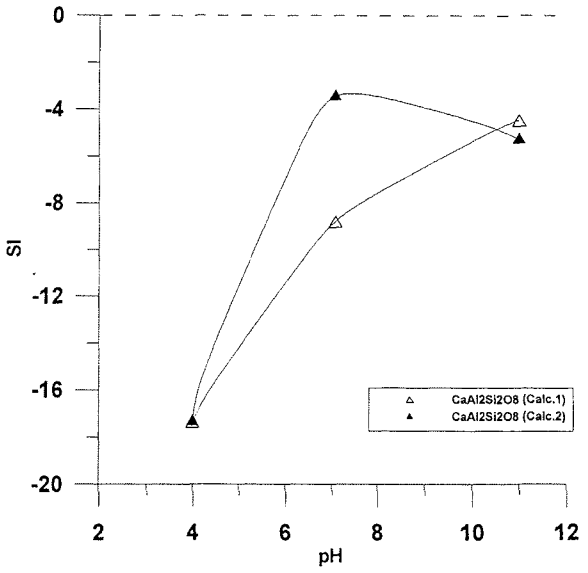

Fig. 7: Saturation indices of anorthite in the leachants of clay admixed with 5 wt.-% PbO annealed at 1000°C. Calc.1 shows the actual SI-value in the leachant, Calc.2 shows the relative solubility dependent on the pH-value.

Copper oxide (CuO) was subsaturated at pH 4 and 7 but in equilibrium at pH 11. The solubility of CuO decreases towards alkaline pH-values (Figure 8).

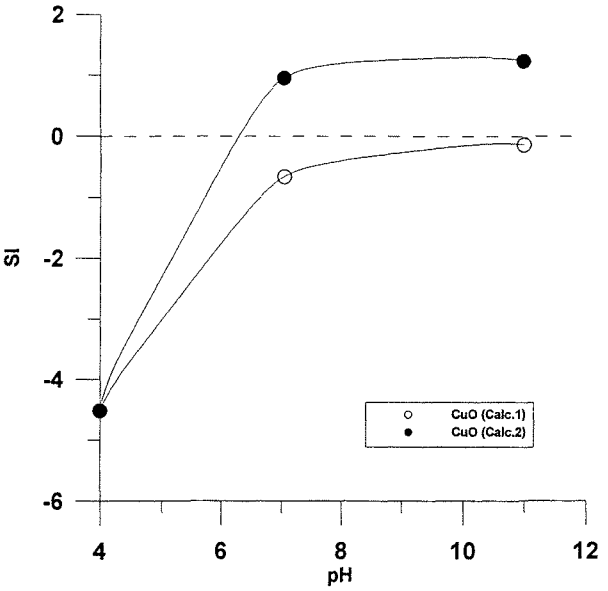

Fig. 8: Saturation indices of CuO in the leachants of clay admixed with 5 wt.-% CuO annealed at 1000°C. Calc.1 shows the actual SI-value in the leachant, Calc.2 shows the relative solubility dependent on the pH-value.

In the vanadium batch no phases containing V were detected by XRD. Vanadium oxides proved to match the observed pH characteristics qualitatively. Subsaturated conditions were found over the investigated pH-range. The solubility of vanadium oxides increases towards alkaline conditions (Figure 9).

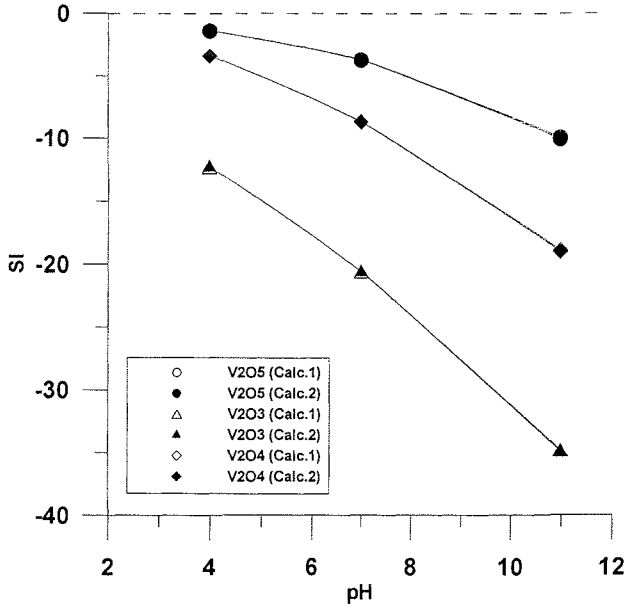

Fig. 9: Saturation indices of vanadium oxides in the leachants of clay admixed with 5 wt.-% V_2O_5 annealed at 1000°C. Calc.1 shows the actual SI-value in the leachant, Calc.2 shows the relative solubility dependent on the pH-value.

Discussion

Whereas XRD analyses yield the phase composition of the samples, the thermodynamic calculations explain the leaching characteristics of Pb, Cu and V with regard to the pH-conditions. The aim of this study is to combine these methods and to discuss which mineral phases are detected by XRD, and to show the solubility behaviour observed during the leaching tests.

The leaching behaviour of lead is determined by lead feldspar. Thermodynamic data of anorthite were used for qualitative simulation of the leachability of lead dependent on the pH-

value. This simulation describes the measured data quite sufficient (Figures 5 and 7). The state of subsaturation at pH 7 seems to be condratictory to the fact that only a very small amount of lead is leached at pH 7. Possible reasons are the slow dissolution kinetics of feldspar or sorption of Pb on the sample material or on a freshly precipitated phase. The qualitative difference between the two calculations for anorthite may be caused by the simultaneous dissolution of other aluminosilicates. It explains the high SI for anorthite at pH 11 in comparison to pH 7.

Calculations with the thermodynamic data of CuO suggest a decrease in solubility of copper with increasing pH-values (Figure 8). The observed minimum of leachability at pH 7 can be explained either with sorption on the sample material or with sorption on a freshly precipitated phase.

The V-containing samples show completely different leaching characteristics (Figure 9). In general, the calculated dissolution behaviour of vanadium oxides matches the observed leaching data. However, powder diffraction patterns revealed no vanadium oxides in this temperature region. But we have to consider that powder diffraction methods are limited by the poor crystallinity of the specimen. Thus, the determination of vanadium oxides which are almost amorphous is impossible.

Furthermore, the solubility characteristics of samples containing vanadium depend on the annealing temperature of the bricks. In general, the leachability above 800°C observed in this study is in good agreement with data from Dondi and others (1997) who examined clays with natural amounts of V (87-124 mg/kg) in a temperature range between 800°C and 1100° C. The maximum mobilization was 20-32 % compared to 29 % in this study. Another study reporting results from leaching tests carried out on ten different bricks revealed a significantly lower mobilization of V (<2 %) (Karius & Hamer 2001). Further comparison of these three studies is problematic because the conditions of the leaching experiments (L/S ratio, leachant, duration of leaching and pH-values) differ significantly.

The following model describes the behaviour of vanadium during leaching processes in our study. Assuming that the leachable vanadium amount of samples synthesized at 700° C is either part of the amorphous phase or of vanadium oxides and that vanadium incorporated in the structure of mullite is not available for leaching anymore, a theoretical leachability can be calculated for the samples of the annealing temperature region between 700° and 1000° C. The fraction of leachable vanadium from the amorphous phase respectively vanadium oxides is assumed to be more or less constant and independent of the annealing temperature. The theoretical leachability is calculated based on the leached amount of vanadium at 700° C, the amount of mullite at a specific temperature and the amount of fixed vanadium in the mullite. The model describes the leachability above 900 °C very well (Figure 6). However, there is a significant lower leachability at 750-800 °C than predicted. In this temperature range the mullite formation starts but obviously the incorporation of vanadium occurs in another phase with low solubility.

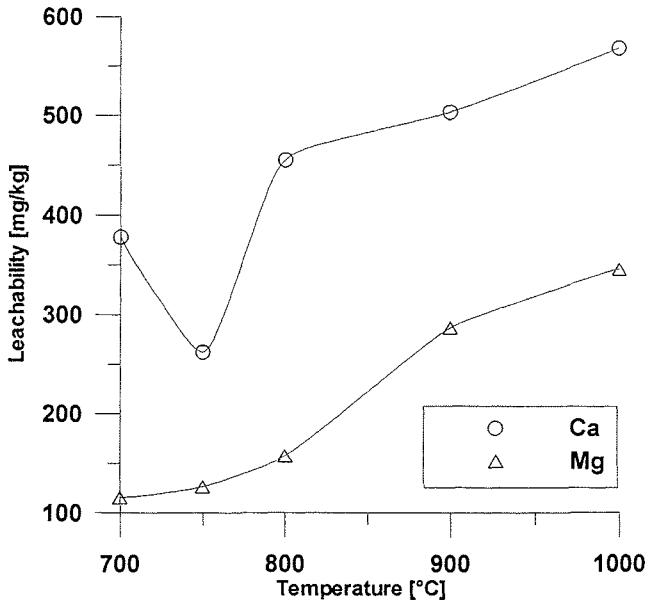

Fig. 10: Leachability (pH 4) of Mg and Ca in clay admixed with 5 wt.-% V_2O_5 at different annealing temperatures

The leaching experiments of samples enriched with vanadium show a significant higher mobilization of Mg and Ca compared with the samples containing lead or copper (Table 3). We assume that this increase in mobilization of Mg and Ca is due to the complete decomposition of the illite phase starting at rather low annealing temperatures. Whereas clay annealed with PbO even at 1000° C shows characteristic illite reflections (Figure 2), no illite is detected in samples containing vanadium (Figure 4). The decomposition occurs between 750° and 800° C and corresponds to the solubility behaviour of Mg and Ca in this temperature region (Figure 10). The powder diffraction pattern of the sample containing CuO still shows residues of intensity at 19.7° 2θ but no further illite reflections are detected (Figure 3). The structure is supposed to decompose in this temperature region but, obviously, Mg and Ca are still incorporated.

Conclusion

Mineralogical and geochemical methods were applied in order to investigate the behaviour of several heavy metals during annealing processes of doped clay. The heavy metal contents used were sufficient for quantitative X-ray powder diffraction analysis and yielded detailed information on the behaviour of Pb, Cu and V during thermal treatment. It could be shown that Pb is incorporated in a lead feldspar. Apart from a minor part of remaining CuO, Copper is mostly incorporated in the amorphous phase. Mullite formation is probably catalyzed by V and a minor part of the V is incorporated in mullite. To a greater extent V is incorporated in the amorphous phase or forms several vanadium oxides.

pH-static experiments yielded information on the mobility of the examined heavy metals after annealing. Pb and Cu were sufficiently immobilized at an annealing temperature of 1000°C. Only 2.8% of Cu was mobile at pH 4 and 0.9% of Pb, respectively. In contrast, more than 29% of V was mobile over the whole examined pH-range (4-11). The mobility of V was

strongly influenced by the annealing temperature. At 800°C the mobility of V showed a minimum. About 11% of V were mobile at this point. For brick production these results implicate that V has to be limited in the raw material in order to avoid high emission rates. There are no environmental specifications available in Germany for V neither for wastes nor for building materials (LAGA, 1996).

Thermodynamic calculations based on data from leaching tests can give some hints about phases which incorporate heavy metals. But care must be taken because the composition of leachants might be influenced by sorption processes or precipitation of secondary minerals.

Acknowledgements

We wish to thank the company Grehl, Humlangen, Germany who kindly provided the investigated clay and Dr. M. Schmücker, DLR, Köln, Germany for ATEM analyses. Funding is gratefully acknowledged from the "Kommission zur Förderung des wissenschaftlichen Nachwuchses", University of Bremen and the government of Bremen.

References

Appelo, C. A. J., Postma, D. (1993): Geochemistry, groundwater and pollution. A. A. Balkema, Rotterdam, 536 pp.

Ban, T., Okada, K. (1992): Structure refinement of mullite by the Rietveld method and a new method for estimation of chemical composition. *J. Am. Ceram. Soc.* **75**, 227-230.

Brindley, G. W., Nakahira, M. (1959): The kaolinite-mullite reaction series:

I. A survey of outstanding problems

II. Metakaolin

III. The high temperature phases. *J. Am. Ceram. Soc.* **42**, 311-324.

Bruhns, P., Fischer, R.X (2000): Crystallization of cristobalite and tridymite in the presence of vanadium. *Eur. J. Mineral.* **12**, 615-624.

Bruhns, P., Fischer, R.X (2001): Phase reactions in the brick firing process of V doped clay. *Eur. J. Mineral.*, in press.

Domínguez, E. A., Ullmann, R. (1996): 'Ecological bricks' made with clays and steel dust pollutants. *App. Clay Sci.* **11**, 237-249.

Dondi, M., Fabbri, B., Mingazzini, C. (1997): Mobilization of chromium and vanadium during firing of structural clay products. *Ziegelindustrie international* **10**, 685-696.

Fischer, R. X., Lengauer, C., Tillmanns, E., Ensink, R. J., Reiss, C. A., Fantner, E. J. (1993): PC-Rietveld Plus, a comprehensive Rietveld analysis package for PC. *Mater. Sci. Forum* **133-136**, 287-292.

Freidin, K., Erell, E. (1995): Bricks Made of Coal Fly-Ash and Slag, Cured in the Open Air. *Cement & Concrete Composites* **17**, 289-300.

Güler, R., Patla, P., Hess, T. R., Vempati, R. K., Cocke, D. L. (1995): Properties of fly-ash bricks produced for environmental applications. *J. Env. Sci. Health* **A30(3)**, 505-524.

Karius, V., Hamer, K., Bäätjer, M, Ulbricht, J.P., Schröter, J., Schulz, H.D. & H. De Vlieger (1999): Thermal treatment of contaminated harbour sediments – Environmental studies and technical experience of producing bricks at an industrial scale – CATS4, Antwerpen, Proceedings, 489-496.

Karius, V., Hamer, K. (2001): pH and grain-size variation in leaching tests with bricks made of harbour sediments compared to commercial bricks. *Sci Total Environ*, in press.

LAGA (1996): Anforderungen an die stoffliche Verwertung von mineralischen Reststoffen / Abfällen – Technische Regeln, Mitteilungen der Länderarbeitsgemeinschaft Abfall (LAGA) 20. Erich Schmidt Verlag, 84 pp.

Margane, J. (1992): Änderung der Schwermetallbindungsformen in thermisch behandeltem Bodenmaterial –Sonderveröffentlichungen Nr. 87. Geol. Institut Universität Köln, Köln, 192 pp.

Obermann, P., Cremer, S. (1991): Mobilisierung von Schwermetallen in Porenwässern von belasteten Böden und Deponien: Entwicklung eines aussagekräftigen Elutionsverfahrens. Materialien zur Ermittlung und Sanierung von Altlasten. Bd. 6. Ruhr-Universität Bochum. i.A.d. Landesamtes für Wasser- und Abfall NRW, Düsseldorf.

Parkhurst, D. L., Appelo, C. A. J. (1999): PHREEQC (Version 2) – A computer program for speciation, batch-reaction, one-dimensional transport and inverse geochemical calculations. Water-Resources Investigations Report 99-4259, U.S. Department of the Interior, U.S. Geological Survey, Denver, Colorado.

Van der Sloot, H. A. (1998): Quick techniques for evaluating the leaching properties of waste materials: their relation to decisions on utilization and disposal. *Trends Anal. Chem.* **17**, 298-310.

Wiebusch, B., Seyfried, C. F. (1997): Utilization of sewage sludge ashes in the brick and tile

industry. *Wat. Sci. Tech.* **36**, 251-258.

Part IV Conclusion

The previous results show the following important points:

- the addition of heavy metal compounds modifies the mineralizations in clay annealed at brick firing temperatures
- the mineralizations depend on the type and on the concentration of the added compounds
- the incorporation of heavy metal ions can be silicatic, oxidic, or may occur in the amorphous compound

Even for small amounts, results can be obtained and interpreted based on the employment of a variety of analytical methods not restricted to just X-ray diffraction. The combination of XRD, XRF, MAS NMR, DTA, IR, ATEM, and leaching experiments yielded a comprehensive knowledge of the reaction sequences during annealing as well as of the phases which incorporate heavy metals and of the leaching behavior of the final products.

Concerning vanadium, complete immobilization has not been achieved. As shown by phase analysis, vanadium is mainly incorporated in the amorphous matrix of the bricks. Leaching experiments yield a rather high solubility of vanadium and showed that the fixation in amorphous compounds is less stable than in crystalline phases. On the other hand, high solubility was not found for copper, which is mainly incorporated in the amorphous compound, too. Obviously, one universal model cannot describe the behavior of different heavy metals.

The detailed determination of the heavy metal ion fixation needs more analytical effort than practical for brick manufacturers. The complex and varying composition of most of the

heavy metal contaminated materials and the rather low concentration of the single components, complicates the analyses.

This study was focussed on the processes occuring in mixtures of clay with just one heavy metal compound. The results cannot be directly transferred to a clay-waste system because the reactions may be influenced by the additional reactants in the system. Therefore, this study only provides the basic facts on the topic. Further research is necessary to determine the behavior of other toxic heavy metals like arsenic, cadmium etc. and the mineralizations in a complex waste mixture.

Acknowledgements

Prof. Dr. R. X. Fischer is acknowledged for providing the topic of this study and for many helpful discussions. Grätitude is owed to Dr. K. Hamer for the second expert opinion. Financial support is gratefully acknowledged from the "Kommission zur Förderung des wissenschaftlichen Nachwuchses" (FNK), University of Bremen.

Dr. H. Eckert, Dr. M. Hengelbrock and Dr. L. van Wüllen (Münster) are acknowledged for performing and discussing the MAS NMR and ESR measurements, and N. Groschopf (Mainz) for XRF analyses. I thank Dr. M. Schmücker (Köln) for performing and discussing the Analytical Transmission Electron Microscopy (ATEM). The Institute of Physical Chemistry (Bremen) is acknowledged for providing access to the infrared spectrometer Special thanks are given to my colleagues from the "AK Kristallographie" for help and discussions.

Publications of this series:

No. 1 **Wefer, G., E. Suess and cruise participants**
Bericht über die POLARSTERN-Fahrt ANT IV/2, Rio de Janeiro - Punta Arenas, 6.11. - 1.12.1985.
60 pages, Bremen, 1986.

No. 2 **Hoffmann, G.**
Holozänstratigraphie und Küstenlinienverlagerung an der andalusischen Mittelmeerküste.
173 pages, Bremen, 1988. (out of print)

No. 3 **Wefer, G. and cruise participants**
Bericht über die METEOR-Fahrt M 6/6, Libreville - Las Palmas, 18.2. - 23.3.1988.
97 pages, Bremen, 1988.

No. 4 **Wefer, G., G.F. Lutze, T.J. Müller, O. Pfannkuche, W. Schenke, G. Siedler, W. Zenk**
Kurzbericht über die METEOR-Expedition No. 6, Hamburg - Hamburg, 28.10.1987 - 19.5.1988.
29 pages, Bremen, 1988. (out of print)

No. 5 **Fischer, G.**
Stabile Kohlenstoff-Isotope in partikulärer organischer Substanz aus dem Südpolarmeer (Atlantischer Sektor). 161 pages, Bremen, 1989.

No. 6 **Berger, W.H. and G. Wefer**
Partikelfluß und Kohlenstoffkreislauf im Ozean.
Bericht und Kurzfassungen über den Workshop vom 3.-4. Juli 1989 in Bremen.
57 pages, Bremen, 1989.

No. 7 **Wefer, G. and cruise participants**
Bericht über die METEOR - Fahrt M 9/4, Dakar - Santa Cruz, 19.2. - 16.3.1989.
103 pages, Bremen, 1989.

No. 8 **Kölling, M.**
Modellierung geochemischer Prozesse im Sickerwasser und Grundwasser.
135 pages, Bremen, 1990.

No. 9 **Heinze, P.-M.**
Das Auftriebsgeschehen vor Peru im Spätquartär. 204 pages, Bremen, 1990. (out of print)

No. 10 **Willems, H., G. Wefer, M. Rinski, B. Donner, H.-J. Bellmann, L. Eißmann, A. Müller, B.W. Flemming, H.-C. Höfle, J. Merkt, H. Streif, G. Hertweck, H. Kuntze, J. Schwaar, W. Schäfer, M.-G. Schulz, F. Grube, B. Menke**
Beiträge zur Geologie und Paläontologie Norddeutschlands: Exkursionsführer.
202 pages, Bremen, 1990.

No. 11 **Wefer, G. and cruise participants**
Bericht über die METEOR-Fahrt M 12/1, Kapstadt - Funchal, 13.3.1990 - 14.4.1990.
66 pages, Bremen, 1990.

No. 12 **Dahmke, A., H.D. Schulz, A. Kölling, F. Kracht, A. Lücke**
Schwermetallspuren und geochemische Gleichgewichte zwischen Porenlösung und Sediment im Wesermündungsgebiet. BMFT-Projekt MFU 0562, Abschlußbericht. 121 pages, Bremen, 1991.

No. 13 **Rostek, F.**
Physikalische Strukturen von Tiefseesedimenten des Südatlantiks und ihre Erfassung in Echolotregistrierungen. 209 pages, Bremen, 1991.

No. 14 **Baumann, M.**
Die Ablagerung von Tschernobyl-Radiocäsium in der Norwegischen See und in der Nordsee.
133 pages, Bremen, 1991. (out of print)

No. 15 **Kölling, A.**
Frühdiagenetische Prozesse und Stoff-Flüsse in marinen und ästuarinen Sedimenten.
140 pages, Bremen, 1991.

No. 16 **SFB 261 (ed.)**
1. Kolloquium des Sonderforschungsbereichs 261 der Universität Bremen (14.Juni 1991):
Der Südatlantik im Spätquartär: Rekonstruktion von Stoffhaushalt und Stromsystemen.
Kurzfassungen der Vorträge und Poster. 66 pages, Bremen, 1991.

No. 17 **Pätzold, J. and cruise participants**
Bericht und erste Ergebnisse über die METEOR-Fahrt M 15/2, Rio de Janeiro - Vitoria,
18.1. - 7.2.1991. 46 pages, Bremen, 1993.

No. 18 **Wefer, G. and cruise participants**
Bericht und erste Ergebnisse über die METEOR-Fahrt M 16/1, Pointe Noire - Recife,
27.3. - 25.4.1991. 120 pages, Bremen, 1991.

No. 19 **Schulz, H.D. and cruise participants**
Bericht und erste Ergebnisse über die METEOR-Fahrt M 16/2, Recife - Belem, 28.4. - 20.5.1991.
149 pages, Bremen, 1991.